Modeling the interplay between membrane lipids and GPCRs

Ramon Guixà González

TESI DOCTORAL UPF / ANY 2014

DIRECTOR DE LA TESI

Dr. Jana Selent

DEPARTAMENT DE CIÈNCIES EXPERIMENTALS I DE LA SALUT

Esta tesis está dedicada a mis padres, Ramón y Mª Teresa,
a mis hermanos, Tete, Dani e Isa,
a mis tíos, Fermín y Amparo,
a mi familia adoptiva catalana, Carlos, Loli, Sara,
i sobretot a la meva amiga Carol, enemiga del meu 'Litost'.

...then the Pink Panther embraced me,
and my world turned Pink...

Acknowledgements

Foremost, I would like to express my gratitude to La Marató de TV3 foundation, the BIOPSYCHO project (Spanish Ministry of Education and Sport), and the FEDER (Fondo Europeo de Desarrollo Regional, Instituto de Salud Carlos III) for the financial support provided during this thesis as well as the Catalan Agency for Management of University and Research Grants (AGAUR) and HPC-EUROPA2 project (with the support of the European Community - Research Infrastructure Action of the FP7) for supporting my predoctoral research with two mobility grants. I would also like to thank the CSC–IT Center for Science (Finland) and the BSC Barcelona Supercomputing Center (Spain) for the computer resources granted.

I owe a very important debt to my supervisor, Dr. Jana Selent, who gave me the opportunity to carry out this project. I am particularly grateful to her for being patient, for supporting and believing my horror tales about lipids and for providing me with the ability to work independently. I would also like to thanks Dr. Manuel Pastor and colleagues at the PharmacoInformatics group and Dr. Ferran Sanz for their support and insightful comments during my thesis. I am grateful to Dr. Ilpo Vattulainen and his group at the Tampere University of Technology for the support they provided during the time I spent in Finland. Likewise, I want to thank Dr. Marta Filizola and her group at the Icahn School of Medicine at Mount Sinai for hosting and helping me during my research stay in New York. Thanks go to Francisco Ciruela too, who trusted our crazy simulations and provided fruitful discussion and motivation for this project.

I particularly want to thank Hector Martinez-Seara and Toni Giorgino, without their guidance and help this dissertation would not have been possible. I also want to thank Matti Javanainen and Pau Carrió for great scientific discussions and their patience dealing with an obtuse biochemist. The advice, comments and support from Jana, Hector, Toni, Matti, Pau, Agnieszka Kazkor, Maria Martí-Solano and Juanma Ramírez-Anguita have been simply indispensable during the preparation of our manuscripts.

Last but of course not least, I would also like to thank all my family

and friends for their support. I want to thank Jose, Javi, Irene, Jéssica, Ignasi y Guillem for those grotesque, hectic and freaky discussions that surprisingly turned out to shape and inspire a substantial part of this work. I also want to thank Dr. Joan for trivializing some of my thesis obstacles and injecting humor into most of them. My special thanks go to my soul mate, Carol, for really understanding my bizarre and aloof behavior during certain periods of this thesis.

Abstract

The lipid composition of cell membranes ultimately determines their biophysical properties, thereby affecting the dynamics and organization of key transmembrane proteins like G protein-couple receptors (GPCRs). The aim of this thesis is to make a step forward towards a better understanding of the nature and extent of the interplay between membrane lipids and GPCRs. We have used molecular dynamics simulations to study the complexity of biological membranes and the effect of the membrane environment on the organization of GPCRs. Thus, we developed a computational framework to comprehensively analyze the properties of lipid bilayers and membrane–protein simulations. In addition, by combining computer simulations and experiments in living cells we demonstrate for the first time that membrane polyunsaturated lipids can modulate the organization of GPCRs. These findings could open new doors to the treatment of several conditions like schizophrenia or Parkinson's disease, where GPCRs have been shown to play an vital role.

Resum

La composició lipídica de les membranes cel·lulars determina, en última instància, les seves propietats biofísiques afectant, així, les dinàmiques i organització de proteïnes transmembrana essencials, com són els receptors acoblats a proteïnes G (GPCRs). L'objectiu d'aquesta tesi és fer un pas endavant en la comprensió de la natura i l'abast de la interacció entre lípids de membrana i GPCRs. Amb aquesta finalitat, hem emprat simulacions de dinàmiques moleculars per tal d'estudiar la complexitat de les membranes biològiques i el seu efecte sobre l'organització de les GPCRs. Així, hem desenvolupat un marc computacional per analitzar amb profunditat les simulacions de bicapes lipídiques i sistemes proteïna-membrana. A més, combinant simulacions computacionals i experiments amb cèl·lules vives, demostrem per primera vegada que els lípids de membrana poliinsaturats poden modular l'organització de les GPCRs. Aquests resultats podrien obrir noves portes en el tractament de condicions diverses com l'esquizofrènia o la malaltia de Parkinson, on s'ha demostrat que les GPCRs juguen un paper vital.

Prologue

This thesis focus on the modulation of G protein-coupled receptors (GPCRs) by membrane lipids, a topic of paramount importance that could revolutionize the development of new drugs by bringing lipids into play. Lipids have been traditionally considered to have a plain structural role in cell membranes, yet, recent studies demonstrate that lipids can modulate the function and dynamics of membrane proteins. Key transmembrane proteins like GPCRs are involved in the most prevalent human diseases including several neurological disorders or even cancer. However, the real contribution of the membrane environment to the function and dynamics of GPCRs is to date largely unknown.

In this scenario, molecular dynamics (MD) simulations of membrane–protein systems have emerged as a extremely valuable technique to examine and support experimental findings. Despite biological membranes are highly complex mixtures, in most of the current molecular simulations of transmembrane proteins, this lipid heterogeneity is underrepresented. Frequently, an important bottleneck of these simulations is the lack of adequate tools to characterize membrane complexity.

In this thesis, we provide a computational framework to biophysically characterize simple and complex lipid bilayers and membrane–protein simulations. We made this framework available to the scientific community through the development of a computational tool, MEMBPLUGING, to automate the analysis of membrane properties in molecular simulations. MEMBPLUGIN offers classical approaches to study the thickness, order or fluidity of membranes but also novel algorithms like the characterization of membrane leaflet interdigitation. We published this unified framework in a leading journal in bioinformatics.

Additionally, we combined MD simulations and experiments in living cells to provide novel results on the effect of membrane lipids on the organization of GPCRs. In particular, we report for the first time the modulation of GPCR oligomerization by docosahexaenoic acid, an omega-3 polyunsaturated fatty acids of high relevance in several brain disorders.

All in all, in this thesis we make a step forward towards a better under-

standing of the interplay between GPCRs and their highly complex lipid environment.

Contents

Chapter 1

INTRODUCTION

1.1 Biological background

1.1.1 G protein-coupled receptors (GPCRs)

The transmission of exogenous signals is the cornerstone of cell functioning in multicellular organisms, where membranes segregate the internal composition of cells from the exterior environment. The real key to understanding cell communication lies in a correct interpretation of how membrane receptors function. The paramount importance of this topic is highlighted by G protein-coupled receptors (GPCRs), the largest family of membrane receptors in the human genome [1]. Among many different proteins, members of this family include receptors for a wide variety of ligands ranging from photons or ions to many neurotransmitters, hormones or chemokines. These molecules are able to stimulate GPCRs to propagate a signal that triggers different second-messenger cascades which are involved in many physiological processes such as vision, taste, odor cell sensing or neurotransmission [2]. Thus, GPCRs are involved in a wide variety of human diseases where impairment in the activation of these receptor occurs and, nowadays, they are therapeutic targets of approximately 50 % of the currently launched drugs [3, 4].

In 1994, Kolakowski presented a comprehensive phylogenetic clas-

sification of GPCRs known as the A–F classification system. While the former nomenclature is still used by the International Union of Pharmacology, a decade later, Fredriksson and colleagues [5] showed that most human GPCRs can be divided in five main families, namely Rhodopsin (class A), Secretin (class B), Adhesion (class B), Glutamate (class C) and Frizzled/Taste2 (class F), a nomenclature system known under the acronym GRAFS. Among these 5 main classes, class A is by far the largest family and includes important receptors like the archetypal GPCR rhodopsin, olfactory receptors, chemokine, angiotensin, opioid, adrenergic, dopamine, histamine or adenosine receptors. However, despite their high ligand idiosyncrasy, all GPCRs share one common structural feature: seven transmembrane (TM) α-helical segments joined by a set of three extracellular and three intracellular loops [4] (Figure: 1.1).

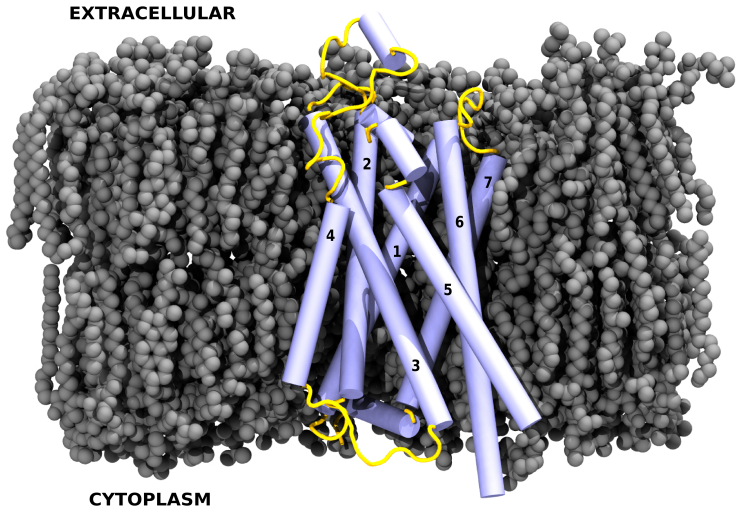

Figure 1.1: **Adenosine A_{2A} receptor embedded in a lipid bilayer.** In all GPCRs, seven transmembrane segments alternatively span from the extracellular side to the cytoplasm joined by protein loops. Helical segments are labeled with numbers and depicted in blue cartoons whereas unstructured protein segments are in thin yellow cylinders. Grey van der Waals spheres represent membrane lipids.

During the last two decades, new developments in protein X-ray crys-

tallography have allowed a rapid and successful crystallization of several new structures of GPCRs [6, 7]. The first atomic structure of a GPCR, rhodopsin, was determined in 2001 by Palczewski et al. [8] and, since then, crystallographic determinations have continued with the solution of several rhodopsin structures (Table: 1.1). This fruitful period has produced a full structural coverage along multiple activated and inactivated states of rhodopsin allowing a reconciliation between the evidence found by biochemists and biophysicists. A breakthrough in the structural study of GPCRs bound to ligands came in 2007, when the X-ray structure of the human β_2-adrenergic receptor bound to an inverse agonist finally saw the light [9]. Two different techniques using antibodies or the well-known T4-lisozyme constructs to stabilize the protein were used to successfully crystallize the first new structures of this receptor [10, 11]. Some years later, a camelid antibody fragment was used to solve a new agonist-bound crystal structure of the β_2-adrenergic receptor in its active-state [12]. Thus, 2007 was the beginning of the advent of new GPCR crystal structures: today the structure of several class A (including adenosine, chemokine, dopamine, muscarinic, opioid, neurotensin, or serotonin receptors), class B, class C and class F GPCRs have been solved (Table: 1.1).

Such good body of new GPCR structures have opened the door for studying differences and similarities of the seven transmembrane regions within class A GPCRs and hence shedding light on the ligand binding network at their transmembrane region or even on their mode of activation. But undoubtedly, a discovery of paramount importance for the field of GPCRs was the structure determination of the β_2-receptor in complex with the G protein [13]. This crystal structure confirmed that slight rearrangements of the GPCR architecture are behind the modulation of signal transduction and set the grounds for future structural studies on the relationship of GPCRs with the intracellular protein machinery.

Recent studies have shown that the function of GPCRs can be modulated by specific lipid-receptor interactions. Consequently, alterations in physiological levels of membrane lipids can markedly affect the behavior of key membrane receptors. Understanding the role of the membrane

Receptor	Class	Number of structures
Adenosine A_{2A}	A (*Rhodopsin*)	**12**
β_2-adrenergic		**15**
β_1-adrenergic		**16**
Chemokine $CXCR_1$		1
Chemokine $CXCR_4$		5
Chemokine $CXCR_5$		1
Dopamine D_3		1
Histamine H_1		1
Muscarinic M_2		4
Muscarinic M_3		1
Neurotensin		5
Nociceptin/orphanin FQ		1
κ-opioid		1
δ-opioid		2
μ-opioid		1
Protease-activated R_1		1
Purinoceptor P2Y12		3
Rhodopsin		**28**
Serotonin 5-HT_{1B}		2
Serotonin 5-HT_{2B}		2
Sphingosine 1P		2
Corticotropin releasing factor	B (*Secretin*)	1
Glucagon		1
Metabotropic glutamate R_1	C (*Glutamate*)	1
Smoothened receptor	F (*Frizzled*)	3

Table 1.1: **GPCR crystal structures solved as of May 2014.** To date, 24 GPCR types has been experimentally solved, including 20 Class A, 2 class B, 1 class C and 1 class F receptor. In this table, GPCRs with more than 10 crystal structures in the PDB have been highlighted in red. Since rhodopsin was the first crystallized GPCR, up to 28 crystal structures of this protein have already been deposited in the Proten Data Bank (PDB).

environment on the dynamics and conformation of GPCRs has therefore become a research priority in this field.

1.1.2 Biological membranes and lipid heterogeneity

Transmembrane proteins like GPCRs live permanently surrounded by membrane lipids. These lipids have been traditionally considered as passive solvents or just physical barriers that confine the whole repertoire of proteins living therein. However, considering membrane lipids simply as structural entities is a misconception of the true global mission of these molecules. The development of new computational and experimental techniques [14] have led to a deeper understanding of membrane lipids and revitalized this field by better defining their role in the dynamics of cell membranes. Today we are aware of the importance of membrane lipids, their specific biological functions, and their involvement in key cell membrane events such as virus budding [15], membrane trafficking or cell signaling [16]. In addition, lipids are involved in wide-spread disorders including neurodegenerative diseases[17] or even cancer [18].

The key physicochemical property that enables the constitution of biological membranes is the amphipatic nature of lipids. Such property is conferred by the presence of one polar and one hydrophobic part within the same lipid molecule (Figure: 1.2), which allows membrane bilayers to assemble, to separate the whole cell from the interior milieu and to compartmentalize internal cell organelles. The lipid composition of these membranes significantly varies across cell compartments and is maintained by cells through an exquisite regulation of the lipid turnover. Two main amphipatic lipid molecules, namely phospholipids and cholesterol, make up the bulk of animal cell membranes. By changing the level of these molecules, cells can modulate the structure of biological membranes with an aim to maximize the function of specific membrane machinery.

In mammals, the level of membrane cholesterol is typically different across cells and tissues. This sterol, synthesized in the endoplasmic reticulum, is a vital element of biological membranes and largely found in the plasma membrane [19]. In terms of the modulation of membrane bio-

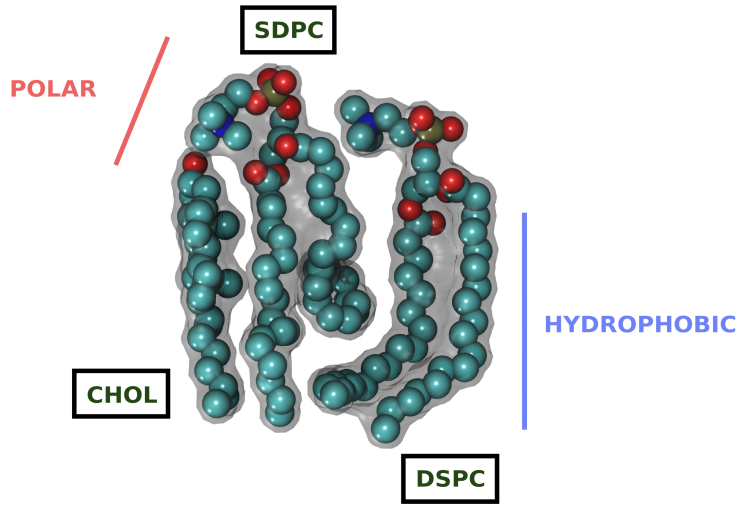

Figure 1.2: **Amphipathic structure of cholesterol and phospholipids.** Snapshot of one cholesterol (left) near two phospholipids, SDPC (1-stearoyl-2-docosahexaenoyl-*sn*-glyerco-3-phosphatidylcholine) (middle) and DSPC (1,2-distearoyl-*sn*-glycero-3-phosphatidylcholine) (right). Both cholesterol and phospholipids are amphipathic molecules, that is, they have both polar and hydrophobic regions. DSPC is an example of a fully saturated phospholipid whereas SDPC contains one saturated and one polyunsaturated unsaturated lipid tail. This snapshot was taken during a molecular dynamics (MD) trajectory of a complex lipid mixture. Carbon atoms are depicted in cyan, phosphorous in ochre, nitrogen in blue and oxygen atoms in red. Hydrogen atoms are not depicted for clarity.

physical properties, cholesterol is widely known to increase the condensation and decrease the fluidity of membranes rich in this molecule [20]. The impact of this effect on the properties of other lipids [21] or, more importantly, on the interaction [22, 23, 24, 25], stability [26], binding properties [27, 28], activation [29], function [30, 31, 32, 33] or even organization[34, 35] of membrane proteins like GPCRs is currently a matter of intense study.

Along with cholesterol levels, the amount and type of phospholipids is an important determinant of the overall membrane biophysical properties.

In general, cells modify two main structural features of phospholipids to design, in the endoplasmic reticulum and Golgi apparatus, most of mammalian species by *de novo* biosynthesis [36, 37] (Figure: 1.3). On the one hand, the type of head group defines five main species of phospholipids, namely phosphatidic acid (PA), phosphatidylethanolamine (PE), phosphatidylcholine (PC), phosphatidylserine (PS) and phosphoinositides (PI) (Figure: 1.3). Each phospholipid species of this colorful assortment, confer biological membranes with specific biophysical and physicochemical properties [19, 38]. For instance, PE phospholipids partially impose a higher curvature stress to the lipid bilayer when compared to membranes rich in PC phospholipids, a property used for budding, fission and fusion events [19, 39] in nature.

On the other hand, the nature of the hydrophobic part of phospholipids (Figure: 1.2) is a key regulator of various structural properties of cell membranes. One important property of these membranes modulated by the architecture of lipid tails is membrane fluidity. The number of double bonds or level of unsaturation was initially thought to provide rigidity to cell membranes, however, recent studies have demonstrated the impressive flexibility of highly unsaturated phospholipids [40]. In fact, subtle changes in membrane levels of unsaturated lipids can severely alter parameters like membrane thickness [41], fluidity [42, 43, 44], lateral pressure [45], or the affinity with other membrane components [46].

In addition to the lipid idiosyncrasy of biological membranes, cells can further stratify the levels of certain lipids across membrane leaflets yielding an asymmetric distribution of lipid molecules within the membrane itself. An elegant set of enzymes modulate the rate of lipid translocation to keep an asymmetry between the plasma and the cytosolic leaflet, hence, granting different biophysical properties to them. For instance, flippases control the so-called flip-flop of membrane phospholipids at the plasma membrane so that the cytosolic leaflet is enriched in PS and PE phospholipids [47]. This lipid imbalance contributes to membrane bending, necessary in biological events where a certain curvature of the membrane is needed (e.g. vesicle formation).

Besides lipid transversal heterogeneity, membranes can locally mod-

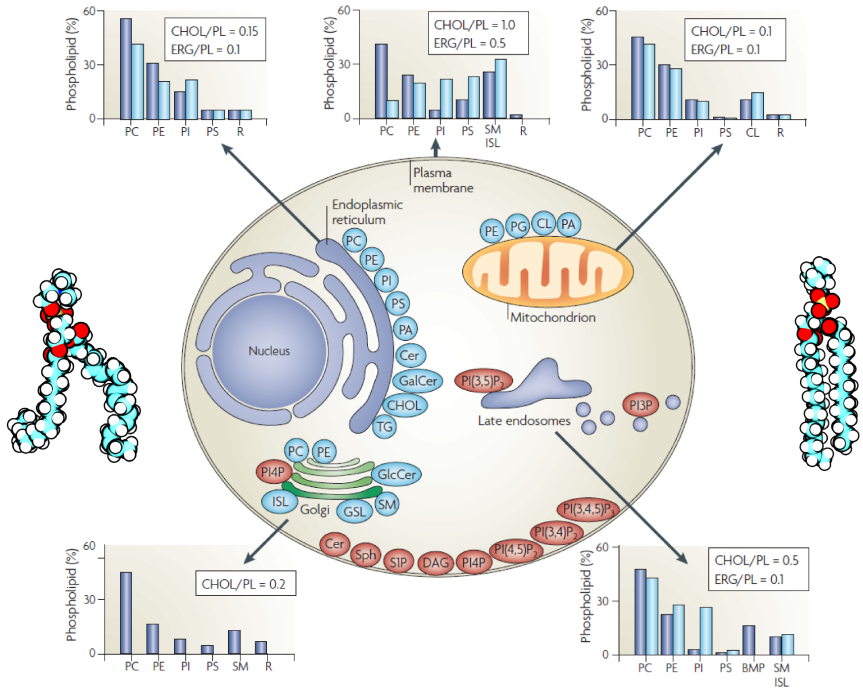

Figure 1.3: **Lipid heterogeneity across cell membranes.** The lipid composition of different membranes varies throughout the cell. Data in graphs are expressed as a percentage of the total phospholipid (PL) in mammals (blue) and yeast (light blue). Major phospholipids in blue and lipids lipids involved in signaling and organelle recognition in red. Abbreviations: Cer, ceramide; GalCer, galactosylceramide; GSLs, glycosphingolipids; DAG, diacylglycerol; ISL, inositol sphingolipid; PA, phosphatidic acid; PC, phosphatidylcholine; PE, phosphatidylethanolamine; PI, phosphatidylinositol; PS, phosphatidylserine; PG, phosphatidylglycerol; PI(3,5)P2 , phosphatidylinositol-(3,5)- bisphosphate; PI(4,5)P2 , phosphatidylinositol-(4,5)-bisphosphate; PI(3,4,5)P3 , phosphatidylinositol-(3,4,5)-trisphosphate; PI4P, phosphatidylinositol-4-phosphate; R, remaining lipids; S1P, sphingosine-1-phosphate; SM, sphingomyelin; Sph, sphingosine; TG, triacylglycerol; CHO, cholesterol (mammals); ERG, ergosterol (yeast). Figure adapted from Van Meer et al. [19].

ify lipid composition by segregating specific lipid and protein species in a lateral fashion to form structures called membrane microdomains [48]. These domains display , when compared to the rest of the membrane they 'float' into, different levels of certain lipids including higher levels of cholesterol. Two types of membrane microdomains, namely lipid rafts [49, 50] and caveolae [51] represent the essence of lipid lateral heterogeneity and have a special biological relevance in the context of protein functioning and dynamics [52, 53]. The fact that membrane microdomains seem to display differences in lipid compositions between healthy and diseased brains [54, 55, 56, 57] highlights the importance of understanding lipid lateral heterogeneity and its impact on the activity of transmembrane proteins like GPCRs.

1.1.3 The modulation of GPCRs by membrane lipids

Despite frequently overlooked, the lipid to protein ratio in native plasma membranes is very high, namely around 50:1 [53, 58]. Characterizing the effect of the membrane environment on protein dynamics is becoming a crucial step for an adequate understanding of key transmembrane proteins [59] like GPCRs. Membrane lipids are known to modulate certain GPCRs directly via specific interactions [60] and indirectly by changing the biophysical properties of the membrane [61]. The most evident example of a specific lipid-GPCR modulation is given by the fact that certain GPCRs can be activated by lipid-derived endogenous ligands [62, 63], as demonstrated by the recent crystal of the sphingosine 1-phosphate receptor [64]. However, the real contribution of specific and unspecific effect of membrane lipids to the function and/or stability of certain GPCRs is to date a widely unknown issue [29].

One typical component of biological membranes, cholesterol, has been intensely studied in the past years in connection to its relationship with GPCRs. A large body of experiments demonstrate that cholesterol modulates the stability and function of several GPCRs including rhodopsin [65], opioid [66, 67, 30], serotonin [68, 69], muscarinic [70] or cannabinoid [71] receptors. However, it is still unknown whether cholesterol exerts such

modulation by directly interacting with the receptor or rather indirectly by changing the biophysical properties of the membrane environment [34, 24]. The presence of specific 'annular' and/or 'nonannular' cholesterol binding sites is thought be involved in the functional modulation of various GPCRs [23]. In fact, the resolution of the β_2- adrenergic receptor crystal structure reported, for the first time, a specific cholesterol binding site in this GPCR [22] and the authors subsequently identified what they termed 'cholesterol consensus motif' within class A GPCRs. Despite cholesterol is known to modulate the function of various GPCRs, little is known about the mechanism behind this effect.

In addition, particular membrane phospholipids and fatty acids have been shown to influence key aspects of GPCR biology including signaling, receptor maturation or desensitization and membrane delivery. One special type of lipid–GPCR interaction is the fatty acylation, a post-translational modification undergone by most membrane proteins including GPCRs [72]. The most common fatty acylation of GPCRs occurs by the addition of palmitate, a saturated fatty acid of 16 carbons (C16:0), frequently to conserved cysteine residues at the last transmembrane domain (helix 8) of the receptor [73, 74]. GPCR mono-, bis- and even tris-palmitoylation has been described in several receptors such as rhodopsin [75] or β_2-adrenergic receptors [76] and, interestingly, in other GPCRs such as the TPα-isoform of the human thromboxane A_2 receptor [77] or the gonadotropin-releasing hormone receptor type 1 [78], no palmitoylation site exists. This particular lipid–protein interaction has been suggested to modulate two relevant biological events of GPCRs, namely the localization of GPCRs into lipid rafts [79, 80, 50] and the dimerization of these receptors [81], although many aspects of both issues still remain unknown.

One particular fatty acid draws, to a greater extent, the attention of scientists due to the essential role it plays on biological membranes: the docosahexaenoic acid (DHA), an omega-3 polyunsaturated fatty acid (PUFA) of 22 carbons and 6 double bonds (22:6n3). The large amount of DHA found in membranes of rod outer segments [82] and neuronal cells [83, 84] seems to provide these membranes with particular biophysical proper-

ties [85] such as increased fluidity [86, 87]. Growing evidence that DHA-rich phospholipids have a special affinity for GPCRs [88] has led scientists to focus on the interaction between DHA and rhodopsin, an archetypal GPCR present in rod outer segments. Over the last few years, various studies have demonstrated the preference of DHA to solvate rhodopsin [89, 60] and the impact of this interaction on the optimization of rhodopsin function [90, 91]. In this context, in vitro experiments have correlated the presence of DHA with with high conformational stability of the protein [92, 93] or the enhancement of the visual signaling pathway [94, 95]. Conversely, reduced rhodopsin activation is observed in response to DHA deficiency [96].

While the aforementioned correlations between rhodopsin and DHA somehow justify the high levels of DHA-rich lipids found in the retina [97], little is known about the interaction between DHA and GPCRs in the brain. In this line, certain studies [98, 99, 100] envisage a similar modulation of other GPCRs by DHA in neuronal membranes, another specialized signaling platform. Moreover, several studies have found substantially low levels of DHA in the brain of subjects suffering from different brain disorders including schizophrenia [101, 102], major depressive disorder [103], bipolar disorder [104], Alzheimer [56] and Parkinson's disease [55]. The special properties of this fatty acid along with its potential effects against neurodegeneration [105, 106] have made DHA a promising candidate against brain aging and certain neurodegenerative disorders [107, 108, 109]. Therefore, in this thesis we have focused on the relationship between DHA and GPCRs, in particular, on the modulation of GPCR organization by this fatty acid.

1.1.4 GPCR dimerization

Recent evidence that GPCR dimers or higher-order oligomers function as dimers or higher-order oligomers add an extra level of complexity to the overall picture of lipid-protein interactions. While some studies show that individual monomers of certain GPCRs are able to respond to ligand binding and activate signaling pathways [110, 111], different ex-

perimental methods have already proven the existence of GPCR-GPCR complexes [112] in living cells. Since the first report of GPCR cross-talk [113], several GPCRs have been reported to dimer- or oligomerize [114, 115, 116, 117]. Moreover, GPCR-GPCR interactions display a very different level of stability, thus, while some dimers have been shown to form only transient complexes [118, 119], certain GPCR complexes exhibit a strong and stable nature [120]. Even after the release of the first crystal structure of a GPCR oligomer[121], the homomeric β_1-adrenergic receptors in their ligand-free state, the exact molecular mechanism, dynamics and biological relevance of the GPCR phenomenon is still unresolved.

GPCR dimerization can have an impact on receptor trafficking and delivery process of these proteins to the cell membrane. The formation of GPCR dimers can up- or down regulate the membrane level of other GPCRs by enhancing their delivery to the cell surface or by regulating their internalization (i.e. endocytosis) [122, 123]. Thus, the co-expression of γ-aminobutyric acid (GABA) R_1 and R_2 receptors has shown to cause a very important enhancement of GABA R_1 receptors [123]. Likewise, certain adrenoceptor subtypes form GPCR oligomers able to modulate the delivery of the αD - adrenoceptor to the membrane [123]. This type of modulation of receptor trafficking is inspiring the development of the so-called pharmacological chaperones, which aim to change the surface expression of specific GPCRs by targeting GPCR dimerization.

In addition, GPCR dimerization is known to impact a variety of cell events by altering ligand binding and the signaling properties of these receptors. Thus, the co-expression of two specific GPCRs can modulate ligand affinity and generate a pharmacological fingerprint attributable to GPCR dimerization [124]. For example, the pharmacology of certain opioid receptors can be altered by targeting dimer complexes such as μ- and δ-opioid heterodimers. In fact, targeting this specific dimer with antagonists of the δ-opioid receptor has been shown to enhance the binding of μ-opioid receptor agonists [125], an approach that has been used to improve the properties of current opioid agonists such as morphine. In addition to ligand binding, GPCR dimerization can alter the

signaling properties of the receptors involved in the protein-protein complex. For example, the selective co-expression of dopamine D_1, D_2, and D_3 receptors in specific areas of the brain differentially modulates the signaling of these receptors via receptor dimerization. Thus, while D_1 and D_2 receptors stimulate and inhibit, respectively, the adenylate cyclase pathway, D_1–D_2 heteromers can activate a different signaling pathway, namely the phospholipase C pathway [126]. Similarly, the co-expression of D_1 and D_3 receptors enhances the signaling properties of the D_1 receptor [127]. But one of the most relevant examples of GPCR dimerization is the adenosine A_{2A} - dopamine D_2 heteromer [128], thought to be involved in certain neuropsychiatric-related conditions including schizophrenia or Parkinson's disease [129]. Since various A_{2A} antagonists have proved able to change the affinity of D_2 agonists in cells, this heteromer is the target of different clinical studies for developing new Parkinson's disease treatments [130].

Therefore, the presence of two particular GPCRs in plasma membranes is clearly able to yield different signals when compared to the monomeric signal of each individual protomer. Whether this functional crosstalk is based on a physical interaction (e.g. conformational changes exerted by protein-protein interactions) is today still widely controversial topic [131, 129]. Since defining the functional relevance of this interaction is a challenging task, the International Union of Basic and Clinical Pharmacology published in 2007 a series of advices for the definition of GPCR complexes [132]. In order to be considered as GPCR heteromers, such complexes need to meet at least two out of the three requirements thereby specified. First, a physical association must be demonstrated by reporting the presence of both subunits in the same cell and documented in native tissue (e.g. coimmunoprecipitation). Second, the complex needs to be linked to, at least, one functional property such as modulation of ligand binding or activation of a specific transduction cascade [132]. Third, the absence of the heteromeric activity is demonstrated by using knockout animals or RNAi technology.

All in all, we are aware of the relevant role played by membrane lipids, GPCRs and GPCR oligomers. We also know that structural ele-

ments of membranes can modulate the activity of GPCRs and that some of them, like the omega-3 PUFAs, have shown to establish a very intense relationship with these receptors. However, only a handful of studies [133, 134, 135, 136] have been devoted to answer this question: do membrane lipids drive or modulate the organization of GPCRs? In this thesis, we partly try to address this question by computational approaches, in particular, all-atom and coarse-grained molecular dynamics (MD) simulations.

1.2 Molecular dynamics (MD) simulations

Modeling biological molecules by molecular dynamics (MD) simulations have yielded deep insights into molecular mechanisms otherwise not approachable by experimental techniques [137, 138]. Classical MD simulations consists on iteratively solving the classical equations of motion on a group of particles (atoms) interacting by a simple harmonic force. In this simplified model, the potential energy of the system is a function of the position of the atoms (coordinates) mathematically expressed by means of a 'force field'. The real experimental parameters behind each force field are built on either quantum mechanics calculations or by fitting different pieces of experimental data. The current principle of molecular mechanics assumes that potentials are additive so that the effective energy can be described as a sum of potentials of the intra- and intermolecular interactions in the system. Despite several force fields of varying levels of complexity exist, the definition of the potential energy in standard force fields generally contains the following terms:

$$U = \overbrace{\sum_{bonds} k_b(r - r_0)^2 + \sum_{angles} k_a(\theta - \theta_0)^2}^{\text{Bonded}} \tag{1.1}$$

$$+ \overbrace{\sum_{dihedrals} k_\phi(1 + \cos(n\phi - \phi_0)) + \sum_{impropers} k_\psi(\psi - \psi_0)^2}^{\text{Bonded}}$$

$$\underbrace{+\sum_{LJ} 4\epsilon_{ij}\left[\left(\frac{\sigma_{ij}}{r_{ij}}\right)^{12}-\left(\frac{\sigma_{ij}}{r_{ij}}\right)^{6}\right]+\sum_{elec}\frac{q_i q_j}{\epsilon_D r_{ij}}}_{\text{Non-bonded}}$$

where the 'bonded' term describes the energy contribution to the potential energy of intramolecular interactions (i.e. bond stretching, angle bending, dihedral and improper torsions) and the 'non-bonded' term represents the contribution from van der Waals and electrostatics forces.

Force fields of two levels of description are commonly used in the molecular modeling of biological systems: all-atom, where each particle represents one atom, and coarse-grained (CG), where groups of atoms are mapped into beads to reduce the level of description hence speeding up the calculations. Force fields widely extended in all-atom simulations are CHARMM [139], [140], GROMOS [141] and OPLS [142]. Similarly, the MARTINI force field [143] is one of the most widely used force fields in CG simulations of biomolecules. These force fields can be used by a vast number of MD engines developed to automate and maximize the numerical solving of the equations of motion by sampling algorithms. Some MD engines including GROMACS [144], NAMD [145], ACEMD [146] or CHARMM [147] are popular in the field of biomolecular simulations.

One of the limitations of MD simulations has always been the computational resources needed to reach long timescales or to simulate large systems. Fortunately, many efforts have been made in recent years to accelerate and parallelize MD simulations[148, 146] reaching timescales previously beyond the computational capacity of computational scientists. Thus, a significant part of the computational work performed during this thesis has exploited the use of MD and high-throughput MD to model cell membranes, GPCR monomers and GPCR oligomers.

1.3 Modeling membranes and GPCRs

1.3.1 Simulating lipid bilayers

Experimental model membranes are useful tools to study lipid mixtures; however, these models are not able to reproduce the high complexity of native-like biological membranes in terms of their lipid composition. As a result, these models normally contain either pure components or a mixture of two to three components [38, 149]. Computer simulations have emerged as a complementary tool to study biological membranes [150] with the potential to model lipid mixtures of higher complexity [151, 152]. Simulation techniques such as Monte Carlo [153, 154] and MD [151] have proven useful to analyze, at a molecular level, the biophysical properties of lipid bilayers. However, it is worth noting that MD simulations also have important limitations due to the long timescales needed to explore all possible states. As stated by Tieleman [155]: 'sampling is often by far the greatest source of errors in MD simulations of lipids and typically much more limiting than relatively modest differences caused by force field choice or choice of simulation algorithms'.

Pressure and temperature are frequently kept constant in MD simulations by the so-called barostats [156, 157, 158, 159] and thermostats [160, 161], respectively. In membrane simulations, due to the presence of the water-membrane interface and the importance of the fluctuations of the area per lipid, pressure control offers more complications than temperature control. The tensionless ensemble or NPT - constant number of particles (N), pressure (P), and temperature (T) - is the method of choice when simulating lipid bilayers [155]. Whereas constant pressure allows an adequate study of structural parameters such as the thickness of the bilayer or its condensation state, the choice of the temperature is also an important factor in membrane simulations. For instance, the interplay between chain-melting transition temperatures (Tm) of lipids will determine the phase behavior of the simulated mixture [162], hence, impacting how long we need to simulate to reach a converged system.

The polar extracellular environment of cells is mimicked in MD sim-

ulations by ions and water molecules. The amount of water confers a specific level of hydration to lipid bilayers, a parameter frequently overlooked when preparing lipid bilayers for simulation. However, water has showed a particular role near hydrophobic surfaces like membrane interfaces [163, 164, 165]. Updates of common force fields are taking this factor into consideration towards a realistic modeling of phospholipids hydration [166]. Different values of membrane hydration are available for phospholipid bilayers, often from PD bilayers [167, 168], where a common experimental parameter to reflect hydration is the number of water molecules per phospholipid. Some of these experiments [169, 170] estimate that in biological membrane each phospholipid tend to be solvated between approximately 20 and 32.5 water molecules. Therefore, 30 water molecules per phospholipid is generally a good approximation for the hydration level when simulating lipid bilayers.

Constructing lipid bilayers for MD simulations is nowadays straightforward thanks to software such as VMD (Visual Molecular Dynamics) [171], a modeling/visualization package commonly used in molecular dynamics simulations. VMD can be used to build lipid bilayers through the 'membrane builder' plugin (http://ks.uiuc.edu/Research/vmd/plugins/membrane/). This tool is yet limited to pure (one-component) mixtures and the use of only a few lipid species of the CHARMM force field repertoire. This limitation has been overcome by a web-based graphical interface of CHARMM: the CHARMM-GUI membrane builder (http://charmm-gui.org), currently one of the most popular and useful tools to build lipid bilayers [172] and membrane-protein systems [173]. Based on the initial parameters specified by the user (e.g. membrane size or water layer thickness), this tool generates the components of the system such as lipids, bulk water, and ions to subsequently assemble them yielding a set of hydrated structures of lipid bilayers ready for an ulterior equilibration phase. Lipids from a structural library of membrane simulations are placed randomly by either a replacement or an insertion method, as indicated by the user. But one of the most interesting advantages of this method is the remarkable number of different lipid species provided (to date 100) which allows constructing highly heterogeneous lipid bilay-

ers even in terms of their leaflet asymmetry. Noteworthy, the area per lipid of each of these lipid types can be adjusted by the user or otherwise suggested by the tool based on experimental values.

Despite building multicomponent mixtures is today an easier task for computational scientists, it is important to remember that mixing is more difficult in highly complex bilayers. In order to favor somehow this mixing, some authors [174] employ, prior to the equilibration phase, classic protocols like the ones based on 'simulated annealing' algorithms. In these approaches, the system undergoes fast heating and cooling cycles to ensure an adequate thermalization of the hydrocarbon tails of phospholipids. This protocol can affect the structure of lipid molecules so it needs to be thoroughly validated prior to its use in production runs. Nevertheless, techniques where high temperature is applied during short periods of time can only help overcoming high energy barriers rather than significantly increase the average lateral diffusion of lipids, which is the real key to an adequate mixing.

1.3.2 Analyzing simulations of lipid bilayers

Two main blocks of biophysical properties can be extracted from the simulated trajectories of lipid bilayers: structural and dynamic properties [175, 176, 177, 46, 178]. While membrane thickness, area per lipid and order parameters are frequently used to characterize membrane structure, dynamic properties are normally linked to the lateral diffusion of lipids. Several MD studies [44, 179, 180] show how varying the level of lipids like cholesterol can change the hydrophobic thickness of membranes, a parameter particularly important in the study of membrane microdomains [181, 182]. The thickness of the bilayer is a structural parameter usually defined by the distance between the phosphate groups of phoshpholipid (head groups) of each membrane leaflet. This value is also known as 'phosphate-to-phosphate' or 'peak-to-peak' distance, the latter in reference to the aspect of the so-called 'electron density profiles' used to interpret thickness and other structural features of membranes (Figure: 1.4).

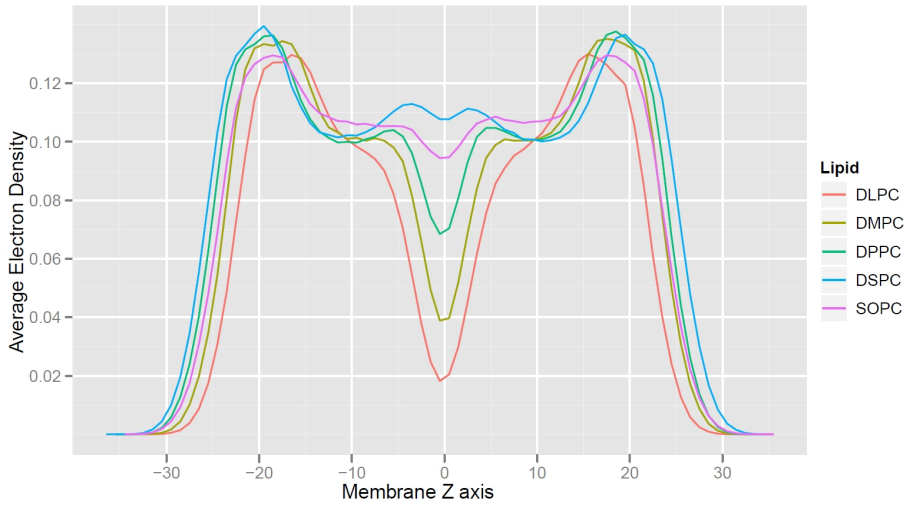

Figure 1.4: **Membrane thickness measured from MD simulations.** Average electron density profiles calculated from the simulated trajectory of 5 membranes of different lipid composition. Abbreviations: DLPC, 1,2-dilauroyl-phosphocholine (diC12:0); DMPC, 1,2-dimyristoyl-phosphocholine (diC14:0); DPPC, 1,2-dipalmitoyl-phosphocholine (diC16:0); DSPC, 1,2-distearoyl phosphocholine (diC18:0); POPC, 1-palmitoyl-2-oleoyl phosphocholine (C16:0-C18:1); SOPC, 1-stearoyl-2- oleoyl phosphocholine (C18:0-C18:1). Figure reprinted with permission from Guixà-González et al. [183]

These profiles give somehow an averaged cross-sectional view of the electron density across the membrane so that the center of the bilayer is located at 0 Å thickness and the maximum distance between peaks is typically around 15–25 Å from the center of the bilayer (Figure: 1.4). The extent of the interaction between the hydrocarbon tails of the phospholipids or 'membrane interdigitation' can be assessed by inspecting the density of lipid tails near the center of the bilayer. For instance, longer and more saturated tails tend to interdigitate more than shorter and unsaturated ones, as shown in Figure: 1.4. Probably due to the controversy around the biological significance of membrane interdigitation, this parameter is not frequently studied in the analysis of MD simulations of lipid bilayers [44, 184, 185].

The inner structure of a lipid bilayer is ultimately defined by the spatial conformation that lipids adopt based on the biophysical properties of the mixture. This characterization can be partly approached by measuring the area per lipid occupied by individual lipid species during the simulation. Calculating the area per lipid is straightforward in simple lipid mixtures (1 or 2 components):

$$A = \frac{xy}{n} \tag{1.2}$$

where xy is the area of the simulation box and n the number of lipid molecules. This calculation is, however, much more complicated for multicomponent membranes[181, 179] or membrane-protein systems [186]. One interesting approximation to calculate the area per lipid of highly heterogeneous mixtures consists of projecting one representative atom of each lipid molecule into a plane and then dividing the space occupied by each individual lipid through a Voronoi tesselation algorithm. In the Voronoi diagrams created by this approach, the area of each of the polygons created corresponds to the area of each lipid molecule.

$$A_{polygon} = \left\langle \frac{1}{2} \sum_{i=0}^{N-1} (x_i + y_{i+1} - y_i + x_{i+1}) \right\rangle \tag{1.3}$$

where N is the number of vertices of the polygon and x_i, y_i the coordinates of each of these vertices in the projected plane. Since groups of lipids can be averaged separately, one can obtain the average area per lipid of each one of the lipid species present in the membrane (Figure: 1.5). Unfortunately, the area per lipid of multicomponent mixtures cannot be measured experimentally and, therefore, the computational data obtained following this method cannot be compared to experiments and should be interpreted with caution.

Thicker membranes are normally more condensed and hence lipids tend to display lower areas per lipid, however, these parameters do not provide direct information on the fine structure of the hydrophobic region (e.g. membrane fluidity). The order of lipid tails or chain structure is is quantified in NMR experiments, among other measurements, by the

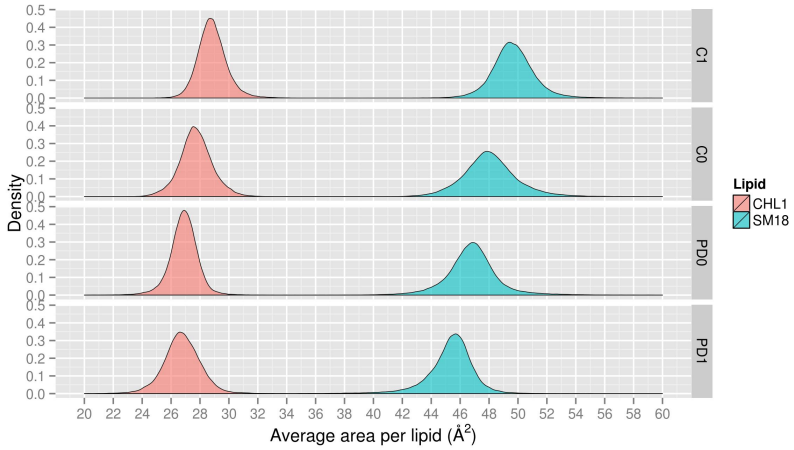

Figure 1.5: **Area per lipid of cholesterol and sphingomyelin in four lipid bilayers.** Probability distributions of the area per lipid of cholesterol (CHL1) and sphingomyelin (SM18) averaged across 500 ns of a simulation of four lipid bilayers with varying degrees of saturation, from more to less unsaturated systems: C1 $>$ C0 $>$ PD0 $>$ PD1.

deuterium order parameters (S_{CD}) [187]. S_{CD} uses the local orientation of phospholipid C–H bonds to give a direct quantification of the disorder of the membrane.

$$S_{CD} = \left| \left\langle \frac{3\cos^2\theta - 1}{2} \right\rangle \right| \tag{1.4}$$

The computational approximation to this calculation is to compute θ, which is the average angle formed between each C–H bond of lipid tails and the normal of the bilayer. S_{CD} results obtained by computational methods are frequently in agreement with experimental values and can be used to explore the impact of membrane composition or other factors on the order of the membrane [188]. The well-known condensing effect of cholesterol [20, 189, 190] can be monitored in computer simulations by measuring its impact on membrane order [191, 192]. Similarly, highly saturated environments yield higher S_{CD} values, which indicates that the hydrophobic core of the lipid bilayer has a lower fluidity (Figure: 1.6).

Membrane order directly affects the level of packing of lipid compo-

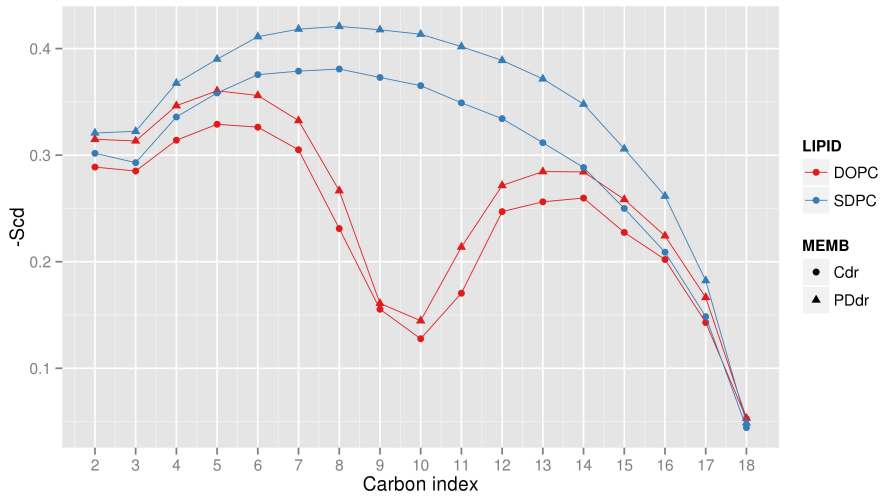

Figure 1.6: **Membrane fluidity between different lipid bilayers.** Order parameters (S_{CD}) of the *sn*-1 chains of DOPC and SDPC compared between two multicomponent membranes with varying levels of chain unsaturation, from more to less unsaturated: Cdr $>$ PDdr. The only double bond present in these analysis is clearly visible by the significant decrease in order at carbon C10 of the *sn*-1 chain of DOPC (18:1). Abbreviations: DOPC, 1,2-dioleyl-sn-glycero-3-phosphocholine; SDPC, 1-stearoyl-2-docosahexaenoyl-sn-glycero-3-phosphocholine.

nents including cholesterol and, therefore, parameters like cholesterol tilt angle can be analyzed to check the packing state of the bilayer [191]. As shown in (Figure: 1.7), more saturated membranes reduce the fluctuations of cholesterol tilt angle due to a higher packing within the hydrophobic core of the membrane.

Data from thickness, area per lipid, order or tilting angles provide an averaged structural view of the simulated system that is rather static. Studying the distribution of molecules or particular atoms around a reference component can give more insights on the organization and dynamic events occurring during the simulation. The so-called radial distribution function (RDF), also known as pair correlation function, is an statistical mechanics concept that can be used in the analysis of membrane simulations to describe the density of certain lipids around another lipid compo-

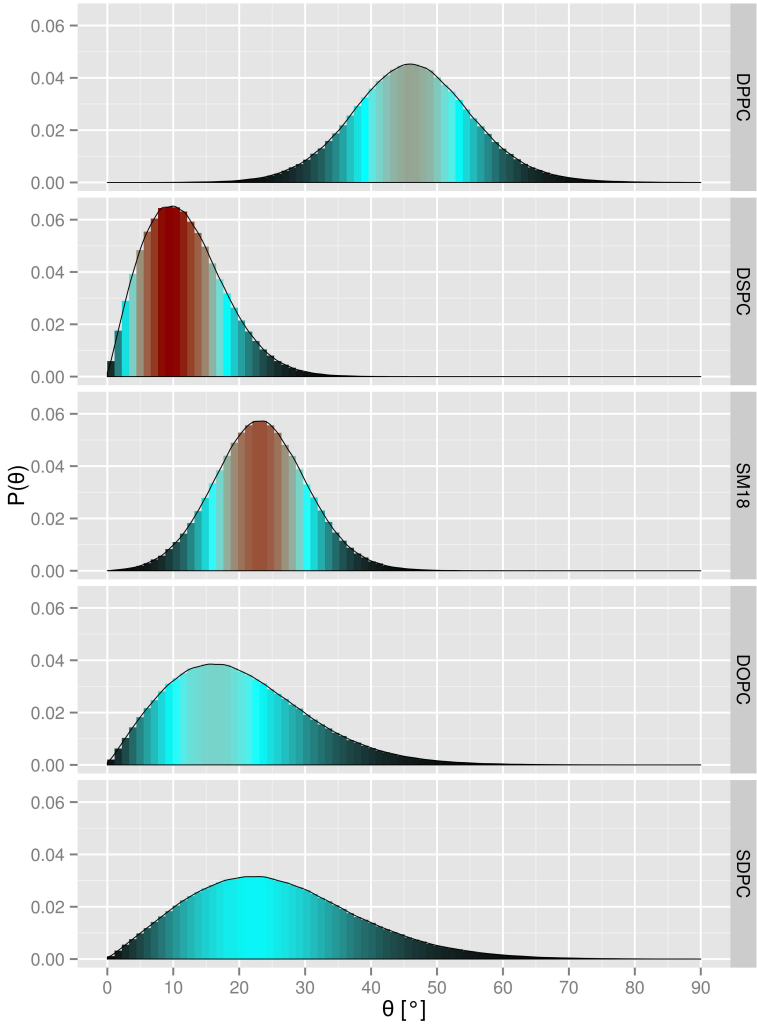

Figure 1.7: **Cholesterol tilt angle distribution in different membrane environment.** The tilt angle of cholesterol (θ) measured in binary mixtures (two components) of one phospholipid (DPPC, DSPC, SM18, DOPC or SDPC) plus a fixed amount of cholesterol. Abbreviations: DPPC, 1,2-dipalmitoyl-sn-glycero-3-phosphocholine; DSPC, 1,2-distearoyl-sn-glycero-3-phosphocholine; DOPC, 1,2-dioleyl-sn-glycero-3-phosphocholine; SM18, sphingomyelin; SDPC, 1-stearoyl-2-docosahexaenoyl-sn-glycero-3-phosphocholine.

nent as a function of the distance [193]. Among many other applications, this parameter is very useful to describe the spatial order of the membrane by inspecting the coordination shell formed by certain membrane lipids [194]. The radial distribution function describes the probability of finding one particle at a certain distance of the other and can be defined as

$$g(r) = \frac{N(r)}{4\pi r^2 \rho \delta r} \tag{1.5}$$

where $g(r)$ is the RDF, $N(r)$ is the number of atoms in the shell between r and $r + \delta r$ around the reference atoms, and ρ is the number density expressed as the ratio of the number of atoms to the volume of the simulation box [195]. This analysis yields information on the radial symmetry of the system in just one dimension, namely distance. However, the interaction of certain lipids with the rest of the membrane environment does not occur in a symmetric fashion. In fact, two different faces exist in the sterol ring of cholesterol molecules, known as α-(or 'smooth') face and β-(or 'rough') based on the absence or presence, respectively, of two off-plane methyl groups. This subtle difference seems to be behind relevant biological functions of cholesterol and drive the interaction pattern of this molecule with other lipid components[196]. Therefore, in asymmetric molecules like cholesterol, information on the angular symmetry of the interaction between lipid molecules can lead to interesting insights. Some authors have enriched the classical RDF approach by calculating bivariate [195, 197] or trivariate [198] forms of the radial distribution function where both the orientation and the position of cholesterol and lipid tails is taken into account. Figure: 1.8 shows an unpublished example of bivariate RDF calculations using two different membrane systems. This figure shows how, after 100 ns, cholesterol-cholesterol interactions seem to be more favored at cholesterol's β-face in more saturated environments.

Finally, simulations of lipid bilayers can provide data on the dynamic properties of the system and hence give a minimal mechanistic explanation to static structural properties. Lipid lateral diffusion describes the ability of lipid components to move across the membrane characteriz-

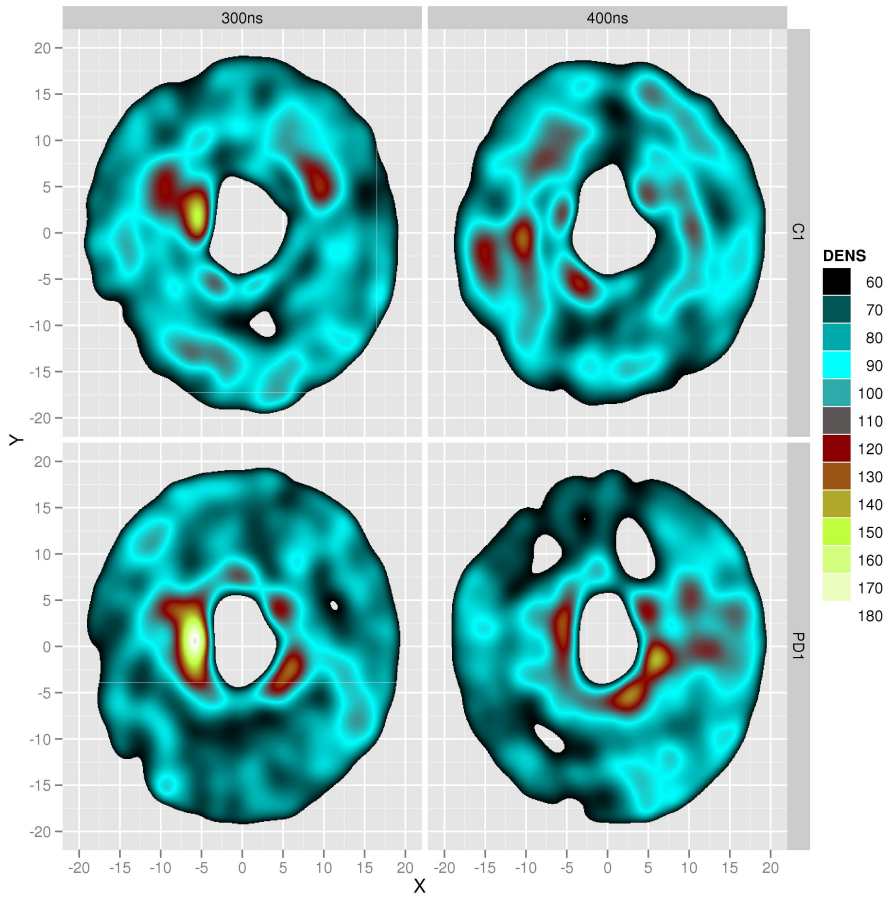

Figure 1.8: **Two-dimensional radial distribution plots of cholesterol.** Average two-dimensional density distributions of cholesterol molecules around cholesterol after 300 and 400 ns simulations of two multicomponent membranes: C1 (less saturated) and PD1 (more saturated). Reference cholesterol molecules are displayed aligned to the center of the plot (shown by a lack of density in this area). Thus, the β-face of cholesterol (rough face) extends towards the positive x axis whereas the α-face (smooth face) extends towards the negative x axis. Color gradient represent the density of cholesterol around reference cholesterol molecules: from black (low density) to white (high density). Cholesterol densities below 60 are not plotted for clarity.

ing, indirectly, the biophysical feature of simple and complex membranes. As discussed above, membrane heterogeneity highly influences the order and packing properties of biological membranes. As a result, estimating the real lateral diffusion of membranes is a matter of intense study and, particularly, in connection to phase separation processes and formation of highly ordered raft-like mixtures [199, 200, 201, 202]. However, in contrast to the structural features of membranes, there is a limited understanding of dynamic processes such as the simple lateral diffusion of lipids [203] or the interplay between the diffusion of lipids and transmembrane proteins [204, 205]. Due to the tight dependence between lipid diffusion and the time scale at which it is observed, dynamic properties of lipid bilayers need to be assessed with real caution.

1.3.3 Simulating GPCR–membrane systems

The success on modeling GPCR–membrane systems significantly relies on an adequate initial structure. Despite the number of GPCR crystal structures and other transmembrane proteins resolved to date is far behind that of soluble proteins, the recent resolution of several new structures (Table: 1.1) has opened the door for MD simulations to contribute to the understanding of GPCR function and dynamics. The high number of available crystal structures has increased the quality of the predicted homology models, where the choice of a template structure is essential. If no crystal structure is available, homology models of the GPCR under study can be built [206, 207] even through web-based automated servers [208]. Like any other protein, modeling a GPCR involves retrieving its protein sequence, performing and refining a sequence alignment against GPCR homologs and calculating a 3D structure using, for instance, protein structure modeling software such as MODELLER [209, 210]. Key manual refinements to complement this modeling includes assigning constraints for geometric optimization of the structure (e.g. highly conserved disulfide bridges), setting the right protonation states of titratable residues or assuring a stereochemically relevant distribution of the backbone dihedral angles (i.e. Ψ and Φ) in the protein structure.

Different protocols have been proposed to easily embed the input structure of a protein into an equilibrated lipid bilayer. One approach is to simply remove a certain amount of lipids and solvent to create a hole where the protein can be placed. This protocol, however, highly depends on the geometry of the protein, alters lipid composition in case of complex mixtures and requires more and longer equilibration steps to obtain an adequate protein-lipid packing. A second popular approach is to make room to the protein by 'inflating' the bilayer, inserting the protein and finally 'deflating' and minimizing the structure to avoid clashes [211]. In addition, a simple and efficient tool of the GROMACS package called 'g_membed' allows to embed proteins by optimally accommodating the protein into the membrane [212]. Lastly, some interesting protocols where lipids diffuse and surround proteins without altering any structure are becoming widely used, mostly in CG simulations [213, 214]. In addition to manual approaches, as mentioned above, the CHARMM-GUI membrane builder (http://charmm-gui.org) is one of the best current tools to automate the process of constructing membrane–protein systems [173].

Several MD simulations have already studied biologically relevant aspects of GPCR biology and provided interesting insights on ligand binding [215, 216, 217], allosteric modulation [218] or GPCR activation [219, 220, 221]. GPCR activation has been traditionally described by conformational changes within the GPCR structure, mainly at the level of the so-called 'ionic lock' but also by assessing more subtle differences such as the concerted motions or formation/rupture of certain networks of residues or 'microswitches'. Partly thanks to larger multiprocessor clusters and specialized high-throughput computer architectures, current MD codes have tremendously increased their performance in MD simulations of GPCRs [219, 221, 222]. However, not even state of the art simulations of GPCRs are exempt of criticism due to the lack of adequate statistical sampling, the main bottleneck in this field [223, 224]. Thus, certain computationally cheaper approaches like elastic network models [225] are currently one interesting option to consider when trying to avoid the convergence issue in GPCR simulations. On the other hand, addressing certain features of GPCR dynamics by GPCR–membrane simulations

clearly requires either reduction in the complexity and/or size of the systems or the enhancement of classical MD methods. CG force fields and/or biased MD techniques have recently been used to better explore the energetic landscape of GPCRs simulated in membranes [226, 227, 228].

In addition, due to the importance of modeling the membrane environment and the influence of membrane biophysics on the function of GPCRs, MD simulations have been recently used to characterize the interplay between membrane deformation/remodeling and the activation and/or organization of GPCRs [229, 230, 231, 134].

1.3.4 CG-MD simulations of GPCR dimers and oligomers

Modeling GPCR dimer- and/or oligomerization is nowadays a challenging task not only due to the large number of particles required but also to the complexity and stochasticity of this reaction. In terms of timescales, most CG approximations outperform any atomistic approach and, therefore, many of the current simulations that aim to model GPCR dimer- and/or oligomerization dynamics use CG-MD. CG models enable the simulation of big systems during long scales (μs to ms regimes), the parallelization of multiple systems for systematic approaches or simply an inexpensive platform for generic studies [232]. MARTINI [143, 233] is a widely used CG model amenable to the GROMACS suite that has proven useful to model membrane–protein systems [234, 235], protein aggregation [236, 204, 237] and, in particular, the formation of GPCR dimers and oligomers [238]. The MARTINI–GROMACS partnership offers a flexible way to build, simulate and analyze large, long and complex simulations of GPCR complexes, which are able to freely diffuse across the membrane and transiently or stably interact with other GPCRs (see Figure: 1.9).

Protein monomers are mapped into CG model either from a crystal structure or from a homology model. One of the useful modeling tools made available by the MARTINI team, namely the 'martinize.py' script allows converting atomistic structures into CG models, generating MARTINI protein input files and fine-tuning important modeling aspects like

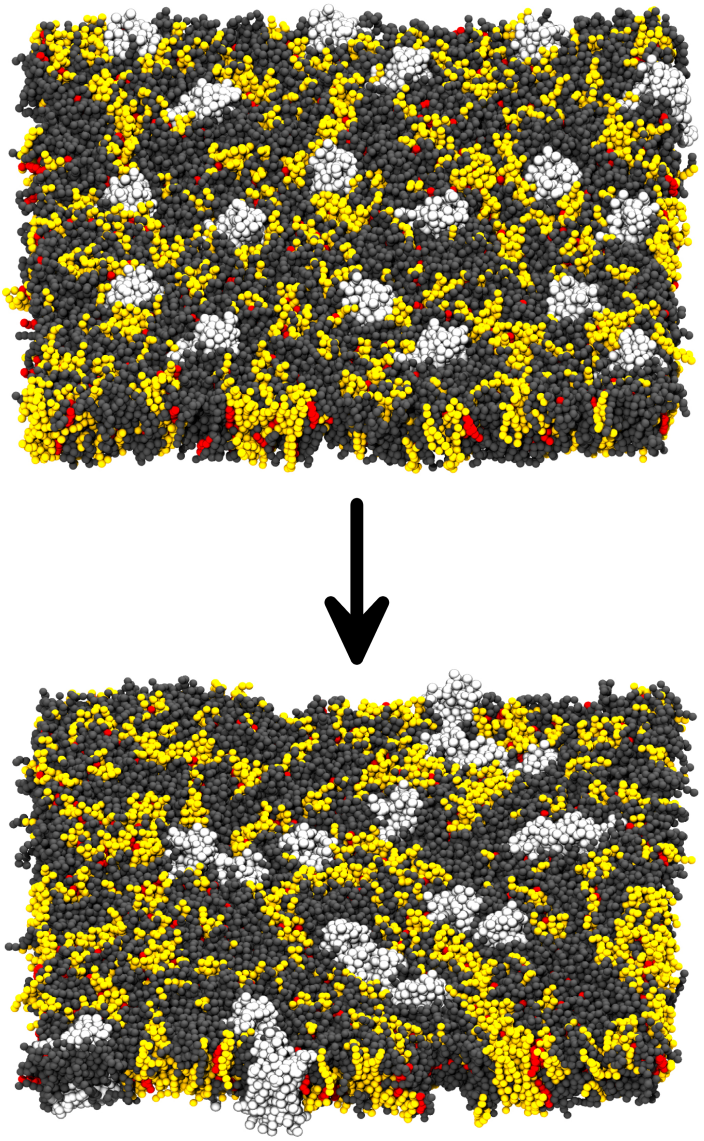

Figure 1.9: **CG-MD simulation of GPCRs self-assembly using MARTINI force field.** 18 GPCR monomers embedded into a multicomponent bilayer (upper) and simulated during 10 μs (bottom). Protein monomers are depicted in white. Grey, yellow and red spheres correspond to a van der Waals representation of polyunsaturated phospholipids, monounsaturated phospholipids and cholesterol, respectively. Solvent particles are not shown for clarity.

secondary structure, disulfide bridges or positional restraints. In addition, this tool allows setting up an elastic network to improve the stability of the protein structure during the simulation. Periole et al. successfully tested the MARTINI force field in combination with an elastic network model by a simple approach the authors called ElNeDyn [239], where certain backbone beads are connected to one another with springs within a predefined distance. Thus, the rigidity and the extent of the network is defined by two parameters, namely the force constant and the cutoff distance, respectively. The ElNeDyn approach has proven useful to quantitatively mimic protein atomistic models in terms of protein deformations, fluctuations of residues and large-amplitude collective motions. An optimal implementation of this model consists of setting up the features of the network by using data on previous atomistic simulations of the same protein. CG-MD simulations of GPCRs have already benefited from the use of the ElNeDyn protocol to study GPCR dimers [240, 241] and oligomers [238]. Since the secondary structure is predefined and restrained by the elastic network, the main drawback of these CG-MD protocols when applied to receptor-receptor interactions lays on the inability of the model to account for any change/transition/folding event in the secondary structure.

Periole et al. [242] first used MARTINI to show that GPCRs self-aggregate in model membranes. In this study, the authors describe the effect of membrane local deformations on the oligomerization of rhodopsin. Using a similar protocol, Mondal et al. [135] approached this issue by studying the energetic cost associated to the protein–membrane hydrophobic mismatch during the oligomerization of adrenergic receptors. Recently, Periole et al. [238] deeply analyzed the self-assembly process of rhodopsin by an impressive set of simulations including 10 parallel simulations of 16 receptors simulated during 5 μs plus a bigger system comprised of 64 receptors simulated for 25 μs. In addition, they performed umbrella sampling simulations to determine the most favored dimer interface by calculating the potential of mean force for the most frequent dimer poses found during the simulation. This combined approach, with approximately 300 μs accumulated, was used to characterize the energetic landscape of rhodopsin's dimer interface and provided new biophysical

insights into this complex.

Moreover, MARTINI and CG-MD simulations have been used in conjunction with biased MD techniques to characterize the dimerization interface of GPCR dimers. The combination of both techniques allows a quantitative and qualitative study of the strength of association and the relative stability between different dimerization interfaces of certain GPCRs. While Provasi et al. studied the lifetime of the δ-opioid receptor dimer by estimating dimer association constants combining CG and umbrella sampling simulations [240], Johnston et al. later characterized the interface of this dimer by CG and metadynamics simulations [241]. In a second study [243], Johnston et al. compared the relative stability of the β_1-and β_2- adrenergic receptor homodimers by a similar approach combining both atomistic, CG metadynamics and CG umbrella sampling simulations. Similarly, these authors recently combined again CG and biased MD techniques to compare the stability of the crystallographic interface of μ-and κ-opioid receptor dimers [244] in a first attempt to rank order viable crystal structures in terms of their energy of association.

To date, there is, however, a clear lack of data regarding the effect of membrane lipids on the GPCR dimer- and/or oligomerization phenomenon.

Chapter 2

OBJECTIVES

2.1 Implementing a computational framework to simulate and analyze highly complex membranes by all-atom and coarse-grained molecular dynamics (MD) simulations

To develop an implement an overall methodology to build, simulate and analyze complex biological membranes in the context of lipid–lipid, lipid–GPCR and GPCR–GPCR interactions. The focus of this objective will lie on the analysis of local properties (e.g. thickness, fluidity, area per lipid, etc.) of membranes and membrane–GPCR simulations.

2.2 Development of a tool that automates the computation of local properties in membranes and membrane–protein simulations

To develop an automated and user-friendly Graphical User Interface (GUI) for the analysis of membrane and membrane–protein simulations in VMD. This tool should offer a full set of computational analyses for a biophys-

ical characterization of these systems by implementing the knowledge built in Objective 2.1.

2.3 Assesing DHA-mediated effects on A_{2A} – dopamine D_2 heteromerization by coarse-grained MD simulations

To study the effect of long-chain omega-3 polyunsaturated fatty acids on the oligomerization of GPCRs in the context of brain disease. As a case study, we aim to shed light on the modulation of A_{2A} – dopamine D_2 heteromerization by DHA-lipids, since both players have a particular relevance for major neuropsychiatric disorders.

Chapter 3

PUBLICATIONS

3.1 Crosstalk within GPCR heteromers in schizophrenia and Parkinson's disease: physical or just functional?

Guixà-González R., Bruno A., Marti-Solano M. and Selent J. *Curr. Med. Chem.*, **19**, 1119–1134 (2012).

Summary
As described in the Introduction section, functional interactions between heteromeric complexes of GPCRs have been shown to modulate the pharmacological and signaling landscape of these receptors. In certain GPCR complexes (e.g. A_{2A} – dopamine D_2), GPCR crosstalk has a particular relevance in neuropsychiatric conditions like schizophrenia and Parkinson's disease. In this article we reviewed the state of the art of GPCR crosstalk for the most relevant heteromers in the context of the former diseases. Here we contrast the current knowledge on the functional aspects of GPCR crosstalk with the structural knowledge that potentially supports a physical interaction between GPCRs. Noteworthy, we profoundly reviewed the state of the art of the A_{2A} – dopamine D_2 complex, the GPCR heteromer we have used in this thesis as a model to study the interplay between membrane lipids and GPCRs.

Guixà-González R., Bruno A., Marti-Solano M. and Selent J.
Crosstalk within GPCR heteromers in schizophrenia and Parkinson's disease: physical or just functional?
Curr. Med. Chem., **19**, 1119–1134 (2012).

3.2 Molecular modeling and simulation of membrane lipid-mediated effects on GPCRs

Guixà-González R., Sadiq SK. K., Dainese E., Pastor M., De Fabritiis G. and Selent J. *Curr. Med. Chem.*, **20**, 22–38 (2013).

Summary
MD simulations, the main computational technique employed in this thesis, is a powerful molecular microscope to study biophysical events and a valuable tool to support experimental techniques. To simulate lipid–GPCR interactions one needs to deeply understand the advantages and pitfalls of modeling lipid bilayers and GPCR–membrane systems. In this paper we revised the current computational approaches to study specific and nonspecific lipid–protein interactions in simple and complex biological membranes. Additionally, we discuss the potential of MD simulations to study the lipid-mediated oligomerization of GPCRs. This publication was extremely helpful to build a solid knowledge base in membrane-based MD simulations.

Guixà-González R., Sadiq SK. K., Dainese E., Pastor M., De Fabritiis G. and Selent J.
Molecular modeling and simulation of membrane lipid-mediated effects on GPCRs
Curr. Med. Chem., **20**, 22–38 (2013).

3.3 Simulating G protein-coupled receptors in native-like membranes: from monomers to oligomers

Guixà-González R., Ramírez-Anguita J. M., Kazcor A. A. and Selent J. *Methods Cell Biol.*, **117**, 63–90 (2013).

Summary
MD simulations of GPCRs and, in particular, simulating GPCR oligomers require a broad expertise building, simulating and analyzing these proteins in their native-like environment. In this publication we cover the modeling process of constructing the lipid bilayer, embedding GPCRs and simulating the self-assembly of GPCR oligomers. In addition, we describe how to analyze these simulations and interpret interesting concepts for membrane–GPCR simulations such as the quantification of membrane remodeling and residual mismatch. With this publication, we managed to put together the basis of the methodology used so far to develop the main objectives of this thesis.

Guixà-González R., Ramírez-Anguita J. M., Kazcor A. A. and Selent J.
Simulating G protein-coupled receptors in native-like membranes: from monomers to oligomers
Methods Cell Biol., **117**, 63–90 (2013).

3.4 MEMBPLUGIN: studying membrane complexity in VMD

Guixà-González R., Rodriguez-Espigares I., Ramírez-Anguita J. M., Carrió-Gaspar P., Martinez-Seara M., Giorgino T. and Selent J. *Bioinformatics*, **30**, 1478–1480 (2014).

Summary
One milestone in this thesis was to develop a modeling tool devoted to the analysis of membrane and membrane–protein simulations and to automatize the biophysical characterization of these systems. In this publication, we present MEMBPLUGIN, a plugin for VMD, one of the most frequently used package in molecular modeling. We developed this tool to offer a wide range of standard structural analyses like membrane thickness, area per lipid or order parameters. Interestingly, MEMBPLUGIN provides a quick and automated way to compute 2D thickness maps and new algorithms for measuring membrane interdigitation. Thanks to this publication we made our expertise available to the scientific community and managed to build an user-friendly tool from a set of individual scripts otherwise hardly usable.

Guixà-González R., Rodriguez-Espigares I., Ramírez-Anguita J. M., Carrió-Gaspar P., Martinez-Seara M., Giorgino T. and Selent J.
MEMBPLUGIN: studying membrane complexity in VMD
Bioinformatics, **30**, 1478–1480 (2014).

MEMBPLUGIN's website.
Software, installation guide, tutorial and case study.

3.4.1 Supplementary: MEMBPLUGIN validation

MEMBPLUGIN: a case study using cholesterol-enriched membranes

Ramon Guixà-González[1], Ismael Rodriguez-Espigares[1] , Juan Manuel Ramírez-Anguita[1], Pau Carrió[1], Hector Martinez-Seara[3], Toni Giorgino[2] and Jana Selent[1]

[1] *Research Programme on Biomedical Informatics (GRIB), Barcelona, Spain;* [2] *Institute of Biomedical Engineering, National Research Council (ISIB-CNR), Padua, Italy;* [3] *Department of Physics, Tampere University of Technology, Tampere, Finland*

MEMBPLUGIN [1] is a versatile tool for the Visual Molecular Dynamics (VMD) package [2] to analyze the results of complex membrane simulations. The plugin can be used to characterize a wide range of biophysical properties of biomembranes such as membrane thickness, fluidity or condensation. In the present case study, we illustrate some of the features of the plugin by analyzing the effect of cholesterol enrichment on a series of lipid bilayers simulations.

Background

Cholesterol, a vital component of cells is know to regulate the biophysical properties of biological membranes. The presence of this sterol in phospholipid membranes has proven to increase membrane condensation [3, 4], ultimately impacting on the overall structure of the bilayer. Thus, cholesterol content can alter key biophysical properties of biological membranes such as thickness, fluidity or area per lipid. Relevant membrane microdomains such as the so-called lipid rafts [5] display a high amount of cholesterol when compared to other regions of the membrane. The study of lipid rafts by experimental means depends upon the development of complex technology due to the fluctuating and heterogeneous nature of these nanoscale assemblies [6]. On the other hand, molecular models can be used in an attempt to offer a molecular perspective (i.e. more detailed) of cholesterol-enriched membranes such as lipid rafts. Despite of the known limitations of current computational techniques, some studies using atomistic [7, 8] and coarse-grained [9] molecular dynamics have already shed some light on the molecular aspects of cholesterol-enriched domains. For this sample case study, we focused on the effect of cholesterol on certain biophysical properties of standard model lipid bilayers.

Methods

We simulated a set of 1-palmitoyl-2-oleyl-sn-glycero-3-phosphocholine (POPC) bilayers containing different amounts of cholesterol. Specifically, we built 4 different POPC:CHO systems, namely 1:0, 5:1, 2:1 and 1:1 (see Table 1). All membranes were built using the CHARMM-GUI membrane builder [10] (`http://www.charmm-gui.org/input/membrane`). Each output was re-hydrated using approximately 30 water molecules (TIP3 model) per lipid and neutralized with 150 mM NaCl. In addition, those lipid tails incorrectly trapped into the cholesterol ring were manually corrected. Subsequently, membranes were run in the NPT ensemble at 1.01325 bar and 310 K for 30 ns, using the ACEMD simulation package [11]. The CHARMM36 [12] force field was used in all simulations. We discarded the first 10 ns of each trajectory and used MEMBPLUGIN [1] to analyze the area per lipid, lipid S_{cd} order parameters, leaflet interdigitation and membrane thickness on the last 20 ns of each system. Usage instructions of each subtool can be found at `https://sourceforge.net/p/membplugin/wiki/Home/`. All figures were rendered using the ggplot2 R package [13] out of MEMBPLUGIN's output files.

	POPC:CHOL			
Component	**1:0**	**5:1**	**2:1**	**1:1**
POPC	106	120	104	86
CHOL	0	24	52	86
CHOL (%) (Aprox.)	0	~ 17	~ 33	50
Sodium	10	10	10	10
Chloride	10	10	10	10
Water	3793	4121	3954	3867

Table 1: **Lipid, water and ion composition of POPC:CHOL membranes.** POPC and CHOL stands for 1-palmitoyl-2-oleyl-sn-glycero-3-phosphocholine and cholesterol, respectively.

Results

Area per lipid

To illustrate the condensing effect of cholesterol on a lipid bilayer, we first measured the average area per lipid of each lipid bilayer using the area per lipid tool of MEMBPLUGIN. This tool calculates both the total area per lipid of the membrane and the area per lipid for each of the lipid species present at the membrane, i.e. POPC or CHOL in our particular case.

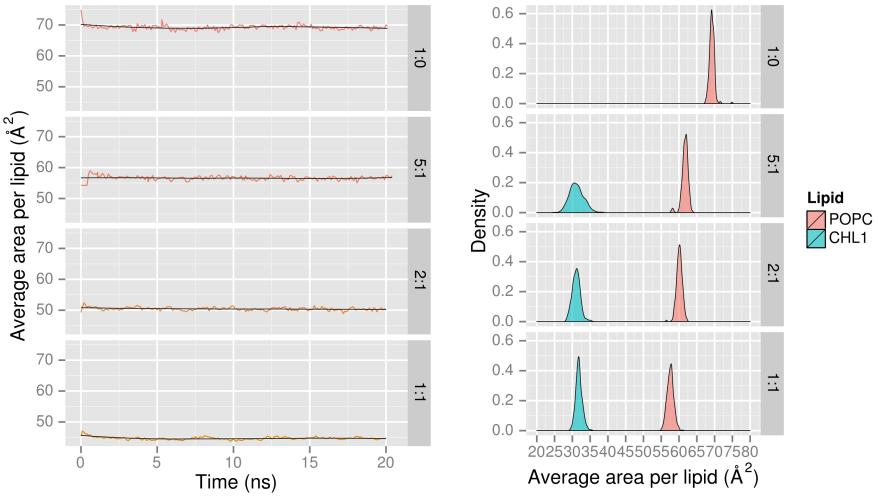

Figure 1: **Average area per lipid of each POPC:CHOL system during the last 20 ns.** The left plot display the total average area per lipid of the system (i.e. POPC plus cholesterol) (x axis, Å^2) over time (y axis, ns). Degraded orange solid lines represent actual values whereas mean values are represented by black solid lines. The average area per lipid of each lipid species during the simulation (Å^2, x axis) is represented by its probability density (arbitrary units, y axis). Color codes as in figure legend.

Apart from the typical equilibration ramp showed within the first 0-5 ns, our simulations do not show major fluctuations in the calculated area per lipid during the last 20 ns of each trajectory. In any case, it is worth to note that due to the short time scale used for this case study, we can not assume the

area per lipid to be in equilibrium. In agreement with experimental [14] and computational [12] estimates, the average area per lipid of POPC, as calculated for system 1:0 (i.e. pure POPC membrane), is 69.26 ± 0.75 Å^2 (see Figure 1). As depicted in Figure 1 left, the addition of cholesterol drops the total area per lipid of the system, in consonance with the known condensing effect of this molecule [3]. Increasing the level of cholesterol from 0% (i.e. system 1:0) to 17% (i.e. system 5:1), 33% (i.e. system 2:1, the approximate cholesterol level found in lipid rafts) and 50% (i.e. system 1:1) decrease the average area per lipid of POPC down to 61.69 ± 0.89 Å^2, 60.11 ± 0.81 Å^2 and 57.56 ± 0.93 Å^2, respectively (see Figure 1 right). As shown in Figure 2, while the condensing effect of cholesterol is most dramatic within 0-17% cholesterol, this effect is less pronounced at higher molar cholesterol concentrations (i.e. 17%-50%).

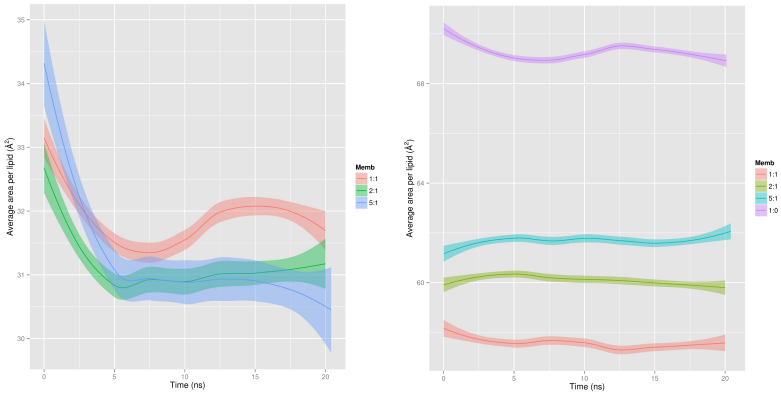

Figure 2: **Average area per lipid of individual lipid species during the simulation.** Solid lines show smoothed values of the area per lipid (Å^2, y axis) for CHOL (top) and POPC (bottom) over time (ns, x axis). Color codes as in figure legend. Confidence intervals around smoothed means are shown as degraded color ribbons.

S_{cd} order parameters

With a view to show the effect of cholesterol on membrane fluidity, we also inspected the chain structure of POPC in our simulations by using the S_{cd} tool of MEMBPLUGIN. This tool can compute the S_{cd} parameters of each

phospholipids present in the membrane under analysis. As described elsewhere [15], highly ordered membranes display high S_{cd} values and vice versa. Our results (see Figure 3) display the highest order near the polar head of the phospholipid (i.e. towards C2) whereas the end of phospholipid tails (i.e. towards C18) are highly disorder, that is, a the typical S_{cd} plot of a lipid bilayer. In addition, the results we obtained for the pure POPC system (i.e. system 1:0) (Figure 3, bottom line) are in agreement with previous experimental [16, 17] and computational [12] studies of this phospholipid.

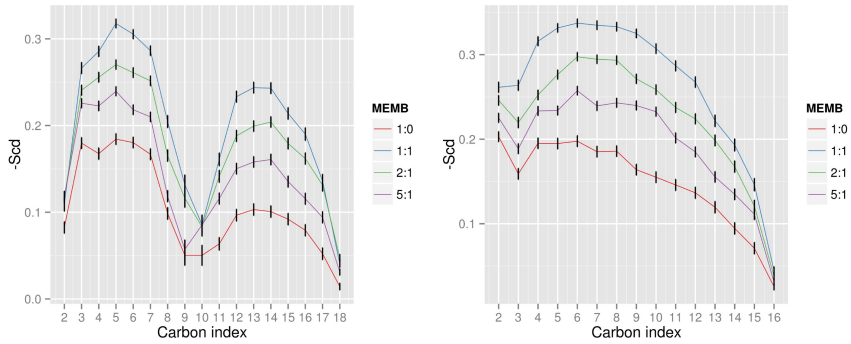

Figure 3: **Average S_{cd} order parameters of POPC tails.** Colored lines represent the average S_{cd} order parameters (x axis) of POPC *sn*-1 (left) and *sn*-2 (right) tails against POPC carbon index (y axis). Color codes as in figure legend. Error bars stand for the standard error of the mean at each carbon.

In our simulations, increasing amounts of cholesterol yield higher S_{cd} values of POPC tails, that is, more ordered membranes. As shown in Figure 3, this trend is clearly visible for both the unsaturated (Figure 3, left) and the saturated (Figure 3, right) chain of POPC. Therefore, as expected, affecting membrane fluidity is one of the underlying mechanisms behind cholesterol condensing effect on POPC membranes.

Membrane thickness

However, are highly-condensed and highly-ordered membranes thicker that more extended and fluid membranes? We address this question using the membrane thickness tool of MEMBPLUGIN to compute the so-called phosphate-to-

phosphate distance of our membrane set. This tool can compute the average thickness of the lipid bilayer between phosphate atoms (or any user-defined atom) and generate local deformations maps based on this analyis. The membrane thickness we obtained for the pure POPC membrane (i.e. system 1:0) goes along the experimental value of this type of lipid bilayers [18]. Likewise, as previously described in experimental [19] and computational [4, 20] studies, we observe that membrane thickness increases with higher molar concentrations of membrane cholesterol. As shown in Figure 4, the results from our simulations confirm that membrane thickness increases by approximately 10%, 18% and 26% in systems containing 17% (i.e. system 5:1), 33% (i.e. system 2:1) and 50% (i.e. system 1:1) of cholesterol, respectively.

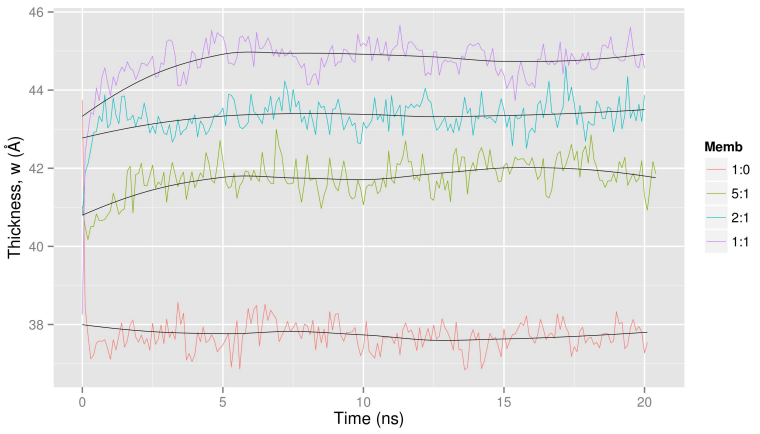

Figure 4: **Evolution of the phosphate-to-phosphate distance during the 20 ns simulation.** Colored lines represent the phosphate-to-phosphate distances for each system ($Å^2$, y axis) over time (ns, x axis). Color codes as in figure legend. The mean value of each plot is represented by a black line.

Specifically, we found an average membrane thickness of 37.73 ± 0.54 Å, 41.76 ± 0.48 Å, 43.31 ± 0.42 Å and 44.72 ± 0.64 Å, during the last 20 ns simulation of system 1:0, 5:1, 2:1 and 1:1, respectively.

Leaflet interdigitation

The concept on leaflet interdigitation remains controversial [21], partly due to the lack of experimental tools able to approach this measurement. However, this parameter can give valuable information on the coupling extent between membrane leaflets. Thus, we used the lipid interdigitation tool of MEMBPLUGIN to study the impact of cholesterol level on the coupling between membrane leaflets during the simulation. This tool offers three estimates of this parameter, namely the fraction mass overlap between the two leaflets, I_ρ, the width of such region, w_ρ, and the fraction of contacts between atoms of different leaflets, I_C, (see https://sourceforge.net/p/membplugin/wiki/Home/LipidInterdigitation/ for more details on this tool). Hereby, we computed the value of I_ρ, w_ρ and I_C for each of the membranes comprising our simulation set.

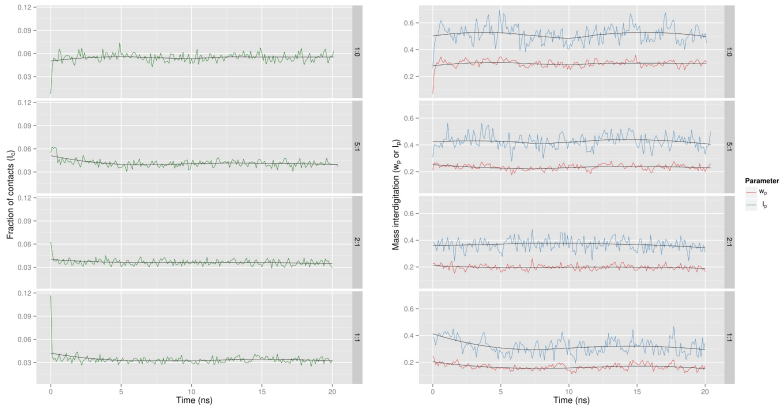

Figure 5: **Leaflet interdigitation represented by I_C, I_ρ, w_ρ and parameters.** Left figure displays the evolution of the fraction of contacts between leaflets, I_C ($0 \leq I_C \leq 1$), during the last 20 ns of the simulations. Likewise, the right figure shows such the evolution for mass interdigitation, namely, I_ρ ($0 \leq I_\rho \leq 1$) and w_ρ (nm). Actual values represented in colored lines, color codes as in figure legend. The moving average value of each plot is represented by a black line.

As for previous calculations, the results show a correlation between membrane cholesterol levels and leaflet interdigitation. In this case, higher cholesterol levels generally seems to decrease the extent of interdigitation between

membrane leaflets (See Figure 5). Thus, Figure 5, right, shows how molar cholesterol concentrations of 17% (i.e. system 5:1), 33% (i.e. system 2:1) and 50% (i.e. system 1:1) gradually decrease both the mass overlap between the two leaflets, I_ρ and the width of such region, w_ρ. Interestingly, as shown in Figure 5, left, the fraction of contacts between leaflets, I_C, does not seem to decrease at the same pace at high cholesterol concentrations (i.e. system 2:1 and system 1:1) when compared to lower ones. In fact, the most pronounced effect of cholesterol addition on this parameter occurs, to a high extent, at the lowest cholesterol level (i.e. 17%, system 5:1) (Figure 5 left).

Conclusions

We used MEMBPLUGIN to analyze the effect of cholesterol on the structure of POPC bilayers. On the one hand, MEMBPLUGIN is able to yield reproducible results in terms of area per lipid, S_{cd} order parameters and membrane thickness and to highlight the already-known condensing effect of cholesterol on phospholipid bilayers. At the same time, the increased amount of leaflet interdigitation showed a probable decrease in the extent of coupling between membrane leaflets, a fact that goes along the increase of membrane thickness. Although the aim of this case study was to highlight the versatility of MEMBPLUGIN using a realistic case, a similar rationale could be followed to analyze the impact of membrane composition on the biophysical properties of more complex and heterogeneous bilayers such as membrane microdomains [7], bacteria model membranes or specific subcellular compartments [22].

Data and citation

The trajectory data to reproduce the analysis of the present study can be downloaded from MEMBPLUGIN's web site. This case study is part of the paper [1], which should be referenced when citing this tool or related results such as the present case study.

References

[1] Ramon Guixà-González, Ismael Rodriguez-Espigares, Juan Manuel Ramírez-Anguita, Hector Martinez-Seara, Toni Giorgino, Pau Carrió, and Jana Selent. MEMBPLUGIN: Studying membrane complexity in VMD. *Bioinformatics*, 2013 (submitted).

[2] W. Humphrey, A. Dalke, and K. Schulten. VMD: visual molecular dynamics. *Journal of molecular graphics*, 14(1):33–38, 1996.

[3] Wei-Chin Hung, Ming-Tao Lee, Fang-Yu Chen, and Huey W Huang. The condensing effect of cholesterol in lipid bilayers. *Biophysical journal*, 92(11):3960–7, June 2007.

[4] Frédérick de Meyer and Berend Smit. Effect of cholesterol on the structure of a phospholipid bilayer. *Proceedings of the National Academy of Sciences of the United States of America*, 106(10):3654–8, March 2009.

[5] Kai Simons and Mathias J. Gerl. Revitalizing membrane rafts: new tools and insights. *Nature Reviews Molecular Cell Biology*, 11(10):688–699, October 2010.

[6] Daniel Lingwood and Kai Simons. Lipid rafts as a membrane-organizing principle. *Science (New York, N.Y.)*, 327(5961):46–50, January 2010.

[7] Perttu Niemelä, Samuli Ollila, Marja T Hyvönen, Mikko Karttunen, Ilpo Vattulainen, and Marja T Hyvo. Assessing the nature of lipid raft membranes. *PLoS Comput. Biol*, 3(2):e34, 2007.

[8] S.A. Pandit, S Vasudevan, S W Chiu, R Jay Mashl, Eric Jakobsson, and H L Scott. Sphingomyelin-cholesterol domains in phospholipid membranes: atomistic simulation. *Biophysical journal*, 87(2):1092–100, August 2004.

[9] H Jelger Risselada and Siewert J Marrink. The molecular face of lipid rafts in model membranes. *Proceedings of the National Academy of Sciences of the United States of America*, 105(45):17367–72, November 2008.

[10] Sunhwan Jo, JB Joseph B Lim, JB Jeffery B Klauda, and Wonpil Im. CHARMM-GUI membrane builder for mixed bilayers and its application to yeast membranes. *Biophysical journal*, 96(1):50–8, July 2009.

[11] MJ J Harvey, G Giupponi, and GD De Fabritiis. ACEMD: accelerating biomolecular dynamics in the microsecond time scale. *Journal of Chemical Theory and Computation*, 5(6):1–9, 2009.

[12] Jeffery B Klauda, Richard M Venable, J Alfredo Freites, Joseph W O'Connor, Douglas J Tobias, Carlos Mondragon-Ramirez, Igor Vorobyov, Alexander D MacKerell, and Richard W Pastor. Update of the CHARMM all-atom additive force field for lipids: validation on six lipid types. *The journal of physical chemistry. B*, 114(23):7830–43, June 2010.

[13] Hadley Wickham. *ggplot2: elegant graphics for data analysis*. Springer New York, 2009.

[14] Norbert Kucerka, Stephanie Tristram-Nagle, and John F Nagle. Structure of fully hydrated fluid phase lipid bilayers with monounsaturated chains. *The Journal of membrane biology*, 208(3):193–202, December 2005.

[15] Louic S Vermeer, Bert L de Groot, Valérie Réat, Alain Milon, and Jerzy Czaplicki. Acyl chain order parameter profiles in phospholipid bilayers: computation from molecular dynamics simulations and comparison with 2H NMR experiments. *European biophysics journal : EBJ*, 36(8):919–31, November 2007.

[16] Saame Raza Shaikh, Michael R Brzustowicz, Noah Gustafson, William Stillwell, and Stephen R Wassall. Monounsaturated PE does not phase-separate from the lipid raft molecules sphingomyelin and cholesterol: role for polyunsaturation? *Biochemistry*, 41(34):10593–602, August 2002.

[17] B Perly, I C Smith, and H C Jarrell. Acyl chain dynamics of phosphatidylethanolamines containing oleic acid and dihydrosterculic acid: 2H NMR relaxation studies. *Biochemistry*, 24(17):4659–65, August 1985.

[18] Fluid phase lipid areas and bilayer thicknesses of commonly used phosphatidylcholines as a function of temperature. *Biochimica et biophysica acta*, 1808(11):2761–71, November 2011.

[19] Norbert Kucerka, Jason D Perlmutter, Jianjun Pan, Stephanie Tristram-Nagle, John Katsaras, and Jonathan N Sachs. The effect of cholesterol on short- and long-chain monounsaturated lipid bilayers as determined by molecular dynamics simulations and X-ray scattering. *Biophysical journal*, 95(6):2792–805, September 2008.

[20] Christofer Hofsäss, Erik Lindahl, and Olle Edholm. Molecular dynamics simulations of phospholipid bilayers with cholesterol. *Biophysical journal*, 84(4):2192–206, April 2003.

[21] Interleaflet coupling mechanisms in bilayers of lipids and cholesterol. *Biophysical journal*, 94(5):L32–4, March 2008.

[22] Björn Sommer, Tim Dingersen, Christian Gamroth, Sebastian E. Schneider, Sebastian Rubert, Jens Krüger, and Karl-Josef Dietz. CELLmicrocosmos 2.2 MembraneEditor: a modular interactive shape-based software approach to solve heterogeneous membrane packing problems. *Journal of Chemical Information and Modeling*, 51(5):1165–1182, May 2011.

3.5 Membrane omega-3 fatty acids modulate the oligomerization of G protein-coupled receptors

Guixà-González R., Javanainen M., Martinez-Seara H., Gomez-Soler M., Cordobilla B., Domingo J. C., Sanz F., Pastor M., Ciruela F. and Selent J. *Nature Commun. (Manuscript under first revision)*, (2014).

Summary
As we have mentioned in the Introduction section, although the modulation of GPCRs by specific membrane lipids has already been reported, there is a clear lack of studies covering the lipid-mediated oligomerization of GPCRs. In addition, DHA and certain GPCR oligomers including the A_{2A} – dopamine D_2 heteromer are linked to brain disease. Therefore, the last milestone of this thesis was to shed light on the effect of DHA on the oligomerization nature of the A_{2A} – dopamine D_2 heteromer. This manuscript describes for the first time the modulation of GPCR oligomerization by membrane omega-3 fatty acids. We predicted this modulation by MD simulations and used living cells to validate experimentally our computational studies. In this work we have generated new interesting results on the interplay between membrane lipids by using the computational framework developed during this thesis.

Membrane omega-3 fatty acids modulate the oligomerization of G protein-coupled receptors

Ramon Guixà-González[1], Matti Javanainen[2], Hector Martinez-Seara[2], Maricel Gómez-Soler[3], Begoña Cordobilla[4], Joan Carles Domingo[4], Ferran Sanz[1], Manuel Pastor[1], Francisco Ciruela[3] and Jana Selent[1⋆]

Abstract

Membrane levels of docosahexaenoic acid (DHA), an essential omega-3 polyunsaturated fatty acid (ω-3 PUFA), are decreased in common neuropsychiatric disorders. DHA modulates key cell membrane properties like fluidity, thereby affecting the behaviour of transmembrane proteins like G protein-coupled receptors (GPCRs). These receptors, which also have special relevance for major neuropsychiatric disorders have recently been shown to form dimers or higher order oligomers, and evidence suggests that DHA levels may affect GPCR function by modulating oligomerization. We assessed the effect of DHA on formation of a particularly interesting oligomer for brain disease: the adenosine A_{2A}–dopamine D_2 heteromer (A_{2A}–D_2). Using computational prediction and experimental validation, we demonstrate that DHA-rich membranes show greater A_{2A}–D_2 oligomerization than DHA-poor membranes. This work reveals for the first time that membrane ω-3 PUFAs play a key role in GPCR oligomerization, which may have important implications for neuropsychiatric conditions like Schizophrenia or Parkinson's disease.

[1]Research Programme on Biomedical Informatics (GRIB), Department of Experimental and Health Sciences Universitat Pompeu Fabra, IMIM (Hospital del Mar Medical Research Institute), Spain; [2] Department of Physics, Tampere University of Technology, Tampere, Finland; [3] Facultat de Medicina, IDIBELL, Universitat de Barcelona, Barcelona, Spain; [4] Facultat de Biologia , Universitat de Barcelona, Barcelona, Spain.

⋆ Correspondence and requests for materials should be addressed to J.S. (email: jana.selent@upf.edu).

Several studies have found substantially lower levels of docosahexaenoic acid (DHA) in the brains of individuals with mental[1–4] or neurological disorders[5,6]. DHA is an omega-3 polyunsaturated fatty acid (ω-3 PUFA) of 22 carbons and 6 double bonds (22:6n3) that has been shown to be essential for the development[7] and maintenance of adequate brain function[8,9]. The high levels of DHA found in specialized cell platforms such as retinal rod outer segments[10,11] or neuronal cells[12,13] seems to provide these membranes with particular biophysical properties[14] such as increased fluidity. The unique biophysical properties of DHA along with its potential neuroprotective effects[8,15] have made DHA a promising candidate against certain neurodegenerative disorders[16–18].

In addition, recent studies have shown that the lipid composition of cell membranes can modulate the function of key membrane proteins such as G protein-coupled receptors (GPCRs)[19,20]. GPCRs are involved in a wide range of diseases and are particularly important for several major psychiatric disorders[21]. Therefore, understanding the role of the membrane environment on the dynamics and function of GPCRs has become a research priority in this field. For instance, a particular relationship is known to exist between DHA and rhodopsin[22], a widely studied GPCR specific to retinal rod cell membranes. The modulatory effect of DHA on rhodopsin was first described by Mitchell et al.[23] and has since been further studied using experimental[24–28] and computational[29,30] methods. DHA is therefore known to influence the biology of rhodopsin and could potentially modulate other GPCRs in other DHA-rich tissues such as the brain[7].

However, an additional level of complexity adds to the overall picture of DHA–GPCR modulation: GPCRs have recently been found to function as dimers or higher order oligomers, and despite initial controversy, the existence and relevance of GPCR oligomerization has gained broad acceptance[31]. Interestingly, impaired crosstalk between specific GPCR heteromers seems to affect GPCR signalling and results in defective neurotransmission and brain dysfunction[32–34]. The study of GPCR oligomers such as the adenosine A_{2A}–dopamine D_2 (A_{2A}–D_2) heteromer is therefore becoming highly relevant in neuropsychiatry[35]. In fact, the A_{2A}–D_2 oligomer is now a promising target against certain neuropsychiatric disorders[33]. The question that naturally arises is do membrane lipids affect GPCR oligomerization? Given the apparent importance of oligomerization for GPCR function, it seems possible that this is the mechanism through which DHA modulates GPCR biology, and subsequently neurological disease processes.

Since current experimental evidence[1–6] links altered levels of DHA to brain dysfunction, in this study we compared the effects of high and low levels of DHA on A_{2A}–D_2 oligomerization. We performed molecular dynamics (MD) simulations of the self-assembly process of A_{2A} and D_2 receptors embedded in multicomponent model membranes reaching an exceptionally long total simulation time of 1.630 ms. We then compared the effect of high and low levels of membrane DHA on protein aggregation and studied the particular affinity between this lipid and GPCRs. We validated our MD molecular dynamics simulations using bioluminescence resonance energy transfer (BRET) experiments in living cells. Our combined results from both the BRET analysis and the MD simulations confirm for the first time that GPCR oligomerization can be modulated by membrane ω-3 PUFAs. These results provide a molecular link between membrane lipid composition and GPCR oligomerization, which could help in the development of new treatments for major neurological disorders.

Results

MD simulations show that ω-3 PUFA enhance GPCR oligomerization. We performed extensive coarse-grained (CG) MD of A_{2A} and D_2 receptors embedded in two model membranes of different lipid composition. Such composition aimed to reflect the general lipid profiles previously observed in post-mortem studies of healthy and diseased individuals[1–6], so we created a 'healthy-like' (rich in DHA) and a 'diseased-like' (low in DHA) membrane. Briefly, the healthy-like and diseased-like models model contained 21 % and 6 % of DHA-rich phospholipids (i.e. SDPC, 1-stearoyl-2-docosahexaenoyl-*sn*-glycero-3-phosphocholine), respectively; the diseased-like model was compensated with a higher fraction of saturated lipids (Table 1a). SDPC contains mixed chains (C22:6 (DHA) and C18:0), so these SDPC levels translate into a DHA content of 11 % and 3 % over total fatty acids, respectively (see Table 1b). First, we simulated 3 replicates of each model system for 60 μs.

We quantified protein aggregation by analysing the number of protein–protein contacts established during the last 20 μs of the simulation. For this purpose, we considered two receptors to be in direct contact if the distance between the positions of their centre of mass (COM) was < 4.2 nm. As shown in Table 2, analysis of all simulations shows that protein aggregation is significantly enhanced in healthy conditions. Specifically, the mean number of protein–protein contacts is ≈ 20 % higher in healthy-like membranes (high DHA) when compared to diseased-like ones (low DHA). This finding suggests that DHA plays an important role in the oligomerization of A_{2A} and D_2 receptors.

DHA treatment enhances A_{2A}–D_2 oligomerization in living cells. BRET experiments were carried out in living cells to study the effect of membrane DHA on the organization of A_{2A} and D_2 receptors. We first determined the fatty acid content of parental HEK-293T cells grown under standard conditions. Under these basal conditions, the cells showed a low relative content of DHA: 0.99 ± 0.03 % of total fatty acids (Fig. 1). To obtain a cell culture with a higher level of DHA we supplemented HEK-293T cells with increasing concentrations of DHA.

Table 1 | Phospholipid and fatty acid composition of healthy- and diseased-like model membranes used in CG- and all-atom MD simulations.

a

PH	Chains	Healthy*	Diseased*
DPPC	diC16:0	21	33
DSPC	diC18:0	7	15
DOPC	diC18:1	15	11
SDPC	C22:6/C18:0	21	6
SM	C18:1/C16:0	36	36
TOTAL	–	100	100

b

Fatty acid	Healthy*	Diseased*
C16:0	39	51
C18:0	43	41
C18:1	7	5
C22:6	11	3
TOTAL	100	100

Phospholipid **(a)** and fatty acid **(b)** levels used in each membrane model. Values are reported as % phospholipid over total phospholipids **(a)** and % fatty acid over total fatty acids **(b)**. The overall composition of both models is inspired by brain lipid profiles of healthy and diseased individuals[1–6]. In both tables, Healthy* and Diseased* refer to healthy- (high DHA) and diseased-like (low DHA) model membranes. In addition to phospholipids, both membrane models contain cholesterol in a phospholipids:cholesterol ratio of 1:3. Abbreviations signify phospholipid (PH), 1,2-dipalmitoyl-*sn*-glycero-3-phosphocholine (DPPC), 1,2-distearoyl-*sn*-glycero-3-phosphocholine (DSPC), 1,2-dioleyl-*sn*-glycero-3-phosphocholine (DOPC), 1-stearoyl-2-docosahexaenoyl-*sn*-glycero-3-phosphocholine (SDPC) and sphingomyelin (SM18).

Table 2 | Mean number of protein–protein contacts established during long-scale CG-MD simulations.

	R1	R2	R3	AVE
Healthy*	1.41	1.48	1.53	1.47
Diseased*	1.27	1.18	1.12	1.19

Mean number of protein–protein contacts per protomer (i.e. the number of protomers that each protomer is in contact with) during the last 20 µs of 60 µs simulations. Healthy* and Diseased* refer to healthy- (high DHA) and diseased-like (low DHA) model membranes. R1, R2, and R3 stand for replicas 1, 2 and 3, respectively. The last column (AVE) displays the mean number of protein–protein contacts per protomer across all replicates.

Interestingly, we observed saturable dose-dependent incorporation of DHA into the membrane of HEK-293T cells with a maximum dose achieved at 200 µM of DHA, yielding a relative DHA content of 6.49 ± 0.32 % of total fatty acids (Fig. 1). While this content is still below the level of DHA found in normal human brains[4], cells supplemented with the maximum dose of DHA still show more than 6-fold higher DHA than cells grown in basal conditions. Therefore, we established non-treated cells and cells treated with 200 µM DHA as representatives of DHA-low and DHA-rich models, respectively. Remarkably, we did not observe significant DHA-mediated cytotoxicity at any dose tested.

Thus, cell viability at 200 µM DHA was 89.5 ± 8.2 % compared to untreated cells (p=0.3045, Student's t test, n=3). With regard to fatty acid profile, while levels of saturated fatty acids remained constant, treatment with DHA induced an increase of PUFA and ω-3 series along with a progressive decrease in monounsaturated and ω-6 series, resulting in a five-fold decrease in the ω-6 / ω-3 ratio (Fig. 1).

Having demonstrated adequate incorporation of DHA into HEK-293T cell membranes, we further investigated its role in A_{2A}–D_2 oligomerization. BRET is a powerful technique for characterizing GPCR oligomers[36] and, in particular, for studying the comparative effect of certain modulators on GPCR oligomerization[37–39]. In our experiments, a positive and saturable BRET signal for the transfer of energy between $A_{2A}{}^{Rluc}$ and $D_2{}^{YFP}$ constructs was observed (Fig. 2a) in cells co-transfected with a constant amount of $A_{2A}{}^{Rluc}$ and increasing concentrations of $D_2{}^{YFP}$. In addition, since the control receptor pair, $A_{2A}{}^{Rluc}$ and $CD4^{YFP}$, led to the typical quasi-linear curve[40,41], the specificity of the saturation (hyperbolic) assay for the $A_{2A}{}^{Rluc}$–$D_2{}^{YFP}$ pair could be established. These results corroborate previous results indicating that A_{2A} and D_2 receptors form constitutive heterodimers in living cells[40].

To assess the effect of DHA on the A_{2A}–D_2 heteromer (i.e. BRET signal), we performed 4 independent BRET titration experiments in the presence and absence of a saturating concentration of DHA (200 µM). Interestingly, preincubation with DHA for 48 h significantly increased the maximum BRET signal ($BRET_{max}$) by 25 ± 8 % ($p < 0.05$) in all the experiments performed with $A_{2A}{}^{Rluc}$–$D_2{}^{YFP}$ co-transfected cells (Fig. 2b). On the other hand, the amount of $D_2{}^{YFP}$ needed to reach 50 % of the maximal BRET signal ($BRET_{50}$) was slightly lower in the presence of DHA, although this effect was not statistically significant (Fig. 2c). Therefore, DHA treatment affects both the propensity of A_{2A} and D_2 protomers to interact and the oligomerization mode of this heteromer.

Overall, these results conclusively demonstrate that DHA treatment increases A_{2A} and D_2 heteromerization.

Polyunsaturated lipids avidly surround GPCRs in CG-MD and all-atom simulations. We used MD simulations to further characterize the affinity between DHA and GPCRs. As shown in the CG-MD simulations (see Supplementary Movie 1), DHA-rich phospholipids (i.e. SDPC) display a striking preference for interaction with GPCRs. In fact, this video shows how a shell of this lipid tends to surround GPCR monomers virtually from the beginning of the simulation, and how, GPCR oligomers are surrounded by SDPC molecules by the end

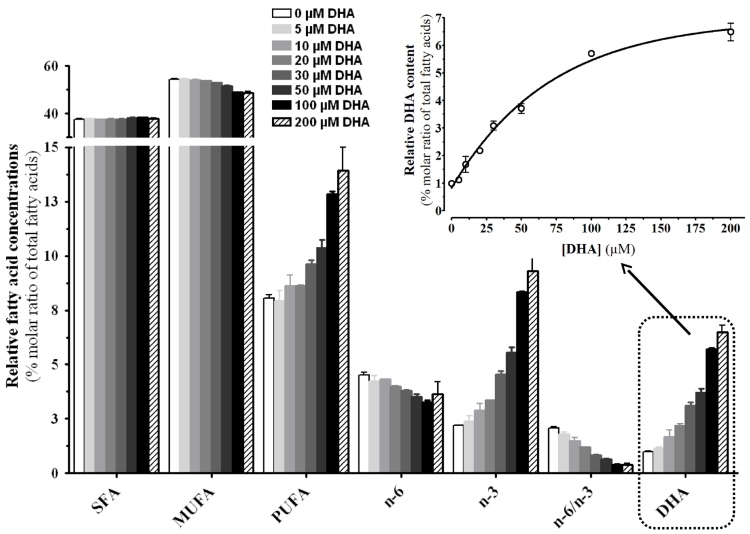

Figure 1 | Effect of DHA treatment in the fatty acids content of HEK cells. HEK-293T cells were incubated with increasing concentrations of DHA (22:6n-3) during 48 h. The effect of increasing doses of DHA in the fatty acid profile was measured by gas chromatography. The specific dose-dependent DHA incorporation is shown (inset panel). The fatty acid content is expressed as the relative molar ratio in percentage. Data shown are the mean ± SEM of three determinations. SFA, MUFA, PUFA, n-6 and n-3 labels stand for saturated fatty acids, monounsaturated fatty acids, polyunsaturated fatty acids, ω-6 PUFA and ω-3 PUFA, respectively)

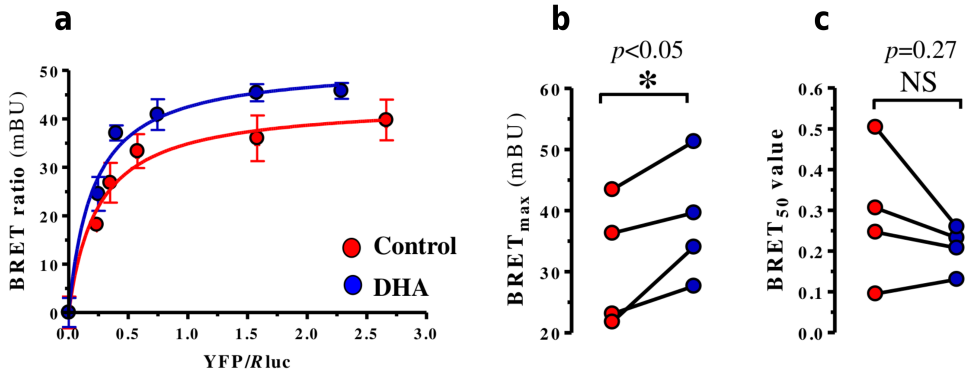

Figure 2 | Effect of DHA on the A_{2A}–D_2 oligomerization state. BRET was measured in HEK-293T cells co-expressing $A_{2A}{}^{Rluc}$ plus $D_2{}^{YFP}$ and preincubated during 24h in the absence (red) or presence of DHA (blue) (see Methods). 4 independent experiments with DHA-treated and non-treated cells were performed. (**a**) shows the BRET saturation curve of one representative experiment where each point measurement was performed in triplicate. Plotted on the x axis is the average fluorescence value of the $D_2{}^{YFP}$ (acceptor), corrected for the background fluorescence, over the average luminescence value of $A_{2A}{}^{Rluc}$ (donor). Values were read after 10 min of h-coelenterazine incubation. The corresponding average BRET ratios (x1000) in mBU (mBRET units), corrected for the background BRET signal, are plotted on the y axis. Values expressed as mean (points) ± SEM (vertical and horizontal error bars; SMEs bars smaller than the point size are not visible). (**b**) and (**c**) plots show, respectively, the $BRET_{max}$ and $BRET_{50}$ results of 4 independent experiments in the absence (red) and presence (blue) of DHA. These results were compared by a paired t test demonstrating statistical significant differences (i.e. $p < 0.05$). Significant differences are marked by the *, whereas NS stands for not significant

of the simulation. To support these observations, we calculated the radial distribution function of each lipid type around the A_{2A} (Fig. 3) and D_2 (Supplementary Fig. 1) receptors. This analysis confirms that during our CG-MD simulations the first solvation shell around the protein is primarily populated by DHA-rich phospholipids (SDPC). This DHA shell cannot completely form when the level of DHA-rich phospholipids is poor (i.e. in diseased-like systems).

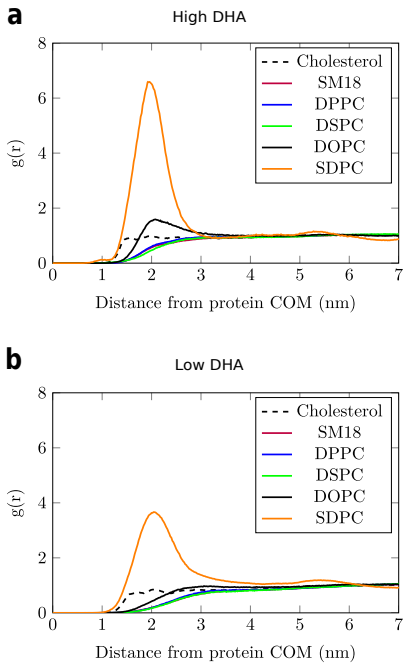

Figure 3 | Radial distribution function of lipids around A_{2A} receptors during CG-MD simulations. Probability density (i.e. radial distribution function, $g(r)$) of lipids around the center of mass of A_{2A} receptors embedded in healthy- (high DHA, **(a)**) and diseased-like (high DHA **(b)**) model membranes. y and x axes represent $g(r)$ (arbitrary units) and distance (nm), respectively. Radial distribution functions for D_2 receptors are shown in Supplementary Fig. 1

To validate the effect we see in our CG-MD simulations, we complemented our simulations using all-atom molecular dynamics of A_{2A} embedded in a healthy-like membrane system (Table 1). A final snapshot of the all-atom simulation at 4 µs (Fig. 4, right) confirms that unsaturated phospholipids, namely DOPC and SDPC, have a strong preference for solvation of the protein. To quantitatively assess this effect, we calculated the mean number of contacts per atom between unsaturated tails and the protein and compared this value with that for saturated tails (see Supplementary Methods). The proportion of lipid-protein contacts between unsaturated tails with respect to saturated ones clearly grows during the simulation (Supplementary Fig. 2). Specifically, DHA tails (i.e. *sn*-2 chain of SDPC) display the highest growth rate (Supplementary Fig. 2b) and confirm the tendency of this fatty acid to interact with the protein. In addition, the contact ratio of SDPC over DOPC remains equilibrated (i.e. around 1) until the end of the simulation, when, proportionally more SDPC is in contact with the protein (Supplementary Fig. 2a and Table 3). These results imply that, as we observe in Fig. 4, DHA gradually populates the closest lipid shell around the GPCR during the all-atom simulation.

In addition, as shown in our CG-MD simulations (Supplementary Movie 1), an SDPC shell seems to act as a lubricating film in many of the dimer and oligomer formation events. It is tempting to suggest that the high affinity between DHA and GPCRs explains the enhancing effect on A_{2A}–D_2 oligomerization we observed in living cells treated with this fatty acid.

Table 3 | Contact ratios established between unsaturated lipid chains and the A_{2A} receptor during 4 µs of the all-atom simulation.

Ratio type	0–1	1–2	2–3	3–4
SDPC / SAT	1.82	2.91	3.56	5.35
SDPC*sn*-1 / SAT	1.64	2.46	2.70	3.48
SDPC*sn*-2 / SAT	2.01	3.37	4.43	7.21
DOPC / SAT	2.03	3.27	4.13	4.24
DOPC*sn*-1 / SAT	1.95	3.04	4.09	3.74
DOPC*sn*-2 / SAT	2.11	3.5	4.16	4.75
SDPC / DOPC	1.15	0.95	0.93	1.38

Ratios represent the relative proportion of mean lipid–protein contacts per atom between two selections. For instance, the SDPC*sn*-1 / SAT ratio corresponds to the average number of lipid–protein contacts per atom established by SDPC*sn*-1 tails with respect to those established by all saturated lipid tails in the membrane (SAT). Each column represent a specific time range expressed in units of µs.

DHA accelerates the kinetics of GPCR aggregation. While the results from our BRET experiments confirms that DHA levels can affect GPCR aggregation in living cells (see above), we wanted to shed more light on the general mechanism behind this effect. Thus, we performed an in-depth characterization of the protein aggregation behaviour observed during our CG-MD simulations. The final snapshots of our CG-MD simulations (Fig. 5a–f) show that protein oligomers tend to form extended rather than looped structures in both healthy- and diseased-like environments. Within these oligomers, protomers establish mostly 1 (dimers) or 2 contacts (trimers) and rarely 3 contacts (tetramers) with other protomers

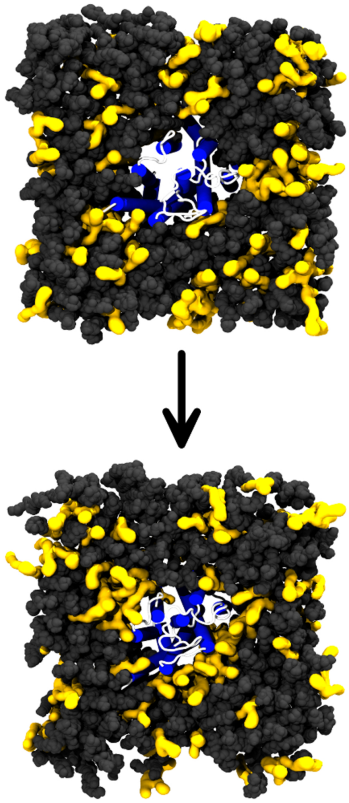

Figure 4 | All-atom simulation of the A_{2A} receptor embedded in a healthy-like model membrane (DHA-high). Initial (top) and final (bottom) snapshots of the simulation were taken at 0 and 4 μs, respectively. A_{2A} helices are depicted in blue cartoons whereas protein loops are in thin white cylinders. Grey van der Waals spheres correspond to a representation of all membrane lipids except unsaturated phospholipids (i.e. SDPC and DOPC molecules) depicted in yellow surface. Water molecules and ions were omitted for clarity.

(Figs. 5a–f). Such array-like disposition has already been described in previous CG-MD simulations of GPCRs[42,43]. To confirm the behaviour of protein oligomers at longer time-scales, we extended one of the simulations (Fig. 5a) up to 260 μs. The final snapshot of this extended simulation displays an extended-like final arrangement of the protein oligomer (Supplementary Fig. 3d) where nearly all protomers form at least one protein–protein contact. It is worth noting that during these 60–260 μs, the number of protein–protein contacts generally remained between one and two contacts per protomer (Supplementary Fig. 3a–d).

The evolution of protein aggregation significantly varied between healthy- and diseased-like systems, as shown by the number of protein–protein contacts over time depicted in Fig. 6. This figure shows that GPCR dimers form significantly quicker in DHA-high (Fig. 6a, left) when compared to DHA-low systems (Fig. 6a, right). To provide more statistical support for this finding, we performed 5 replicate simulations for of the two membrane environments. Analysis of the first 16 μs (Fig. 6b, right) of these simulations shows that protein aggregation is again reduced in all replicates of the diseased-like model. More importantly, however, these replicate simulations confirm that protein aggregates consolidate earlier in the presence of healthy levels of DHA (Fig. 6b, left). As shown in Table 4, the mean number of protein–protein contacts per protomer during the first 0–4 μs is similar in healthy- and diseased-like systems. In contrast, during the 4–8 μs interval of the simulation, protomers embedded in healthy-like model membranes were able to engage in twice as many protein–protein contacts compared to diseased-like membranes. Therefore, increasing levels of membrane ω-3 PUFAs (i.e. DHA) seems to speed up GPCR oligomerization by promoting a higher numbers of protein–protein contacts in shorter times.

Table 4 | Mean number of protein–protein contacts established during short replicates of CG-MD simulations.

	0–4	4–8	8–12	12–16	0–16
Healthy*	0.25	0.62	0.78	0.91	0.64
Diseased*	0.22	0.29	0.49	0.67	0.42

The mean number of protein–protein contacts per protomer in 5 replicates of short 16 μs simulations. Time frames (columns) are expressed in μs. Healthy* and Diseased* refer to healthy- (high DHA) and diseased-like (low DHA) model membranes. Starting from the left, each column shows the mean number of protein–protein contacts during sequential 4 μs intervals, and the last column displays the same value for the whole simulation (0–16 μs).

Finally, we performed further CG-MD simulations to confirm whether the initial arrangement of protomers could modulate the effect of DHA on protein aggregation. We used new starting configurations of the proteins, where protomers of each receptor type occupied one half of the simulation box, and ran 3 replicates of healthy- and diseased-like systems for 120 μs. This analysis confirmed that the enhancing effect of DHA on protein aggregation is not markedly affected by the initial configuration of protomers (Supplementary Fig. 4).

DHA-rich membranes speed up protein and lipid diffusion. To study the effect of DHA on protein diffusion, we performed a new set of CG-MD simulations based on single monomers (i.e. A_{2A} or D_2) and measured protein diffusion (see details in Supplementary Methods). As shown in (Supplementary Fig. 5), proteins display higher mean squared displacements (MSDs) when diffusing in the more fluid environment of a healthy-like (DHA-

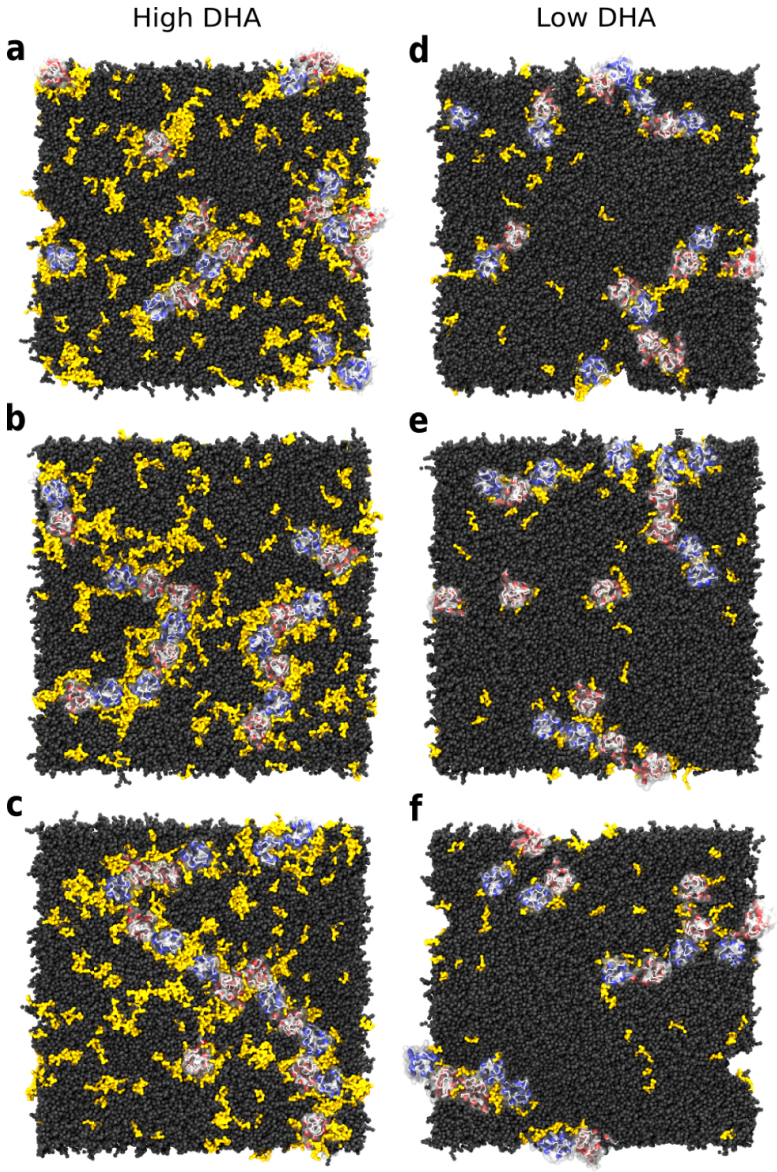

Figure 5 | Final snapshot of healthy- and diseased-like systems after 60 µs of CG-MD simulation. Left and right columns display 3 replicates of healthy- (high DHA, left) and diseased-like (low DHA, right) systems. Each figure correspond to one replica. A_{2A} and D_2 helices are depicted in red and blue cartoons, respectively, whereas protein loops are in thin white cylinders. Protein monomers are surrounded by a white transparent surface. Grey spheres correspond to a van der Waals representation of all membrane lipids except for SDPC molecules depicted in yellow surface. Water molecules, ions, and anti-freezing particles are not shown for clarity.

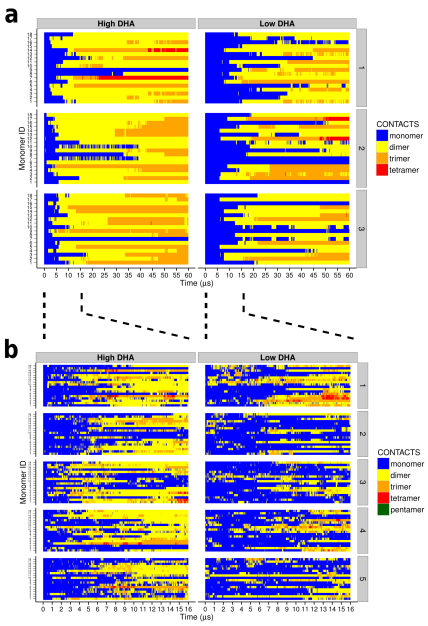

Figure 6 | Time-dependence of protein aggregation in CG-MD simulations. Long (**a**) and short (**b**) simulations (60 µs and 16 µs, respectively) of healthy-like (i.e. high DHA, left) and diseased-like (low DHA, right) systems. Each cell represents one replicate, as three long (**a**) and 5 short replicates (**b**) were run for each system. Each number in the y axis represents one GPCR protomer and time extends along the x axis.

rich) membrane than in diseased-like (DHA-low) membranes. Specifically, A_{2A} and D_2 receptors simulated in healthy-like membranes display an average diffusion coefficient (± error estimate; see Supplementary methods) of 4.8 ± 1.3 × 10^{-9} cm^2/s and 4.6 ± 1.0 × 10^{-9} cm^2/s, respectively. In contrast, when simulated in diseased-like membranes, A_{2A} and D_2 receptors show a slower diffusion of 1.8 ± 0.6 × 10^{-9} cm^2/s and 2.2 ± 0.6 × 10^{-9} cm^2/s, respectively. Similarly, the calculated protein rotational motion is slower in diseased-like membranes (Supplementary Fig. 6a), a trend particularly evident for the D_2 receptor (Supplementary Fig. 6b).

In general, the simulation data suggest that higher levels of DHA allow proteins to travel longer distances and sample a higher number of potential dimerization interfaces due to enhanced translational and rotational diffusion, respectively. Likely as a result of a faster diffusion, proteins aggregate more rapidly in healthy-like model membranes (Fig. 6a–b, left), where we find that nearly all monomeric structures (blue) disappear within 5–10 µs, making room for dimers (yellow), trimers (orange) or even higher-order arrangements such as tetramers (red) or pentamers (green). In contrast, in diseased-like systems (Fig. 6a–b, right), most of the monomeric structures need 15–20 µs to form higher-order structures. Similarly, lipids generally move faster in highly unsaturated environments (Supplementary Fig. 7). It is worth noting that out of the six lipid species, SDPC displays the lowest diffusion coefficient in both healthy- and diseased-like systems (Table 5). Such low diffusion is consistent with the fact that SDPC is the most common lipid of the protein-solvating lipid shell (Figs. 3 and Supplementary Fig. 1). Hence, a plausible explanation for the low diffusion values shown by SDPC is that the high number of DHA–protein interactions slows down the diffusion of this lipid, in agreement with previous work[44].

Table 5 | Average diffusion coefficients of lipids during long CG-MD simulations

Lipid	Healthy*	Diseased*
CHOL	3.43 ± 0.19	2.60 ± 0.19
SM	2.72 ± 0.17	2.52 ± 0.20
DPPC	2.87 ± 0.35	2.48 ± 0.15
DSPC	2.87 ± 0.15	2.36 ± 0.07
DOPC	2.90 ± 0.33	2.44 ± 0.09
SDPC	2.08 ± 0.16	1.34 ± 0.11

Diffusion coefficients of lipids in each model membrane. Healthy* and Diseased* refer to healthy- (high DHA) and diseased-like (low DHA) model membranes. Values are reported in 10^{-8} cm^2/s ± the error estimate. The calculation of error estimates is described in the Supplementary Methods.

Discussion

Experimental evidence suggests that both GPCR oligomerization and DHA play a relevant role in brain functioning. In this study we report for the first time a molecular link between membrane levels of DHA and GPCR oligomerization, which could have important implications for the treatment of major psychiatric disorders. In addition, this work opens the door for studying the effect of ω-3 PUFAs on other GPCR oligomers known to be involved in neurological diseases.

We have used computational prediction methods backed up by laboratory validation to assess the effect of DHA levels on the formation of A_{2A}–D_2 heteromers. Our CG-MD simulations predict that GPCR aggregation is driven by membrane DHA levels. Specifically, low levels of DHA significantly diminished the ability of A_{2A} and D_2 receptors to engage in protein–protein contacts during these simulations (Table 2). To validate these findings we used BRET measurements in living cells to

monitor the oligomerization mode of these receptors in DHA-high and DHA-low membrane environments. The results from these experiments provide a striking validation of our computational prediction, and showed that enriching cell membranes with DHA enhances the intensity of A_{2A}–D_2 oligomerization (Fig. 2).

In addition, the results from the CG-MD simulations show that membrane DHA levels modulate the diffusion of membrane components (Table 5 and Supplementary Fig. 6) and, ultimately, the rate of spontaneous protein–protein interactions (Fig. 6). Thus, A_{2A} and D_2 receptors can travel longer distances and sample a higher number of potential dimerization interfaces in DHA-rich membranes. These results suggest that higher levels of DHA accelerate protein aggregation and highlights the role of kinetics in modulating GPCR oligomerization. Intriguingly, this effect of DHA on GPCR oligomerization could partly underlie the neuroprotective properties of DHA supplementation reported previously in animal studies[8,17]. In that case, restoring membrane DHA levels in individuals with Schizophrenia or Parkinson's disease could improve the impaired crosstalk of the A_{2A}–D_2 oligomer observed in these disorders[33].

A question now arises about the molecular mechanism through which DHA enhances the kinetics of GPCR aggregation. In line with previous studies[22,29], both our CG- and all-atom MD simulations confirm the strong tendency of DHA-rich phospholipids to solvate GPCRs (Fig. 3 and Table 3). In fact, a ubiquitous shell of DHA-rich lipids constantly surrounded the proteins during our millisecond-scale CG-MD simulations (Supplementary Movie 1). This distinctive solvation shell seems to provide proteins with a complete DHA armour that enhances GPCR aggregation kinetics by facilitating the establishment and consolidation of proteinprotein interactions in the membrane. It is tempting to speculate on whether this DHA-dependent effect is a general mechanism that cell membranes use to drive transmembrane proteins like GPCRs into signalling platforms (e.g. lipid microdomains), which is currently a matter of intense discussion[45–47].

In conclusion, our results represent the first reported evidence of a molecular link between membrane levels of ω-3 polyunsaturated fatty acids and GPCR oligomerization. They provide an important advance in understanding the interplay between membrane lipids and key transmembrane proteins like GPCRs, a topic of current special interest in biophysics. Most importantly, these findings create new opportunities to explore the use of membrane lipids as a therapeutic tool for major neuropsychiatric conditions, specifically Schizophrenia or Parkinson's disease, in which the A_{2A}–D_2 heteromer has been shown to have particular importance.

Methods

CG-MD simulations. The MARTINI force field for lipids v2.0[48] and amino acids v2.1[49] and the GROMACS 4.5 simulation package[50] were employed to build and perform all CG-MD simulations. The exact lipid composition of each model is represented in Table 1 and Supplementary Table 1. The extension of MARTINI force field to proteins[49] was used to model A_{2A} and D_2 receptors. All CG-MD simulations were carried out in the NPT ensemble at 37°C and at 1 bar. We report all CG-MD simulation using effective times, a standard 4-fold speed-up conversion factor that accounts for the loss of friction of the MARTINI CG-MD model and employed in similar CG-MD[48] studies using GPCRs[42]. Protein self-assembly was first simulated for 60 μs using 3 healthy-like and 3 diseased-like replicates. One of the former simulations, namely healthy-like replicate 1 (see Fig. 5a), was simulated up to 260 μs to observe potential changes on the protein oligomer arrangement over long time-scales. A different initial arrangement of protein monomers embedded in 3 healthy-like and 3 diseased-like membrane models was used to validate the effect of DHA on protein aggregation. These systems were simulated for 60 μs to study protein aggregation and further extended up to 120 μs to inspect the stability of protein oligomers over longer time-scales. In addition, to validate the behaviour of protein aggregation in short times, 10 extra systems (i.e. 5 healthy-like and 5 diseased-like) were simulated for 16 μs. Lastly, to calculate the diffusion of protein monomers, A_{2A} and D_2 receptors were individually simulated for 32 μs in both healthy- and diseased-like environments. Altogether, an accumulated simulation time of approximately 1,630 ms was used in this study. A detailed description of the construction of the systems along with their simulation protocol can be found in the Supplementary Methods.

Cell culture and transfection. Human embryonic kidney 293T (HEK-293T) cells were grown at 37°C in an atmosphere of 5 % CO_2 in Dulbecco's modified Eagle's medium (Sigma-Aldrich, St. Louis, MO, U.S.A.) supplemented with 1 mM sodium pyruvate, 2 mM L-glutamine, 100 mg/mL streptomycin, 100 U/mL penicillin and 5 % (v/v) fetal bovine serum. The cells were seeded into six-well plates at 300,000 cells/well and transiently transfected with the corresponding cDNA constructs using Transfectin (Bio-Rad, Hercules, CA, U.S.A.) following manufacturer's instructions.

DHA fatty acid supplementation and cell viability assay. Triglyceride fish oil was kindly provided by Brudy Technology (Barcelona, Spain). This oil contains more than 70 % of DHA in total fatty acids and more than 90 % ω-3 fatty acid triglycerides. Transfected cells were incubated with media containing different amounts of DHA (namely 5, 10, 20, 30, 50, 100 and 200 μM) for 48 h. To determine the effect of DHA on cell viability we used the CALcein-AcetoxyMethyl Ester, Diacetate, (CAL-AM), a cell-permeable dye (EMD Millipore, MA, USA). In brief, HEK-293T cells (1 × 104 cells/well) were cultured in a 96-well plate at 37°C, and exposed to varying concentrations of DHA for 48 h. Cells treated with plain medium served as a negative control group, whereas cells warmed at 65°C for 1 min were used as a positive control of cell death. After removing the supernatant of each well and washing twice with PBS, a solution of 100 μl of 1.0 μM calcein-AM diluted in warm (37°C) PBS was added to cells. After an incubation period of 30 min at 37°C, fluorescence was measured in a POLARstar Optima plate-reader (BMG LABTECH GmbH, Ortenberg, Germany) at 485/535 nm.

Fatty acid analysis. The composition of fatty acids was determined using the method by Lepage and Roy[51]. The total lipids, containing 0.01 % butylhydroxytoluene as antioxidant, were transesterified with acetyl chloride during 60 min at 100°C. Gas chromatography analysis was performed on a Shimadzu GCMS-QP2010 Plus gas chromatograph-mass spectrometer (Shimadzu, Kyoto, Japan). Fatty acid methyl ester peaks were identified by their elution pattern and relative retention times with respect to a reference mixture (GLC-744 Nu-Chek Prep. Inc., Elysian MN, USA). The results were expressed in relative amounts (molar percentage of total fatty acids).

BRET experiments. HEK-293T cells were transiently trans-

fected with a constant amount (0.3 µg) of $A_{2A}{}^{Rluc}$ and increasing amounts of plasmid encoding $D_2{}^{YFP}$, namely from 0.25 to 3.7 µg. The cDNA encoding $A_{2A}{}^{Rluc}$, $D_2{}^{YFP}$ and $CD4^{YFP}$ were previously described in[40,41]. Both fluorescence and luminescence signals from each sample were measured prior to experiments to confirm equal expression of the Rluc construct while monitoring the increase in YFP expression. Cells were then treated with DHA 200 µM for 48 h and rapidly washed twice with phosphate-buffered saline, detached and re-suspended in the same buffer. Triplicate samples of cell suspension (20 µg protein) were distributed in black bottom 96-well black microplates or white bottomed 96-well white microplates (Fisher Scientific, Madrid, Spain) for fluorescence or BRET experiments, respectively. For BRET measurements, colenterazine-h substrate (NanoLight Technology, Pinetop, Arizona, USA.) was added to a final concentration of 5 µM. BRET readings were performed at 1 and 10 min using the POLARstar Optima plate reader (BMG Labtech, Durham, NC, USA). This plate reader allows detection and sequential integration of both luminescence (Rluc) and fluorescence (YFP) signals by two filter settings: 440–500 nm and 510–560 nm windows to detect 485 nm (Rluc, donor) and 530 nm (YFP, acceptor) signals, respectively. The BRET ratio (i.e. the fluorescence signal over the luminescence signal) was defined as described previously[40] and measured in 4 independent experiments where cells were treated with DHA. The values of $BRET_{MAX}$ (i.e. the maximal signal reached at saturation) and $BRET_{50}$ (i.e. BRET ratio giving 50 % of the $BRET_{MAX}$) were also calculated as in[40]. The statistical assessment of $BRET_{MAX}$ and $BRET_{50}$ values across experiments was performed using a paired t test comparing DHA-treated versus non-treated cells.

All-atom simulations. The CHARMM36[52], CHARMM36c[53] and CHARMM27[54] force fields were used to represent lipids, cholesterol and proteins, respectively. An all-atom structure of the adenosine A_{2A} receptor was embedded into an equilibrated healthy-like membrane patch (see Table 1). A equilibration phase in the NPT ensemble at 37°C and 1 bar was then carried out to allow lipids to accommodate to the protein. Subsequently, a production run of 4 µs in the NVT ensemble was performed. All-atom simulations were performed using the ACEMD simulation package[55]. A detailed description of the construction and simulation protocols is provided in the Supplementary Methods.

Analysis of MD simulations. Procedures used in the analysis of both CG- and all-atom MD simulations are shown in the Supplementary Methods.

References

1. McNamara, R. K. *et al.* Abnormalities in the fatty acid composition of the postmortem orbitofrontal cortex of schizophrenic patients: gender differences and partial normalization with antipsychotic medications. *Schizophr. Res.* **91,** 37–50 (2007).
2. McNamara, R. K. *et al.* Selective deficits in the omega-3 fatty acid docosahexaenoic acid in the postmortem orbitofrontal cortex of patients with major depressive disorder. *Biol. Psychiat.* **62,** 17–24 (2007).
3. McNamara, R. K. *et al.* Deficits in docosahexaenoic acid and associated elevations in the metabolism of arachidonic acid and saturated fatty acids in the postmortem orbitofrontal cortex of patients with bipolar disorder. *Psychiat. Res.* **160,** 285–299 (2008).
4. Taha, A. Y., Cheon, Y., Ma, K., Rapoport, S. I. & Rao, J. S. Altered fatty acid concentrations in prefrontal cortex of schizophrenic patients. *J. Psychiat. Res.* **47,** 636–643 (2013).
5. Martín, V. *et al.* Lipid alterations in lipid rafts from Alzheimer's disease human brain cortex. *J. Alzheimers Dis.* **19,** 489–502 (2010).
6. Fabelo, N. *et al.* Severe alterations in lipid composition of frontal cortex lipid rafts from Parkinson's disease and incidental Parkinson's disease. *Mol. Med.* **17,** 1107–1118 (2011).
7. Innis, S. M. Dietary omega 3 fatty acids and the developing brain. *Brain Res.* **1237,** 35–43 (2008).
8. Calon, F. & Cole, G. Neuroprotective action of omega-3 polyunsaturated fatty acids against neurodegenerative diseases: evidence from animal studies. *Prostag. Leukotr. Ess.* **77,** 287–293 (2007).
9. Tanaka, K., Farooqui, A. A., Siddiqi, N. J., Alhomida, A. S. & Ong, W.-Y. Effects of Docosahexaenoic Acid on Neurotransmission. *Biomol. Ther.* **20,** 152–157 (2012).
10. Wiegand, R. & Anderson, R. Phospholipid molecular species of frog rod outer segment membranes. *Exp. Eye Res.* **37,** 159–173 (1983).
11. Jeffrey, B. G., Weisinger, H. S., Neuringer, M. & Mitchell, D. C. The role of docosahexaenoic acid in retinal function. *Lipids* **36,** 859–871 (2001).
12. Breckenridge, W., Gombos, G. & Morgan, I. The lipid composition of adult rat brain synaptosomal plasma membranes. *Biochim. Biophys. Acta* **266,** 695–707 (1972).
13. Sun, G. & Sun, A. Phospholipids and acyl groups of synaptosomal and myelin membranes isolated from the cerebral cortex of squirrel monkey (Saimiri sciureus). *Biochim. Biophys. Acta* **280,** 306–315 (1972).
14. Valentine, R. C. & Valentine, D. L. Omega-3 fatty acids in cellular membranes: a unified concept. *Prog. Lip. Res.* **43,** 383–402 (2004).
15. Salem, N., Litman, B., Kim, H. Y. & Gawrisch, K. Mechanisms of action of docosahexaenoic acid in the nervous system. *Lipids* **36,** 945–959 (2001).
16. Akter, K. *et al.* A review of the possible role of the essential fatty acids and fish oils in the aetiology, prevention or pharmacotherapy of schizophrenia. *J. Clin. Pharm. Ther.* **37,** 132–139 (2012).
17. Bousquet, M., Calon, F. & Cicchetti, F. Impact of omega-3 fatty acids in Parkinson's disease. *Ageing Res. Rev.* **10,** 453–463 (2011).
18. Siegel, G. & Ermilov, E. Omega-3 fatty acids: benefits for cardiocerebro-vascular diseases. *Atherosclerosis* **225,** 291–295 (2012).
19. Mondal, S., Khelashvili, G., Johner, N. & Weinstein, H. *How The Dynamic Properties And Functional Mechanisms Of GPCRs Are Modulated By Their Coupling To The Membrane Environment* 55–74 (Springer Netherlands, 2014).
20. Gawrisch, K., Soubias, O. & Mihailescu, M. Insights from biophysical studies on the role of polyunsaturated fatty acids for function of G-protein coupled membrane receptors. *Prostag. Leukotr. Ess.* **79,** 131–134 (2008).
21. Catapano, L. a. & Manji, H. K. G protein-coupled receptors in major psychiatric disorders. *Biochim. Biophys. Acta* **1768,** 976–93 (2007).
22. Soubias, O., Teague, W. E. & Gawrisch, K. Evidence for specificity in lipid-rhodopsin interactions. *J. Biol. Chem.* **281,** 33233–33241 (2006).
23. Mitchell, D. C., Straume, M. & Litman, B. J. Role of *sn*-1-saturated,*sn*-2-polyunsaturated phospholipids in control of membrane receptor conformational equilibrium: effects of cholesterol and acyl chain unsaturation on the metarhodopsin I↔metarhodopsin II equilibrium. *Biochemistry-US* **31,** 662–670 (1992).
24. Polozova, A. & Litman, B. J. Cholesterol dependent recruitment of di22:6-PC by a G protein-coupled receptor into lateral domains. *Biophys. J.* **79,** 2632–2643 (2000).
25. Litman, B. J., Niu, S. L., Polozova, A. & Mitchell, D. C. The role of docosahexaenoic acid containing phospholipids in modulating G protein-coupled signaling pathways: visual transduction. *J. Mol. Neurosci.* **16,** 237–242 (2001).
26. Mitchell, D. C., Niu, S.-L. & Litman, B. J. Enhancement of G protein-coupled signaling by DHA phospholipids. *Lipids* **38,** 437–443 (2003).
27. Mitchell, D. C., Niu, S.-L. & Litman, B. J. DHA-rich phospholipids optimize G-protein-coupled signaling. *J. Pediatr.* **143,** S80–S86 (2003).

28. Niu, S.-L. *et al.* Reduced G protein-coupled signaling efficiency in retinal rod outer segments in response to n-3 fatty acid deficiency. *J. Biol. Chem.* **279,** 31098–31104 (2004).
29. Feller, S. E., Gawrisch, K. & Woolf, T. B. Rhodopsin exhibits a preference for solvation by polyunsaturated docosohexaenoic acid. *J. Am. Chem. Soc.* **125,** 4434–4435 (2003).
30. Grossfield, A., Feller, S. E. & Pitman, M. C. Contribution of omega-3 fatty acids to the thermodynamics of membrane protein solvation. *J. Phys. Chem. B* **110,** 8907–8909 (2006).
31. Milligan, G. The prevalence, maintenance, and relevance of G protein-coupled receptor oligomerization. *Mol. Pharmacol.* **84,** 158–169 (2013).
32. Ferré, S., Ciruela, F., Woods, A. S., Lluis, C. & Franco, R. Functional relevance of neurotransmitter receptor heteromers in the central nervous system. *Trends Neurosci.* **30,** 440–446 (2007).
33. Guixà-González, R., Bruno, A., Marti-Solano, M. & Selent, J. Crosstalk within GPCR heteromers in schizophrenia and Parkinson's disease: physical or just functional? *Curr. Med. Chem.* **19,** 1119–1134 (2012).
34. Ciruela, F. *et al.* G protein-coupled receptor oligomerization for what? *J. of Recept. and Signal Tr. R.* **30,** 322–330 (2010).
35. Ferré, S. *et al.* Adenosine A_{2A}-dopamine D_2 receptor-receptor heteromers. Targets for neuro-psychiatric disorders. *Parkinsonism R. D.* **10,** 265–271 (2004).
36. Ayoub, M. A. & Pfleger, K. D. G. Recent advances in bioluminescence resonance energy transfer technologies to study GPCR heteromerization. *Curr. Opin. Pharmacol.* **10,** 44–52 (2010).
37. Percherancier, Y. *et al.* Bioluminescence resonance energy transfer reveals ligand-induced conformational changes in $CXCR_4$ homo- and heterodimers. *J. Biol. Chem.* **280,** 9895–9903 (2005).
38. Marquer, C. *et al.* Influence of MT7 toxin on the oligomerization state of the M_1 muscarinic receptor. *Biol. Cell* **102,** 409–420 (2010).
39. Romero-Fernandez, W. *et al.* Agonist-induced formation of FGFR1 homodimers and signaling differ among members of the FGF family. *Biochem. Biophys. Res. Co.* **409,** 764–768 (2011).
40. Canals, M. *et al.* Adenosine A_{2A}-dopamine D_2 receptor-receptor heteromerization: qualitative and quantitative assessment by fluorescence and bioluminescence energy transfer. *J. Biol. Chem.* **278,** 46741–46749 (2003).
41. Casado, V. *et al.* Detection of heteromerization of more than two proteins by sequential BRET-FRET. *Nat. Methods* **5,** 727–733 (2008).
42. Periole, X., Knepp, A., Sakmar, T. P., Marrink, S. J. & Huber, T. Structural determinants of the supramolecular organization of G protein-coupled receptors in bilayers. *J. Am. Chem. Soc.* **134,** 10959–10965 (2012).
43. Mondal, S. *et al.* Membrane driven spatial organization of GPCRs. *Sci. Rep.* **3,** 2909 (2013).
44. Niemelä, P. *et al.* Membrane proteins diffuse as dynamic complexes with lipids. *J. Am. Chem. Soc.* **132,** 7574–7575 (2010).
45. Langelier, B., Linard, A., Bordat, C., Lavialle, M. & Heberden, C. Long chain-polyunsaturated fatty acids modulate membrane phospholipid composition and protein localization in lipid rafts of neural stem cell cultures. *J. Cell. Biochem.* **110,** 1356–1364 (2010).
46. Wassall, S. R. & Stillwell, W. Docosahexaenoic acid domains: the ultimate non-raft membrane domain. *Chem. Phys. Lip.* **153,** 57–63 (2008).
47. Shaikh, S. R. Biophysical and biochemical mechanisms by which dietary N-3 polyunsaturated fatty acids from fish oil disrupt membrane lipid rafts. *J. Nutr. Biochem.* **23,** 101–105 (2012).
48. Marrink, S. J., Risselada, H. J., Yefimov, S., Tieleman, D. P. & de Vries, A. H. The MARTINI force field: coarse grained model for biomolecular simulations. *J. Phys. Chem. B* **111,** 7812–7824 (2007).
49. Monticelli, L. *et al.* The MARTINI Coarse-grained force field: extension to proteins. *J. Chem. Theory Comput.* **4,** 819–834 (2008).
50. Hess, B. & Kutzner, C. GROMACS 4: algorithms for highly efficient, load-balanced, and scalable molecular simulation. *J. Chem. Theory Comput.* **4,** 435–447 (2008).
51. Lepage, G. & Roy, C. C. Direct transesterification of all classes of lipids in a one-step reaction. *J. Lipid Res.* **27,** 114–120 (1986).
52. Klauda, J. B. *et al.* Update of the CHARMM all-atom additive force field for lipids: validation on six lipid types. *J. Phys. Chem. B* **114,** 7830–7843 (2010).
53. Lim, J. B., Rogaski, B. & Klauda, J. B. Update of the cholesterol force field parameters in CHARMM. *J. Phys. Chem. B* **116,** 203–210 (2012).
54. MacKerell, A. & Bashford, D. All-atom empirical potential for molecular modeling and dynamics studies of proteins. *J. Phys. Chem. B* **5647,** 3586–3616 (1998).
55. Harvey, M., Giupponi, G. & Fabritiis, G. ACEMD: accelerating biomolecular dynamics in the microsecond time scale. *J. Chem. Theory Comput.* **5,** 1–9 (2009).

Acknowledgements

J.S. and R.G-G. acknowledge support from Fundació La Marató de TV3 (091010) / Instituto de Salud Carlos III FEDER (CP12/03139) / Ministerio de Educacin y Ciencia (Grant number: SAF2009-13609-C04-04) and the GLISTEN European Research Network. R.G-G. was also supported by the HPC-Europa2 project (project number: 228398) with the support of the European Commission - Capacities Area - Research Infrastructures. R.G-G., M.J. and H.M-S. thank the CSC–IT Center for Science for the computational resources provided. M.J. acknowledges financial support from the Finnish Doctoral Programme in Computational Sciences (FICS). H.M-S. acknowledges financial support from the Academy of Finland through its Centre of Excellence Programs. F.C. acknowledges support from SAF2011-24779 / Consolider-Ingenio CSD2008-00005 from Ministerio de Economía y Competitividad and ICREA Academia-2010 from the Catalan Institution for Research and Advanced Studies. Also, M.G-S. and F.C. belong to the "Neuropharmacology" and "Pain" accredited research group (Generalitat de Catalunya, 2009 SGR 232). We thank Marta Filizola's team for fruitful discussion and especially to Jennifer M. Johnston and Davide Provasi for giving critical insights and carefully reading the manuscript. We also thank Toni Giorgino, Mike Gilligan and Maria Marti-Solano for reading this manuscript. We are grateful to thank Gavin Lucas at *The Paper Mill* (www.thepapermill.eu) for critical reading and language review.

Author contributions

The whole project was conceived by R.G-G., M.J. and H.M-S. and supervised by J.S. F.C. designed all cell-based experiments. J.C.-D. designed the fatty acid analysis experiment. R.G-G., M.J. and H.M-S. performed and analysed all CG-MD simulations. R.G-G. performed and analysed the all-atom simulations. B.C. and J.C.-D. performed the fatty acid analysis. M.G-S. and F.C. performed and analysed all cell-based experiments. M.P. and F.S. gave technical support and conceptual advise. R.G-G. wrote the paper with contributions from J.S., H.M-S and M.J. and comments from all authors.

Membrane omega-3 fatty acids modulate the oligomerization of G protein-coupled receptors

Ramon Guixà-González[1], Matti Javanainen[2], Hector Martinez-Seara[2], Maricel Gómez-Soler[3], Begoña Cordobilla[4], Joan Carles Domingo[4], Ferran Sanz[1], Manuel Pastor[1], Francisco Ciruela[3] and Jana Selent[1⋆]

Supplementary Methods

COARSE-GRAINED (CG) MOLECULAR DYNAMICS SIMULATIONS.

CG models of A_{2A} and D_2 receptors. While a crystal structure[1] (PDB:3EML) was directly used as an all-atom representation of the adenosine A_{2A} receptor, a homology model of the D_2 receptor was built based on the crystal structure of the highly homologous dopamine D_3 receptor (PDB:3PBL). The intracellular loop 3, not resolved in any of the current GPCR crystal structures, was omitted in both cases and all titratable residues were left in the dominant protonation state at pH 7.0. A structure and the corresponding topology compatible with Martini force field v2.1[2] were created based on the former atomistic structure files. To preserve the tertiary structure of proteins during the simulation, an elastic network was applied between beads as a structural scaffold following the ElNeDyn approach[3]. Based on the fluctuations observed in C_α atoms during all-atom simulations of A_{2A} and D_2 receptors, force constants of 1000 kJ/mol and 250 kJ/mol were applied to the helical regions and the loops, respectively.

Construction of CG systems. Inspired by brain postmortem studies of healthy and diseased subjects[4–9], we built two multi-component lipid bilayers, namely 'healthy-like' and 'diseased-like' model membranes. To keep an adequate balance between lipid components we followed key general tendencies observed in the former studies rather than exact proportions. The aim was to create two native-like model membranes, one DHA-rich (healthy-like) and one DHA-low (diseased-like), by modifying DHA levels while preserving adequate amounts of other relevant membrane components (i.e. saturated lipids, monounsaturated lipids and cholesterol). In short, two lipid bilayers were created by arranging 450 lipids (see Table 1 in the manuscript). All lipids were initially placed randomly. The relative lipid composition of each bilayer is given in the manuscript (see Table 1). These bilayers were subsequently solvated and 10 % of the water was replaced by the antifreeze particle of Martini force field. This was followed by an equilibration phase. Thereafter, one A_{2A} and one D_2 receptors were embedded into the equilibrated lipid bilayers without compromising the lipid composition and protein excess charge was neutralized with chloride beads. Subsequently, larger systems were created based on these patches by replicating their contents independently 9 times (3×3) in the membrane plane using the `genconf` utility of GROMACS[10].The composition of these constructed systems is detailed in Supplementary Table 1a. The systems were equilibrated with protein beads constrained. Eight different starting structures were then constructed to be simulated as independent replicas for both compositions (i.e. healthy- and diseased-like). The initial coordinates for these replicas were extracted at large time intervals of 2 to 8 µs from the simulation where protein beads were constrained. This enabled a proper mixing to the lipid environment surrounding each protein. For each membrane type, three replicas were simulated for 60 µs while the remaining 5 replicas were just simulated for 16 µs to validate the effect of DHA at shorter times. One healthy-like simulations was extended up to 260 µs to observe the arrangement of protein oligomers at longer time-scales. Likewise, a similar pair of the initial systems (i.e. $3 \times$ healthy- and $3 \times$ diseased-like) were subsequently built following the same protocol but using a different initial arrangement of protein monomers. The exact composition of these second set of simulations is detailed in Supplementary Table 1b. Finally, single protein diffusion was studied

[1]Research Programme on Biomedical Informatics (GRIB), Barcelona, Spain; [2] Department of Physics, Tampere University of Technology, Tampere, Finland; [3] Facultat de Medicina, IDIBELL, Universitat de Barcelona, Barcelona, Spain; [4] Facultat de Biologia , Universitat de Barcelona, Barcelona, Spain.

⋆ Correspondence and requests for materials should be addressed to J.S. (email: jana.selent@upf.edu).

by simulating monomeric A_{2A} and D_2 receptors embedded in the initially constructed small membrane patches of both healthy- and diseased-like compositions. These systems were simulated for 32 µs.

Table 1 | Number of residues comprising both sets of CG simulations.

(a)

	Healthy-like	**Diseased-like**
DPPC	576 (14 %)	900 (22 %)
DSPC	198 (5 %)	396 (10 %)
DOPC	396 (10 %)	288 (7 %)
SDPC	576 (14 %)	162 (4 %)
SM	972 (24 %)	972 (24 %)
CHO	1332 (33 %)	1332 (33 %)
TOTAL LIPIDS	4050 (100 %)	4050 (100 %)
A_{2A}	9	9
D_2	9	9
W	44865	44028
WF	5004	4905
IONS (Cl^-)	153	153

(b)

	Healthy-like	**Disease-like**
DPPC	512 (14 %)	832 (22 %)
DSPC	192 (5 %)	384 (10 %)
DOPC	352 (10 %)	288 (7 %)
SDPC	512 (14 %)	128 (3 %)
SM	864 (24 %)	960 (25 %)
CHO	1184 (33 %)	1280 (33 %)
TOTAL LIPIDS	3616 (100 %)	3872 (100 %)
A_{2A}	8	8
D_2	8	8
W	44488	48360
WF	4960	5384
IONS (Cl^-)	136	136

Composition of **(a)** initial simulations (i.e. $2 \times [3 \times 60$ µs $+ 5 \times 16$ µs]) and **(b)** validation systems (i.e. $2 \times [6 \times 120$ µs]). In brackets, lipid percentages over total number of lipids. Lipid composition in **(a)** and **(b)** yields a protein–to–lipid ratio of 1:151 and 1:162, respectively. Abbreviations stand for for 1,2-dipalmitoyl-*sn*-glycero-3-phosphocholine (DPPC), 1,2-distearoyl-*sn*-glycero-3-phosphocholine (DSPC), 1,2-dioleyl-*sn*-glycero-3-phosphocholine (DOPC), 1-stearoyl-2-docosahexaenoyl-*sn*-glycero-3-phosphocholine (SDPC) and sphingomyelin (SM18), cholesterol (CHO), water beads (W) and Martini antifreeze particles (WF), respectively.

CG simulation protocol. All simulations were performed using the GROMACS 4.5 simulation package[10] using a time step of 10 fs in the NPT ensemble. The temperature was kept constant at 37°C with the Berendsen thermostat[11] using a relaxation time constant of 1 ps. Membrane and solvent components were coupled separately. The pressure was coupled semi-isotropically with the Berendsen barostat[11] using a relaxation time constant of 5 ps and a reference pressure of 1 bar. The shift approach was employed for non-bonded interactions. The electrostatic interactions were shifted to zero between 0 and 1.2 nm whereas for Lennard-Jones interactions the shifting was conducted between 0.9 and 1.2 nm. The neighbour list with a radius of 1.2 nm was updated every 10 steps. Periodic boundary conditions were employed in all three dimensions.

Protein and lipid diffusion. The `g_msd` tool of GROMACS package[10] was used to perform all mean squared displacement (MSD) calculations. Lipid lateral diffusion was studied in multi-protein systems once most of the protein–protein contacts were established. Thus, the last 30 µs of the trajectories were employed for the analysis. All lipid species were considered separately and the center of mass of the whole membrane was removed. Lipid diffusion coefficients were extracted as the slope of a linear fit to the calculated MSD data, as defined in equation (1):

$$D = \lim_{\tau \to \infty} \frac{\mathrm{MSD}(\tau)}{4\tau} = \lim_{\tau \to \infty} \frac{\langle [\vec{r}(t+\tau) - \vec{r}(t+0)]^2 \rangle_t}{4\tau}, \tag{1}$$

where t is the simulation time and τ is the lag time. The fits were performed to the MSD curve in the lag time interval between 3 and 27 µs.
Protein lateral and rotational diffusion was studied in the single-protein systems described earlier. Protein lateral diffusion coefficients were obtained from a linear fit of equation (1) to the lag time interval of 0.8–4 µs. In the calculation of both protein and lipid diffusion coefficients, error estimates were reported as the difference of the diffusion coefficients obtained from fits to two halves of the whole fit interval. Rotational diffusion of proteins was also studied on single-protein simulations using the `g_rotacf` tool of GROMACS[10]. The 2nd order Legendre polynomial was employed and the obtained curves were fitted using an exponentially decaying function.

Radial Distribution Functions (RDFs). The RDFs of lipids around proteins were calculated using the `g_rdf` tool of GROMACS[10]. RDF values are reported as averages over the three 60 µs replicas for both compositions.

ALL-ATOM MOLECULAR DYNAMICS SIMULATIONS.

Construction of all-atom systems. A healthy-like model membrane (see Table 1 in the manuscript) of approximately 100 × 100 Å^2 (in the membrane plane) was built using the CHARMM-GUI membrane builder[12]. Since sphingomyelin is not a standard lipid of CHARMM force field, a VMD1.9[13] script was employed to mutate the pertinent fraction of DSPC molecules into 18-carbon sphingomyelin (SM). SM topology and additional parameters were created by a generalization approach using the CGenFF force field[14,15] version 2b6 using the CHARMM ParamChem interface v0.9.1 (https://www.paramchem.org). No high penalty scores were obtained in the former process. Thereafter, a VMD1.9[13] script was used to re-hydrate the membrane patch using approximately 30 water molecules (TIP3 model) per lipid and the system was neutralize with 150 mM NaCl. Subsequently, the membrane was equilibrated for 1 µs in the NPT ensemble. Next, the crystal structure of the adenosine A_{2A} receptor[1] (PDB:3EML) was manually embedded into the equilibrated membrane patch using VMD1.9[13]. This protein structure was prepared as described earlier. The final combined membrane–protein system comprised a total of 112,357 atoms. Table 2 gives a detailed composition of such system.

Table 2 | Number of residues comprising the atomistic simulation.

Component	Num
DPPC	48 (15 %)
DSPC	18 (6 %)
DOPC	36 (11 %)
SDPC	44 (14 %)
SM	79 (24 %)
CHO	112 (34 %)
TOTAL LIPIDS	337 (100 %)
A_{2A}	1
W	8155
Na^-	75
Cl^-	65

The number of residues of each component is shown. In brackets, lipid percentages over total number of lipids. The lipid composition yields a protein–to–lipid ratio of 1:337. Abbreviations stand for for 1,2-dipalmitoyl-*sn*-glycero-3-phosphocholine (DPPC), 1,2-distearoyl-*sn*-glycero-3-phosphocholine (DSPC), 1,2-dioleyl-*sn*-glycero-3-phosphocholine (DOPC), 1-stearoyl-2-docosahexaenoyl-*sn*-glycero-3-phosphocholine (SDPC) and sphingomyelin (SM18), cholesterol (CHO) and water (W), respectively.

An NPT equilibration phase was then carried out on so that lipids and water molecules could accommodate to the protein. To this end, harmonic positional constraints were applied to the C_α atoms of the protein and the system was simulated for 10 ns. Such constraints were gradually released from the receptor over 5 ns and the system was further equilibrated for 100 ns. In the production run, we simulated the system for 4 µs in the NVT ensemble. The ACEMD simulation package[16] was used. NPT simulations were carried out at 37°C and 1 bar using the Berendsen barostat[11] with a relaxation time of 400 fs and 2 fs integration time step. NVT simulations were run at 37°C, using the Langevin thermostat[17] with a damping coefficient of 5 ps^{-1} and 4 fs integration time step. In all simulation phases, van der Waals and short-range electrostatic interactions were cut off at 9 Å and the particle mesh Ewald method[18] was used to compute the long-range electrostatic interactions.

Analysis of lipid–protein contact ratios in all-atom MD simulations. We measured the ratio of lipid–protein contact between two groups (e.g. two lipid species) by calculating the number of contacts per atom of the first group divided by the number of contact per atom of the second group. Atoms were considered in contact when located at < 4.2 Å of the COM of the protein. For this analysis only atoms in the lipid tails are considered. To facilitate the interpretation of the results, each contact value was previously normalized by the the total number of atoms belonging to that particular selection. For example, in the SDPC/SAT ratio, SDPC is calculated as the number of atoms of any SDPC chain < 4.2 Å of protein's COM divided by the total number of SDPC chain atoms in the system. Likewise, SAT is calculated in the former ratio as the number of atoms of any saturated chain < 4.2 Å of protein's COM divided by the total number atoms of saturated chains in the system.

FIGURE ART.

The built-in Tachyon ray tracer of VMD1.9[13] was used to render all snapshots from both CG and all-atom simulations. The ggplot2 R package[19] was used to generate plots on protein aggregation and lipid–protein contact ratios.

References

1. Jaakola, V., Griffith, M. & Hanson, M. The 2.6 Angstrom crystal structure of a human A_{2A} adenosine receptor bound to an antagonist. *Science* **322,** 1211–1217 (2008).
2. Monticelli, L. *et al.* The MARTINI coarse-grained force field: extension to proteins. *J. Chem. Theory Comput.* **4,** 819–834 (2008).
3. Periole, X., Cavalli, M., Marrink, S. J. & Ceruso, M. A. Combining an elastic network with a coarse-grained molecular force field: structure, dynamics, and intermolecular recognition. *J. Chem. Theory Comput.* **5,** 2531–2543 (2009).
4. McNamara, R. K. *et al.* Selective deficits in the omega-3 fatty acid docosahexaenoic acid in the postmortem orbitofrontal cortex of patients with major depressive disorder. *Biol. Psychiat.* **62,** 17–24 (2007).
5. McNamara, R. K. *et al.* Abnormalities in the fatty acid composition of the postmortem orbitofrontal cortex of schizophrenic patients: gender differences and partial normalization with antipsychotic medications. *Schizophr. Res.* **91,** 37–50 (2007).
6. Deficits in docosahexaenoic acid and associated elevations in the metabolism of arachidonic acid and saturated fatty acids in the postmortem orbitofrontal cortex of patients with bipolar disorder. *Psychiat. Res.* **160,** 285–299 (2008).
7. Martín, V. *et al.* Lipid alterations in lipid rafts from Alzheimer's disease human brain cortex. *J. Alzheimers Dis.* **19,** 489–502 (2010).
8. Fabelo, N. *et al.* Severe alterations in lipid composition of frontal cortex lipid rafts from Parkinson's disease and incidental Parkinson's disease. *Mol. Med.* **17,** 1107–1118 (2011).
9. Taha, A. Y., Cheon, Y., Ma, K., Rapoport, S. I. & Rao, J. S. Altered fatty acid concentrations in prefrontal cortex of schizophrenic patients. *J. Psychiat. Res.* **47,** 636–643 (2013).
10. Hess, B. & Kutzner, C. GROMACS 4: algorithms for highly efficient, load-balanced, and scalable molecular simulation. *J. Chem. Theory Comput.* **4,** 435–447 (2008).
11. Berendsen, H. J., Postma, J. P. M., van Gunsteren, W. F., DiNola, A. & Haak, J. Molecular dynamics with coupling to an external bath. *J. Chem. Phys.* **81,** 3684–3690 (1984).
12. Jo, S., Lim, J. J. B., Klauda, J. J. B. & Im, W. CHARMM-GUI membrane builder for mixed bilayers and its application to yeast membranes. *Biophys. J.* **96,** 50–58 (2009).
13. Humphrey, W., Dalke, A. & Schulten, K. VMD: visual molecular dynamics. *J. Mol. Graphics* **14,** 33–38 (1996).
14. Vanommeslaeghe, K & MacKerell, A. D. Automation of the CHARMM General Force Field (CGenFF) I: bond perception and atom typing. *J. Chem. Inf. Model* **52,** 3144–3154 (2012).
15. Vanommeslaeghe, K, Raman, E. P. & MacKerell, A. D. Automation of the CHARMM General Force Field (CGenFF) II: assignment of bonded parameters and partial atomic charges. *J. Chem. Inf. Model* **52,** 3155–3168 (2012).
16. Harvey, M., Giupponi, G & Fabritiis, G. ACEMD: accelerating biomolecular dynamics in the microsecond time scale. *J. Chem. Theory Comput.* **5,** 1–9 (2009).
17. Grest, G. & Kremer, K. Molecular dynamics simulation for polymers in the presence of a heat bath. *Phys. Rev. A* **33,** 3628–3631 (1986).
18. Darden, T., York, D. & Pedersen, L. Particle mesh Ewald: An $N \cdot \log(N)$ method for Ewald sums in large systems. *J. Chem. Phys.* **27709,** 13–16 (1993).
19. Wickham, H. *Ggplot2: Elegant Graphics For Data Analysis* (Springer New York, 2009).

Membrane omega-3 fatty acids modulate the oligomerization of G protein-coupled receptors

Ramon Guixà-González[1], Matti Javanainen[2], Hector Martinez-Seara[2], Maricel Gómez-Soler[3], Begoña Cordobilla[4], Joan Carles Domingo[4], Ferran Sanz[1], Manuel Pastor[1], Francisco Ciruela[3] and Jana Selent[1⋆]

Supplementary Figures

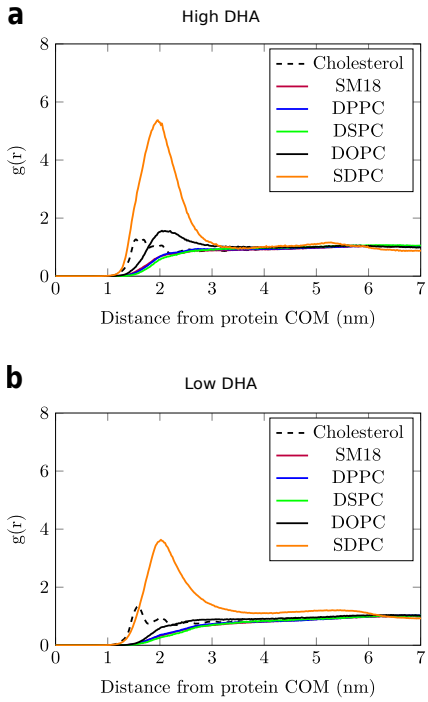

Figure 1 | Radial distribution function of lipids around proteins during CG-MD simulations. Probability density (i.e. radial distribution function, $g(r)$) of lipids around the center of mass of D_2 receptors embedded in healthy- (high DHA, **(a)**) and diseased-like (low DHA, **(b)**) model membranes. y and x axes represent $g(r)$ (arbitrary units) and distance (nm), respectively.

[1]Research Programme on Biomedical Informatics (GRIB), Department of Experimental and Health Sciences Universitat Pompeu Fabra, IMIM (Hospital del Mar Medical Research Institute), Spain; [2] Department of Physics, Tampere University of Technology, Tampere, Finland; [3] Facultat de Medicina, IDIBELL, Universitat de Barcelona, Barcelona, Spain; [4] Facultat de Biologia , Universitat de Barcelona, Barcelona, Spain.

⋆ Correspondence and requests for materials should be addressed to J.S. (email: jana.selent@upf.edu).

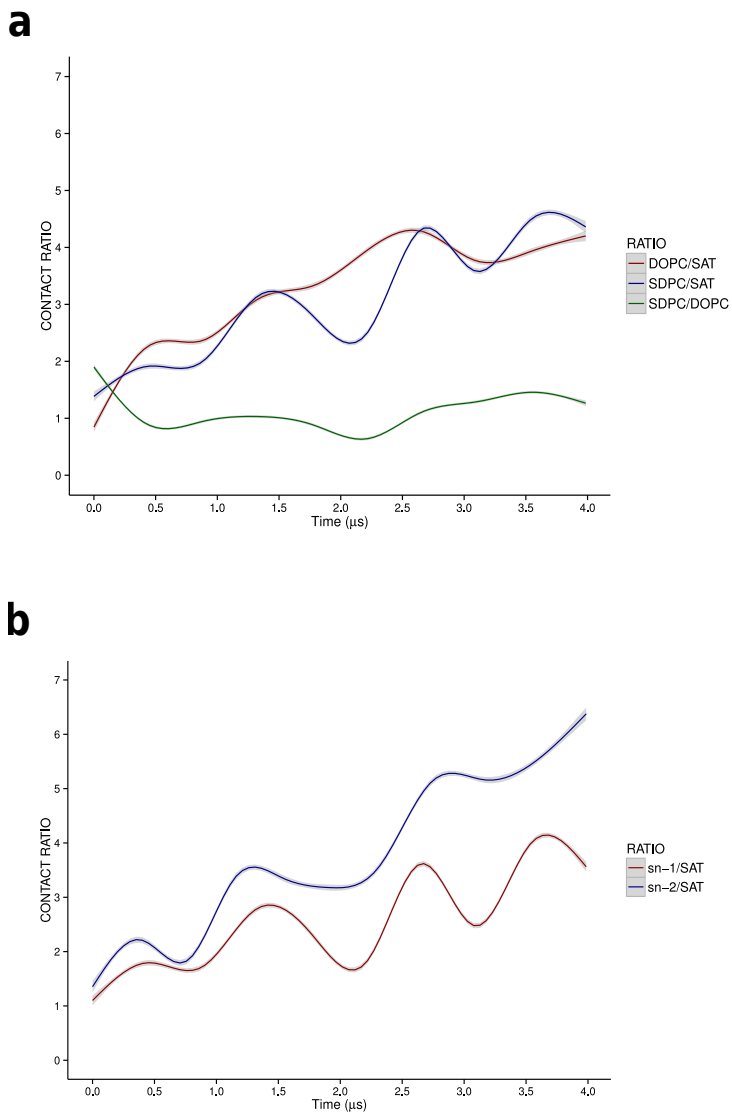

Figure 2 | Evolution of lipid–protein contacts during the all-atom simulation. The relative proportion of atomic lipid–protein contacts (x axis) over time (y axis) is displayed (details on the calculation of these ratios are given in the Supplementary Methods). Fig **(a)** shows the evolution of 3 different contact ratios during the simulation, namely DOPC chains versus all saturated chains (i.e. DOPC / SAT), SDPC chains versus all saturated chains (i.e. SDPC /SAT) and DOPC chains versus SDPC chains (i.e. DOPC / SDPC). Fig **(b)** display the contact ratio of each SDPC chain versus all saturated chains (i.e. *sn*-1 / SAT and *sn*-2 /SAT). In all plots, SAT stands for all saturated chains. Coloured lines represent the smoothed average surrounded by the standard error.

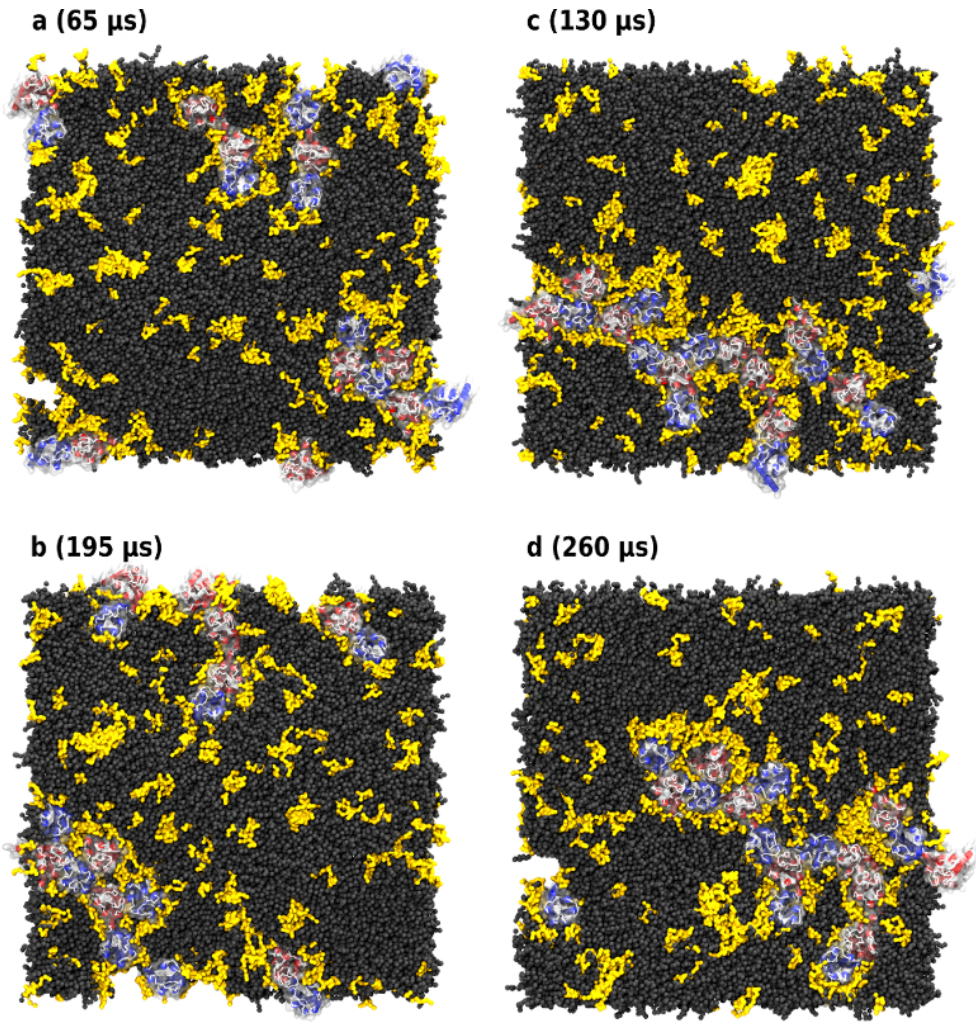

Figure 3 | Long-scale behaviour of protein oligomers. To study long-scale behaviour of protein oligomers, we extended the simulation of one of healthy-like systems from 60 to 260 µs (see Methods). **(a)**, **(b)**, **(c)** and **(d)** display snapshot of the extended simulation at 65, 130, 195 and 260 µs, respectively. A_{2A} and D_2 helices are depicted in red and blue cartoons, respectively, whereas protein loops are in thin white cylinders. Protomers are surrounded by a white transparent surface. Grey spheres correspond to a van der Waals representation of all membrane lipids except for SDPC molecules, depicted in yellow surface. Water molecules, ions and anti-freezing particles were omitted for clarity.

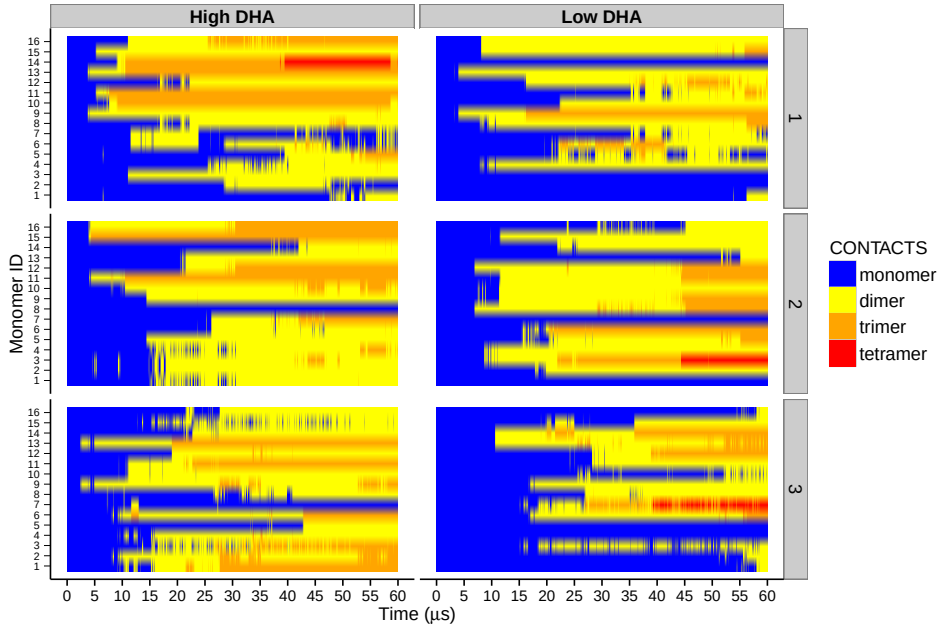

Figure 4 | Time-dependence of protein aggregation in CG-MD simulations starting from different initial arrangements of protomers. Healthy-like (i.e. DHA-high, left) and diseased-like (DHA-low, right) systems where each cell represents one replicate. Each number in the y axis represents one GPCR protomer and time extends along the x axis.

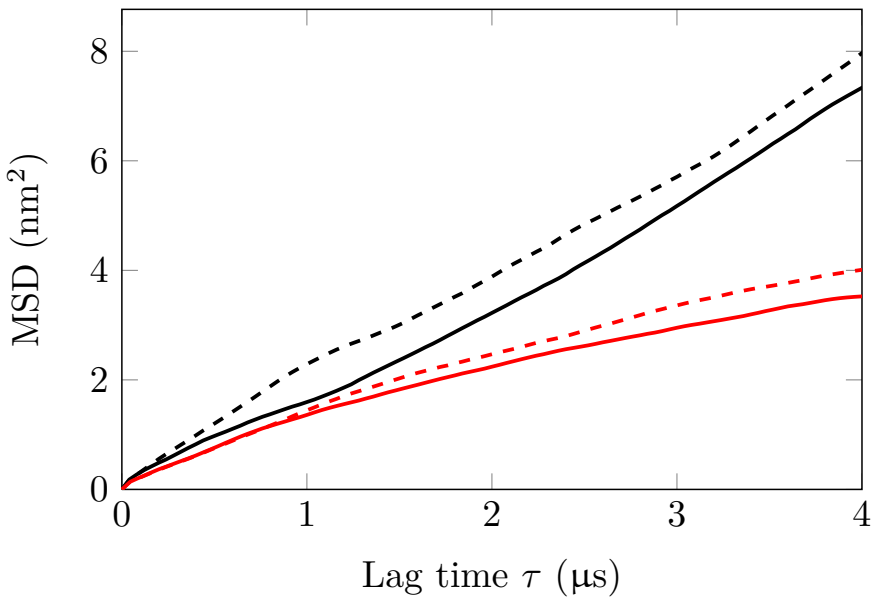

Figure 5 | Mean squared displacement (MSD) of proteins. Data show the average MSD of proteins embedded in healthy-like (black curve) and diseased-like (red curve) membrane environments.

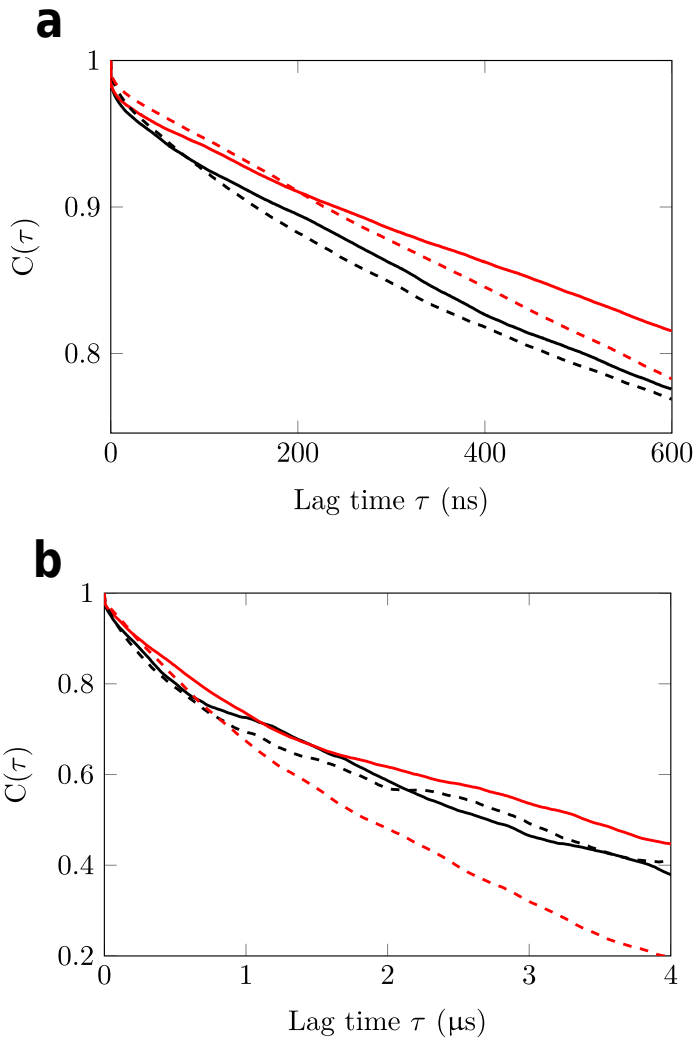

Figure 6 | Rotational autocorrelation of protein motion over short (a) and long (b) times. Second order Lagrange polynomial is employed as the rotational autocorrelation function, $C(\tau)$, and plotted in the y axis. Lag time τ, in µs, extends along the x axis. Solid and dashed lines correspond to A_{2A} and D_2 whereas black and red stand for healthy- and diseased-like systems, respectively.

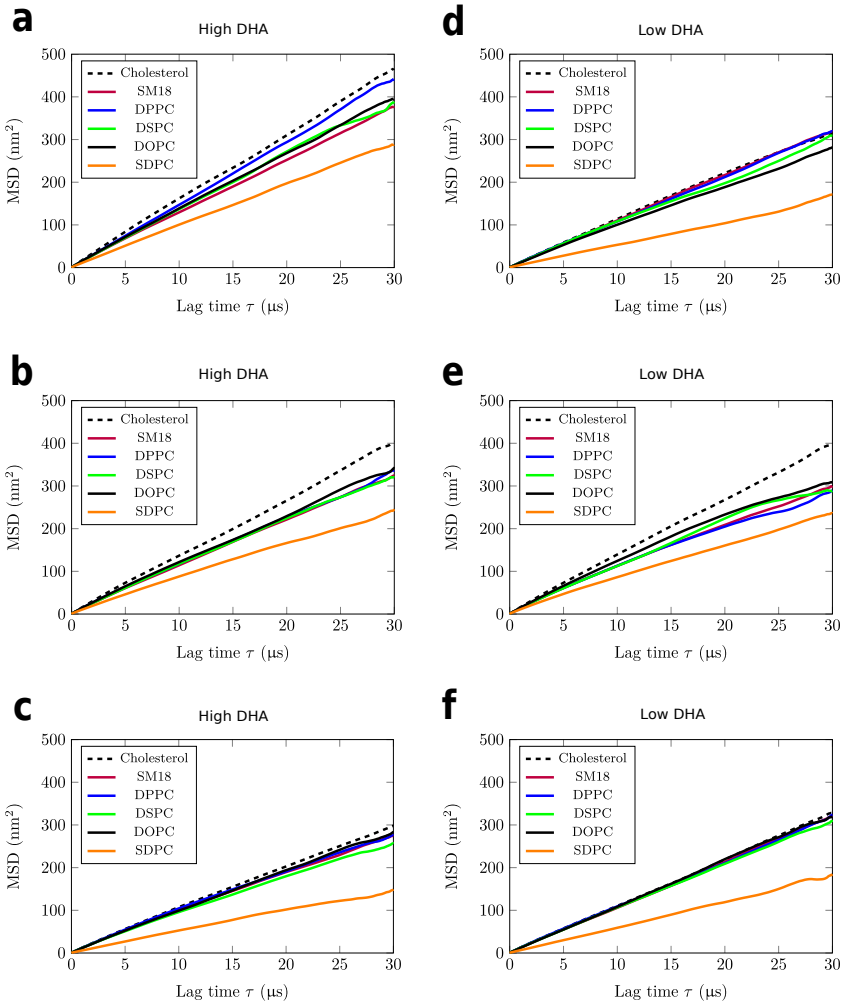

Figure 7 | Mean squared displacement (MSD) of lipids during CG-MD simulations. The mean squared displacement for each lipid species in healthy- (high DHA, **(a–c)**) and diseased-like systems (low DHA, **(d–e)**). MSDs are plotted in the y axis, in nm^2, while lag time τ, in µs, extends along the x axis. Each cell represents one replicate

Chapter 4

DISCUSSION

Molecular dynamics simulations (MD) have emerged as one of the most useful computational approaches to complement experimental techniques in the field of membrane and membrane–protein biophysics. However, native-like membranes and membrane–protein systems require highly complex analyses and simulation techniques to adequately characterize their biophysical properties. Therefore, in this thesis, we first built and developed a solid knowledge base of the MD protocols needed to model complex protein–lipid environments (Publications 3.1, 3.2 and 3.3). Secondly we developed a tool devoted to the analysis of lipid bilayers and membrane–protein simulations (Publication 3.4.1) and, lastly, we shed light on the coupling between the membrane and G protein-coupled receptors (GPCRs) by a mixed computational/experimental case study highly relevant to brain disease (Publication 3.5.

A comprehensive analysis and biophysical characterization of membrane simulations by computational approaches covers a wide set of structural parameters. These parameters are rather of different nature so that frequently each measurement needs different methodologies, algorithms and tools. To date, there is a lack of tools that have unified the analysis of the structural properties of membranes and membrane–protein simulations. Some studies have separately approached methods like the calculation of membrane thickness maps [245, 246], area per lipid [247,

248, 249] or membrane deformation profiles [231]. Recently, an interesting collection of methods to calculate membrane local properties has been developed [177] as an analysis tool of the simulation package GROMACS [144]. This versatile software efficiently computes local membrane thickness, area per lipid, curvature and deuterium order parameters from molecular simulations.

None one of the former methodologies offers, however, a graphical user interface for the automated analysis of membrane–protein simulations in VMD [171], a popular open-source package for molecular modeling and visualization. This thesis was partly devoted to the development of MEMBPLUGIN [250] (Publication 3.4.1), a graphical user interface plugin for VMD that unifies the calculation of chain order parameters, area per lipid, membrane thickness and deformation profiles, and tilt angle. In addition to standard measurements, MEMBPLUGIN provides novel algorithms to measure lipid chain interdigitation, a parameter that gives valuable information on the coupling extent between membrane leaflets and is thought to be involved in membrane events of biological relevance[184].

The first release of MEMBPLUGIN is hosted in Sourceforge: http://sourceforge.net/projects/membplugin/, and licensed under the General Public License version 3.0 (GPLv3). Overall, MEMBPLUGIN offers an unified computational framework for a comprehensive biophysical characterization of membrane and membrane–protein simulations which is multi-platform and freely available to the scientific community. In addition, we created a hands-on tutorial and a validation case study, where we use MEMBPLUGIN to characterize the effect of gradually increasing cholesterol content in a series of lipid bilayer simulations (Publication 3.4.1). Future efforts will be made to release new versions of this tool that cover the analysis of more complex membranes such as non-planar bilayers or new biophysical characterizations such as bivariate radial distribution functions.

The final aim of this thesis was to apply MD simulations to study the interplay between membrane lipids and the organization of GPCRs. This aim was partly inspired by the observation that levels of certain membrane

polyunsaturated fatty acids (PUFAs) are reduced in the brains of individuals with relevant neurological disorders like schizophrenia [101, 102, 103], Alzheimer [56], or Parkinson's disease [55]. This deficiency could affect the function of key membrane proteins like GPCRs, which are also especially relevant for psychiatric conditions. The fact that GPCR dimers and higher order oligomers regulate the function of these receptors raises one intriguing question: do the reduced levels of certain membrane lipids found in diseased brains affect GPCR oligomerization?

Recent studies [134, 135, 61] have demonstrated the influence of the hydrophobic mismatch in the spatial organization of GPCRs. These approaches have focused on the contribution of the energy penalty associated to the inability of membranes to deform around GPCRs [133, 231] and highlight the potential role of different lipid matrices on the aggregation of GPCRs [251, 252]. Moreover, Goddard et al. have validated experimental protocols using fluorescence energy transfer techniques in liposomes to shed light on the contribution of various lipid types to the oligomerization of neurotensin receptor 1 [136]. However, there is no reported evidence of specific fatty acids like the docosahexeanoic acid (DHA), which seem to have a special affinity for GPCRs, modulating the aggregation of these receptors in the membrane.

Demonstrating a connection between ω-PUFAs like DHA and GPCR oligomerization could change treatment paradigms for neurological disorders by creating an opportunity to explore the use of membrane lipids as a therapeutic tool. As we review in [129], the adenosine A_{2A} and dopamine D_2 receptors have shown to establish an antagonistic crosstalk in certain parts of the brain. In fact, the the adenosine A_{2A}-D_2 heteromer [128] seems to be specially relevant in schizophrenia and Parkinson's disease and the target of current clinical studies [130]. Therefore, the ultimate effort of this thesis has been dedicated to study the influence of DHA-rich and DHA-poor membranes on the organization of the adenosine A_{2A}-D_2 heteromer in the membrane.

We have used computational prediction methods backed up by laboratory validation to show that DHA-rich membranes enhance A_{2A}-D_2 oligomerization (Publication 3.5). These results provide the first reported

evidence of a molecular link between membrane levels of ω-PUFAs and GPCR oligomerization. This represents an important advance in understanding the interplay between membrane lipids and key transmembrane proteins like GPCRs, which is a current research priority in membrane biophysics. Most importantly, these findings create new opportunities to explore the use of membrane lipids as a therapeutic tool for major neuropsychiatric conditions, specifically Schizophrenia or Parkinson's disease, in which the A2A-D2 heteromer has been shown to have particular importance. In addition, this work opens the door for similar studies on other GPCR oligomers known to be involved in neurological diseases.

All in all, in this thesis we have advanced in the understanding of the interplay between membrane lipid and GPCRs using MD simulations. Nonetheless, MD simulations have inherent limitations and the results from analyzing MD trajectories need to be interpreted with caution. As we have discussed here, the lack of adequate statistical sampling is one of the main drawback of most current MD simulations [223, 224] and, particularly, when studying biological events that evolve in long timescales. We strongly believe that combined approaches of experiments and computer simulations are not only needed to validate theoretical results but should be established as a standard framework.

Chapter 5

CONCLUSIONS

1. The biophysical characterization of highly complex membranes and membrane–protein simulations requires a comprehensive study of their biophysical properties. Therefore, we have developed and validated an analytical framework to compute membrane local properties by using classical and novel algorithms.

2. Only a few computational tools have been developed to study the complexity of biological membranes and membrane–protein simulations through an automated application. To bridge this gap, we have wrapped up our analytical framework in one open-source tool, MEMBPLUGIN, which we have made available to the scientific community as a plugin for VMD, one of the most popular software for molecular visualization and modeling.

3. The role of membrane lipids on the dimerization of GPCRs remains, to date, largely unknown. In this thesis, we have demonstrated that different levels of membrane ω-3 polyunsaturated fatty acids modulate the oligomerization of adenosine A_{2A}-dopamine D_2 receptors, a relevant heteromer in major neuropsychiatric conditions such as schizophrenia and Parkinson's disease. Thus, we show how combining molecular dynamics simulations and experiments is a suitable tool to study membrane-dependent oligomerization of G protein-coupled receptors.

Chapter 6

LIST OF COMMUNICATIONS

ARTICLES

1. Guixà-González R., Bruno A., Marti-Solano M. and Selent J. Crosstalk within GPCR heteromers in schizophrenia and Parkinson's disease: physical or just functional? *Curr. Med. Chem.*, **19**, 1119–1134 (2012).

2. Kazcor A. A., Guixà-González R., Carrió P., Obiol-Pardo C., Pastor M. and Selent J. Fractal dimension as a measure of surface roughness of G protein-coupled receptors: implications for structure and function. *J. Mol. Model.*, **18**, 4465–4475 (2012).

3. Selent J., Kazcor A. A., Guixà-González R., Carrió P., Pastor M. and Obiol-Pardo C. Rational design of the survivin/CDK4 complex by combining protein-protein docking and molecular dynamics simulations. *J. Mol. Model.*, **19**, 1507–1514 (2013).

4. Guixà-González R., Sadiq SK. K., Dainese E., Pastor M., De Fabritiis G. and Selent J. Molecular modeling and simulation of membrane lipid-mediated effects on GPCRs. *Curr. Med. Chem.*, *20*, 22–38 (2013).

5. Guixà-González R., Ramírez-Anguita J. M., Kazcor A. A. and Selent J. Simulating G Protein- Coupled Receptors in Native-Like

Membranes: From Monomers to Oligomers. *Methods Cell Biol. (Elsevier*, **117**, 63–90 (2013).

6. Marti-Solano M., Guixà-González R., Sanz F., Pastor M. and J. Selent. Novel insights into biased agonism at G protein-coupled receptors and their potential for drug design. *Curr. Pharm. Design*, **19**, 5156–5166 (2013).

7. Guixà-González R., Rodriguez-Espigares I., Ramírez-Anguita J. M., Carrió-Gaspar P., Martinez-Seara M., Giorgino T. and Selent J. MEMBPLUGIN: studying membrane complexity in VMD. *Bioinformatics*, **30**, 1478-1480 (2014).

8. Kazcor A. A., Marti-Solano M., Guixà-González R., and Selent J. Recent Progress on Modeling G Protein-Coupled Receptors (GPCRs). *Biotechnology (Studium Press LLC)*, In press (2014).

9. Marti-Solano M., Kazcor A. A., Guixà-González R., and Selent J. Computational Strategies to Incorporate GPCR Complexity in Drug Design. *Frontiers in Computational Chemistry (Bentham Science Publishers)*, In press (2014).

10. Guixà-González R., Javanainen M., Martinez-Seara H., Gomez-Soler M., Cordobilla B., Domingo J. C., Sanz F., Pastor M., Ciruela F. and Selent J. Membrane omega-3 fatty acids modulate the oligomerization of G protein-coupled receptors. *Nature Commun.*, Manuscript under first revision, (2014).

CONFERENCES

1. *Exploring G protein-coupled receptors oligomerization interface with Adaptive Poisson-Boltzmann solver (APBS)*. Membrane Proteins: Structure and Function, MGMG Spring Meeting, Oxford (UK). April 2010.

2. *A novel approach for predicting GPCR oligomerization based on classical protein-protein docking and surface roughness*. International Symposium on Medicinal Chemistry, Brussels (Belgium). September 2010.

3. *Fractal properties of GPCRs I: analysis of surface roughness*. International Symposium on Medicinal Chemistry, Brussels (Belgium). September 2010.

4. *Fractal properties of GPCRs II: identification of classical and novel binding sites*. International Symposium on Medicinal Chemistry, Brussels (Belgium). September 2010.

5. *Fractal properties of GPCRs III: is the oligomerization interface smooth or rough?*. International Symposium on Medicinal Chemistry, Brussels (Belgium). September 2010.

6. *Allosteric modulation of GPCRs by the membrane environment*. 22nd International Symposium on Medicinal Chemistry, EFMC-ISMC, Berlin (Germany). September 2012.

7. *In the search of electrostatic complementarity in GPCR dimer interfaces*. 22nd International Symposium on Medicinal Chemistry, EFMC-ISMC, Berlin (Germany). September 2012.

8. *Lipid rafts behavior in CNS disorders: a computational case-study for Parkinson's disease*. 22nd International Symposium on Medicinal Chemistry, EFMC-ISMC, Berlin (Germany). September 2012.

9. *Multi-component protocol for modeling dimers of G protein-coupled receptors*. 22nd International Symposium on Medicinal Chemistry, EFMC-ISMC, Berlin (Germany). September 2012.

10. *Searching for dimerization interface of the D2R-mGluR5 heterodimer in different conformational states*. 22nd International Symposium on Medicinal Chemistry, EFMC-ISMC, Berlin (Germany). September 2012.

11. *Building the Survivin/CDK4 complex by combining protein-protein docking and molecular dynamics simulations*. 22nd International Symposium on Medicinal Chemistry, EFMC-ISMC, Berlin (Germany). September 2012.

12. *Excessive order of lipid rafts in Parkinson's disease*. Lipid-Protein Interactions Meeting, Biophysical Society. Hyderabad (India), November 2013.

13. *Modeling GPCR dimerization*. Drug Discovery and Selection - When Chemical Biology meets Drug Design, Nice (France). July 2013.

14. *Cell membrane composition affects GPCR aggregation*. Biophysical Society 58th Annual Meeting, San Francisco (USA). February 2014.

15. *Studying complex membrane environments and GPCRs using MEMBPLUGIN*. GPCR Spring Conference, Barcelona (Spain). April 2014.

16. ORAL COMMUNICATION: *Membrane omega-3 fatty acids modulate the oligomerization of G protein-coupled receptors)*. GPCR Spring Conference, Barcelona (Spain). April 2014.

Chapter 7

BIBLIOGRAPHY

[1] Pierce K.L., Premont R.T., and Lefkowitz R.J. Seven-transmembrane receptors. *Nat. Rev. Mol. Cell Bio.* **3**, 639–650 (2002).

[2] De Mendoza A., Sebé-Pedrós A., and Ruiz-Trillo I.n. The Evolution of the GPCR Signaling System in Eukaryotes: Modularity, Conservation, and the Transition to Metazoan Multicellularity. *Genome Bio. and Evol.* **6**, 606–619 (2014).

[3] Overington J.P., Al-Lazikani B., and Hopkins A.L. How many drug targets are there? *Nat. Rev. Drug Discov.* **5**, 993–996 (2006).

[4] Katritch V., Cherezov V., and Stevens R.C. Structure-function of the G protein-coupled receptor superfamily. *Annu. Rev. of Pharmacol.* **53**, 531–556 (2013).

[5] Fredriksson R., Lagerström M.C.M., Lundin L.G., and Schiöth H.B. The G-protein-coupled receptors in the human genome form five main families. Phylogenetic analysis, paralogon groups, and fingerprints. *Mol. Pharmacol.* **63**, 1256–1272 (2003).

[6] Salon J.A., Lodowski D.T., and Palczewski K. The Significance of G Protein-Coupled Receptor Crystallography for Drug Discovery. *Pharmacol. Rev.* **63**, 901–937 (2011).

[7] Stevens R.C., Cherezov V., Katritch V., Abagyan R., Rosen H., and Wüthrich K. GPCR Network: a large-scale collaboration on GPCR structure and function. *Nat. Rev. Drug Discov.* **12**, 25–34 (2014).

[8] Palczewski K., Kumasaka T., Hori T., Behnke C.A., Motoshima H., Fox B.A., Le Trong I., Teller D.C., Okada T., Stenkamp R.E., Yamamoto M., and Miyano M. Crystal structure of rhodopsin: AG protein-coupled receptor. *Science* **289**, 739–745 (2000).

[9] Cherezov V., Rosenbaum D.M., Hanson M.A., Rasmussen S.r.G.F., Thian F.S., Kobilka T.S., Choi H.j., Kuhn P., Weis W.I., Kobilka B.K., and Stevens R.C. High-resolution crystal structure of an engineered human beta2-adrenergic G protein-coupled receptor. *Science* **318**, 1258–1265 (2007).

[10] Rasmussen S.r.G.F., Choi H.J., Rosenbaum D.M., Kobilka T.S., Thian F.S., Edwards P.C., Burghammer M., Ratnala V.R.P., Sanishvili R., Fischetti R.F., Schertler G.F.X., Weis W.I., and Kobilka B.K. Crystal structure of the human beta2 adrenergic G-protein-coupled receptor. *Nature* **450**, 383–387 (2007).

[11] Rosenbaum D.M., Cherezov V., Hanson M.A., Rasmussen S.r.G.F., Thian F.S., Kobilka T.S., Choi H.J., Yao X.J.J., Weis W.I., Stevens R.C., and Kobilka B.K. GPCR engineering yields high-resolution structural insights into beta2-adrenergic receptor function. *Science* **318**, 1266–1273 (2007).

[12] Rasmussen S.r.G.F., Choi H.J., Fung J.J., Pardon E., Casarosa P., Chae P.S., Devree B.T., Rosenbaum D.M., Thian F.S., Kobilka T.S., Schnapp A., Konetzki I., Sunahara R.K., Gellman S.H., Pautsch A., Steyaert J., Weis W.I., and Kobilka B.K. Structure of a nanobody-stabilized active state of the $\beta(2)$ adrenoceptor. *Nature* **469**, 175–180 (2011).

[13] Rasmussen S.r.G.F., DeVree B.T., Zou Y., Kruse A.C., Chung K.Y., Kobilka T.S., Thian F.S., Chae P.S., Pardon E., Calinski D.,

Mathiesen J.M., Shah S.T.a., Lyons J.a., Caffrey M., Gellman S.H., Steyaert J., Skiniotis G., Weis W.I., Sunahara R.K., and Kobilka B.K. Crystal structure of the $\beta 2$ adrenergic receptor-Gs protein complex. *Nature* **477**, 549–555 (2011).

[14] Wenk M.R. Lipidomics: new tools and applications. *Cell* **143**, 888–895 (2010).

[15] Schley D., Whittaker R.J., and Neuman B.W. Arenavirus budding resulting from membrane curvature. *J. R. Soc. Interface* **10** (2013).

[16] Li X., Garrity A.G., and Xu H. Regulation of membrane trafficking by signalling on endosomal and lysosomal membranes. *J. Physiol.* **591**, 4389–4401 (2013).

[17] Walter J. and van Echten-Deckert G. Cross-talk of membrane lipids and Alzheimer-related proteins. *Mol. Neurodegener.* **8**, 34 (2013).

[18] Peetla C., Vijayaraghavalu S., and Labhasetwar V. Biophysics of cell membrane lipids in cancer drug resistance: Implications for drug transport and drug delivery with nanoparticles. *Adv. Drug Delivery Rev.* **65**, 1686–1698 (2013).

[19] van Meer G., Voelker D.R., and Feigenson G.W. Membrane lipids: where they are and how they behave. *Nat. Rev. Mol. Cell Bio.* **9**, 112–124 (2008).

[20] Hung W.C., Lee M.T., Chen F.Y., and Huang H.W. The condensing effect of cholesterol in lipid bilayers. *Biophys. J.* **92**, 3960–3967 (2007).

[21] de Meyer F. and Smit B. Effect of cholesterol on the structure of a phospholipid bilayer. *P. Natl. Acad. Sci. USA* **106**, 3654–3658 (2009).

[22] Hanson M.A., Cherezov V., Griffith M.T., Roth C.B., Jaakola V.P., Chien E.Y.T., Velasquez J., Kuhn P., and Stevens R.C. A specific

cholesterol binding site is established by the 2.8 A structure of the human β2-adrenergic receptor. *Structure* **16**, 897–905 (2008).

[23] Paila Y.D., Tiwari S., and Chattopadhyay A. Are specific nonannular cholesterol binding sites present in G-protein coupled receptors? *Biochim. Biophys. Acta* **1788**, 295–302 (2009).

[24] Paila Y.D. and Chattopadhyay A. The function of G-protein coupled receptors and membrane cholesterol: specific or general interaction? *Glycoconjugate J.* **26**, 711–720 (2009).

[25] Wiegand V. and Gimpl G. Specification of the cholesterol interaction with the oxytocin receptor using a chimeric receptor approach. *Eur. J. Pharmacol.* **676**, 12–19 (2012).

[26] Oates J., Faust B., Attrill H., Harding P., Orwick M., Watts A., O'Malley M.a., Helgeson M.E., Wagner N.J., and Robinson A.S. The role of cholesterol on the activity and stability of neurotensin receptor 1. *Biochim. Biophys. Acta* **1818**, 2228–2233 (2012).

[27] Michal P., Rudajev V., El-Fakahany E.E., and Dolezal V. Membrane cholesterol content influences binding properties of muscarinic M2 receptors and differentially impacts activation of second messenger pathways. *Eur. J. of Pharmacol.* **606**, 50–60 (2009).

[28] Gaibelet G., Millot C., Lebrun C., Ravault S., Sauliere a., Andre a., Lagane B., and Lopez a. Cholesterol content drives distinct pharmacological behaviours of micro-opioid receptor in different microdomains of the CHO plasma membrane. *Mol. Memb. Bio.* **25**, 423–435 (2008).

[29] Oates J. and Watts A. Uncovering the intimate relationship between lipids, cholesterol and GPCR activation. *Curr. Op. Struct. Biol.* **21**, 802–807 (2011).

[30] Lagane B., Gaibelet G., Meilhoc E., Masson J.M., Cézanne L., and Lopez a. Role of sterols in modulating the human mu-opioid

receptor function in Saccharomyces cerevisiae. *J. Biol. Chem.* **275**, 33197–33200 (2000).

[31] Sjögren B., Csöregh L., and Svenningsson P. Cholesterol reduction attenuates 5-HT1A receptor-mediated signaling in human primary neuronal cultures. *N.-S. Arch. of Pharmacol.* **378**, 441–446 (2008).

[32] O'Malley M.a., Helgeson M.E., Wagner N.J., and Robinson A.S. The morphology and composition of cholesterol-rich micellar nanostructures determine transmembrane protein (GPCR) activity. *Biophys. J.* **100**, L11–L13 (2011).

[33] Morioka S., Shigemori T., Hara K., Morisaka H., Kuroda K., and Ueda M. Effect of sterol composition on the activity of the yeast G-protein-coupled receptor Ste2. *Appl. Microbiol. Biotechnol.* **97**, 4013–4020 (2013).

[34] Pucadyil T.T.J. and Chattopadhyay A. Role of cholesterol in the function and organization of G-protein coupled receptors. *Prog. Lipid Res.* **45**, 295–333 (2006).

[35] Prasanna X., Chattopadhyay A., and Sengupta D. Cholesterol Modulates the Dimer Interface of the β2-Adrenergic Receptor via Cholesterol Occupancy Sites. *Biophys. J.* **106**, 1290–1300 (2014).

[36] Fagone P. and Jackowski S. Membrane phospholipid synthesis and endoplasmic reticulum function. *J. Lipid Res.* **50**, S311–S316 (2009).

[37] Blom T., Somerharju P., and Ikonen E. Synthesis and biosynthetic trafficking of membrane lipids. *Cold Spring Harbor Bio.* **3**, a004713 (2011).

[38] Feigenson G.W.G. Phase boundaries and biological membranes. *Annu. Rev. of Biophys. Biom.* **36**, 63–77 (2007).

[39] Marsh D. Lateral pressure profile, spontaneous curvature frustration, and the incorporation and conformation of proteins in membranes. *Biophys. J.* **93**, 3884–3899 (2007).

[40] Huber T., Rajamoorthi K., Kurze V.F., Beyer K., and Brown M.F. Structure of docosahexaenoic acid-containing phospholipid bilayers as studied by (2)H NMR and molecular dynamics simulations. *J. Am. Chem. Soc.* **124**, 298–309 (2002).

[41] Heberle F.a., Petruzielo R.S., Pan J., Drazba P., Kučerka N., Standaert R.F., Feigenson G.W., and Katsaras J. Bilayer thickness mismatch controls domain size in model membranes. *J. Am. Chem. Soc.* **135**, 6853–6859 (2013).

[42] Saiz L. and Klein M.L. Influence of highly polyunsaturated lipid acyl chains of biomembranes on the NMR order parameters. *J. Am. Chem. Soc.* **123**, 7381–7387 (2001).

[43] Hyvönen M.T. and Kovanen P.T. Molecular dynamics simulations of unsaturated lipid bilayers: effects of varying the numbers of double bonds. *Eur. Biophys. J.* **34**, 294–305 (2005).

[44] Hyvo M.T., Niemelä P.S., Hyvönen M.T., and Vattulainen I. Influence of chain length and unsaturation on sphingomyelin bilayers. *Biophys. J.* **90**, 851–863 (2006).

[45] Ollila S., Hyvönen M.T., and Vattulainen I. Polyunsaturation in lipid membranes: dynamic properties and lateral pressure profiles. *J. Phys. Chem. B* **111**, 3139–3150 (2007).

[46] Martinez-Seara H., Róg T., Pasenkiewicz-gierula M., Vattulainen I., Karttunen M., Reigada R., Health P., Complete M., and Ro T. Interplay of unsaturated phospholipids and cholesterol in membranes: effect of the double-bond position. *Biophys. J.* **95**, 3295–3305 (2008).

[47] Pomorski T. and Menon a.K. Lipid flippases and their biological functions. *Cell. Mol. Life Sci.* **63**, 2908–2921 (2006).

[48] Schmitz G. and Grandl M. Update on lipid membrane microdomains. *Curr. Op. Clin. Nutr. Metabol. Care* **11**, 106–12 (2008).

[49] Lingwood D. and Simons K. Lipid rafts as a membrane-organizing principle. *Science* **327**, 46–50 (2010).

[50] Sonnino S. and Prinetti a. Membrane domains and the "lipid raft" concept. *Curr. Med. Chem.* **20**, 4–21 (2013).

[51] Parton R.G. and del Pozo M.a. Caveolae as plasma membrane sensors, protectors and organizers. *Nat. Rev. Mol. Cell Biol.* **14**, 98–112 (2013).

[52] Simons K. and Gerl M.J. Revitalizing membrane rafts: new tools and insights. *Nat. Rev. Mol. Cell Bio.* **11**, 688–699 (2010).

[53] Jacobson K., Mouritsen O.G., and Anderson R.G.W. Lipid rafts: at a crossroad between cell biology and physics. *Nat. Cell Biol.* **9**, 7–14 (2007).

[54] Fabelo N., Martín V., Marín R., Moreno D., Ferrer I., and Díaz M. Altered lipid composition in cortical lipid rafts occurs at early stages of sporadic Alzheimer disease and facilitates APP/BACE1 interactions. *Neurobiol. Aging* 1–12 (2014).

[55] Fabelo N., Martín V., Santpere G., Marín R., Torrent L., Ferrer I., and Díaz M. Severe alterations in lipid composition of frontal cortex lipid rafts from Parkinson's Disease and Incidental Parkinson's Disease. *Mol. Med.* **17**, 1107 (2011).

[56] Martín V., Fabelo N., Santpere G., Puig B., Marín R., Ferrer I., and Díaz M. Lipid alterations in lipid rafts from Alzheimer's disease human brain cortex. *J. Alzheimer's Disease* **19**, 489–502 (2010).

[57] Fabelo N., Martín V., Marín R., Santpere G., Aso E., Ferrer I., and Díaz M. Evidence for Premature Lipid Raft Aging in APP / PS1 Double-Transgenic. *J. Neuropathol. Exp. Neurol.* **71**, 868–881 (2012).

[58] Dupuy A.D. and Engelman D.M. Protein area occupancy at the center of the red blood cell membrane. *P. Natl. Acad. Sci. USA* **105**, 2848–2852 (2008).

[59] Lee A.G. How lipids affect the activities of integral membrane proteins. *Biochim. Biophys. Acta* **1666**, 62–87 (2004).

[60] Soubias O., Teague W.E., and Gawrisch K. Evidence for specificity in lipid-rhodopsin interactions. *J. Biol. Chem.* **281**, 33233–33241 (2006).

[61] Mondal S., Khelashvili G., Johner N., and Weinstein H. *How The Dynamic Properties And Functional Mechanisms Of GPCRs Are Modulated By Their Coupling To The Membrane Environment*, volume 796 of *Advances in Experimental Medicine and Biology*. Springer Netherlands (2014).

[62] Hurst D.P., Grossfield A., Lynch D.L., Feller S., Romo T.D., Gawrisch K., Pitman M.C., and Reggio P.H. A lipid pathway for ligand binding is necessary for a cannabinoid G protein-coupled receptor. *J. Biol. Chem.* **285**, 17954–64 (2010).

[63] Hurst D.P., Schmeisser M., and Reggio P.H. Endogenous lipid activated G protein-coupled receptors: emerging structural features from crystallography and molecular dynamics simulations. *Chem. Phys. Lipids* **169**, 46–56 (2013).

[64] Hanson M.A., Roth C.B., Jo E., Griffith M.T., Scott F.L., Reinhart G., Desale H., Clemons B., Cahalan S.M., Schuerer S.C., Sanna M.G., Han G.W., Kuhn P., Rosen H., and Stevens R.C. Crystal structure of a lipid G protein-coupled receptor. *Science* **335**, 851–855 (2012).

[65] Albert A.D. and Boesze-Battaglia K. The role of cholesterol in rod outer segment membranes (2005).

[66] Huang P., Xu W., Yoon S.I., Chen C., Chong P.L.G., and Liu-Chen L.Y. Cholesterol reduction by methyl-β-cyclodextrin attenuates the delta opioid receptor-mediated signaling in neuronal cells but enhances it in non-neuronal cells. *Biochem. Pharmacol.* **73**, 534–549 (2007).

[67] Xu W., Yoon S.i., Huang P., Wang Y., Chen C., and Chong P.L.g. Localization of the Opioid Receptor in Lipid Rafts. *J. Pharmacol. Exp. Therapeut.* **317**, 1295–1306 (2006).

[68] Prasad R., Paila Y.D., Chattopadhyay A., and Jafurulla M. Membrane cholesterol depletion enhances ligand binding function of human serotonin1A receptors in neuronal cells. *Biochem. Biophys. Res. Co.* **390**, 93–96 (2009).

[69] Pucadyil T.J. and Chattopadhyay A. Cholesterol depletion induces dynamic confinement of the G-protein coupled serotonin(1A) receptor in the plasma membrane of living cells. *Biochim. Biophys. Acta* **1768**, 655–668 (2007).

[70] Colozo A.T., Park P.S.H., Sum C.S., Pisterzi L.F., and Wells J.W. Cholesterol as a determinant of cooperativity in the M2 muscarinic cholinergic receptor. *Biochem. Pharmacol.* **74**, 236–255 (2007).

[71] Bari M., Paradisi A., Pasquariello N., and Maccarrone M. Cholesterol-dependent modulation of type 1 cannabinoid receptors in nerve cells. *J. Neurosci. Res.* **81**, 275–283 (2005).

[72] Escribá P.V., Wedegaertner P.B., Goñi F.M., and Vögler O. Lipid-protein interactions in GPCR-associated signaling. *Biochim. Biophys. Acta* **1768**, 836–852 (2007).

[73] Chini B. and Parenti M. G-protein-coupled receptors, cholesterol and palmitoylation: facts about fats. *J. Mol. Endocrinology* **42**, 371–379 (2009).

[74] Goddard A.D. and Watts A. Regulation of G protein-coupled receptors by palmitoylation and cholesterol. *BMC Biol.* **10**, 27 (2012).

[75] O'Brien P.J. and Zatz M. Acylation of bovine rhodopsin by [3H]palmitic acid. *J. Biol. Chem.* **259**, 5054–5057 (1984).

[76] O'Dowd B.F., Hnatowich M., Caron M.G., Lefkowitz R.J., and Bouvier M. Palmitoylation of the human beta 2-adrenergic receptor. Mutation of Cys341 in the carboxyl tail leads to an uncoupled nonpalmitoylated form of the receptor. *J. Biol. Chem.* **264**, 7564–7569 (1989).

[77] Reid H.M. and Kinsella B.T. Palmitoylation of the TPβ isoform of the human thromboxane A2 receptor. Modulation of G protein: Effector coupling and modes of receptor internalization. *Cell. Signal.* **19**, 1056–1070 (2007).

[78] Navratil A.M., Farmerie T.A., Bogerd J., Nett T.M., and Clay C.M. Differential impact of intracellular carboxyl terminal domains on lipid raft localization of the murine gonadotropin-releasing hormone receptor. *Biol. Reprod.* **74**, 788–797 (2006).

[79] Chini B. and Parenti M. G-protein coupled receptors in lipid rafts and caveolae: how, when and why do they go there? *J. Mol. Endocrinology* **32**, 325–338 (2004).

[80] Levental I., Grzybek M., and Simons K. Greasing their way: lipid modifications determine protein association with membrane rafts. *Biochemistry* **49**, 6305–6316 (2010).

[81] Dainese E., Oddi S., and Maccarrone M. Lipid-mediated dimerization of beta2-adrenergic receptor reveals important clues for cannabinoid receptors. *Cell. Mol. Life Sci.* **65**, 2277–2279 (2008).

[82] Wiegand R. and Anderson R. Phospholipid molecular species of frog rod outer segment membranes. *Exp. Eye Res.* **37**, 159–173 (1983).

[83] Gombos G., Morgan I.G., and Breckenridge W. The lipid composition of adult rat brain synaptosomal plasma membranes. *Biochim. Biophys. Acta* **266**, 695–707 (1972).

[84] Squirrel O.F., Sun G., and Sun A. Phospholipids and acyl groups of synaptosomal and myelin membranes isolated from the cerebral cortex of squirrel monkey(Saimiri sciureus). *Biochim. Biophys. Acta* **280**, 306–325 (1972).

[85] Valentine R.C. and Valentine D.L. Omega-3 fatty acids in cellular membranes: a unified concept. *Prog. Lipid Res.* **43**, 383–402 (2004).

[86] Wassall S.R. and Stillwell W. Docosahexaenoic acid domains: the ultimate non-raft membrane domain. *Chem. Phys. Lip.* **153**, 57–63 (2008).

[87] Shaikh S.R. Biophysical and biochemical mechanisms by which dietary N-3 polyunsaturated fatty acids from fish oil disrupt membrane lipid rafts. *J. Nutr. Biochem.* **23**, 101–105 (2012).

[88] Gawrisch K., Soubias O., and Mihailescu M. Insights from biophysical studies on the role of polyunsaturated fatty acids for function of G-protein coupled membrane receptors. *Prostag. Leukotr. ESS* **79**, 131–134 (2008).

[89] Feller S.E., Gawrisch K., and Woolf T.B. Rhodopsin exhibits a preference for solvation by polyunsaturated docosohexaenoic acid. *J. Am. Chem. Soc.* **125**, 4434–4435 (2003).

[90] Litman B.J. and Mitchell D.C. A role for phospholipid polyunsaturation in modulating membrane protein function. *Lipids* **31 Suppl**, S193–S197 (1996).

[91] Mitchell D.C., Niu S.L., and Litman B.J. Enhancement of G protein-coupled signaling by DHA phospholipids. *Lipids* **38**, 437–443 (2003).

[92] Bennett M.P. and Mitchell D.C. Regulation of membrane proteins by dietary lipids: effects of cholesterol and docosahexaenoic acid acyl chain-containing phospholipids on rhodopsin stability and function. *Biophys. J.* **95**, 1206–1216 (2008).

[93] Sánchez-Martín M.J., Ramon E., Torrent-Burgués J., and Garriga P. Improved conformational stability of the visual G protein-coupled receptor rhodopsin by specific interaction with docosahexaenoic acid phospholipid. *Chembiochem* **14**, 639–644 (2013).

[94] Mitchell D.C., Niu S.L., and Litman B.J. DHA-rich phospholipids optimize G-protein-coupled signaling. *J. Pediatr.* **143**, S80–S86 (2003).

[95] Mitchell D.C., Niu S.L., and Litman B.J. Quantifying the differential effects of DHA and DPA on the early events in visual signal transduction. *Chem. Phys. Lip.* **165**, 393–400 (2012).

[96] Niu S.L., Mitchell D.C., Lim S.Y., Wen Z.M., Kim H.Y., Salem N., and Litman B.J. Reduced G protein-coupled signaling efficiency in retinal rod outer segments in response to n-3 fatty acid deficiency. *J. Biol. Chem.* **279**, 31098–31104 (2004).

[97] Jeffrey B.G., Weisinger H.S., Neuringer M., and Mitchell D.C. The role of docosahexaenoic acid in retinal function. *Lipids* **36**, 859–871 (2001).

[98] Niu S.L., Mitchell D.C., and Litman B.J. Optimization of receptor-G protein coupling by bilayer lipid composition II: formation of metarhodopsin II-transducin complex. *J. Biol. Chem.* **276**, 42807–42811 (2001).

[99] Litman B.J., Niu S.L., Polozova A., and Mitchell D.C. The role of docosahexaenoic acid containing phospholipids in modulating G protein-coupled signaling pathways: visual transduction. *J. Mol. Neurosci.* **16**, 237–242 (2001).

[100] Mitchell D.C., Niu S.L., and Litman B.J. Optimization of receptor-G protein coupling by bilayer lipid composition I: kinetics of rhodopsin-transducin binding. *J. Biol. Chem.* **276**, 42801–42806 (2001).

[101] McNamara R.K., Jandacek R., Rider T., Tso P., Hahn C.G., Richtand N.M., and Stanford K.E. Abnormalities in the fatty acid composition of the postmortem orbitofrontal cortex of schizophrenic patients: gender differences and partial normalization with antipsychotic medications. *Schizophr. Res.* **91**, 37–50 (2007).

[102] Taha A.Y., Cheon Y., Ma K., Rapoport S.I., and Rao J.S. Altered fatty acid concentrations in prefrontal cortex of schizophrenic patients. *J. Psychiat. Res.* **47**, 636–643 (2013).

[103] McNamara R.K., Hahn C.G., Jandacek R., Rider T., Tso P., Stanford K.E., and Richtand N.M. Selective deficits in the omega-3 fatty acid docosahexaenoic acid in the postmortem orbitofrontal cortex of patients with major depressive disorder. *Biol. Psychiat.* **62**, 17–24 (2007).

[104] McNamara R.K., Jandacek R., Rider T., Tso P., Stanford K.E., Hahn C.G., and Richtand N.M. Deficits in docosahexaenoic acid and associated elevations in the metabolism of arachidonic acid and saturated fatty acids in the postmortem orbitofrontal cortex of patients with bipolar disorder. *J. Psychiat. Res.* **160**, 285–299 (2008).

[105] Salem N., Litman B., Kim H.Y., and Gawrisch K. Mechanisms of action of docosahexaenoic acid in the nervous system. *Lipids* **36**, 945–959 (2001).

[106] Calon F. and Cole G. Neuroprotective action of omega-3 polyunsaturated fatty acids against neurodegenerative diseases: evidence from animal studies. *Prostag. Leukotr. ESS* **77**, 287–293 (2007).

[107] Akter K., Gallo D.A., Martin S.A., Myronyuk N., Roberts R.T., Stercula K., and Raffa R.B. A review of the possible role of the

essential fatty acids and fish oils in the aetiology, prevention or pharmacotherapy of schizophrenia. *J. Clin. Pharm. Ther.* **37**, 132–139 (2012).

[108] Bousquet M., Calon F., and Cicchetti F. Impact of omega-3 fatty acids in Parkinson's disease. *Ageing Res. Rev.* **10**, 453–463 (2011).

[109] Siegel G. and Ermilov E. Omega-3 fatty acids: benefits for cardio-cerebro-vascular diseases. *Atherosclerosis* **225**, 291–295 (2012).

[110] Whorton M.R., Bokoch M.P., Rasmussen S.r.G.F., Huang B., Zare R.N., Kobilka B., and Sunahara R.K. A monomeric G protein-coupled receptor isolated in a high-density lipoprotein particle efficiently activates its G protein. *P. Natl. Acad. Sci. USA* **104**, 7682–7687 (2007).

[111] Ernst O.P., Gramse V., Kolbe M., Hofmann K.P., and Heck M. Monomeric G protein-coupled receptor rhodopsin in solution activates its G protein transducin at the diffusion limit. *P. Natl. Acad. Sci. USA* **104**, 10859–10864 (2007).

[112] Kasai R.S. and Kusumi A. Single-molecule imaging revealed dynamic GPCR dimerization. *Curr. Op. Cell Bio.* **27**, 78–86 (2014).

[113] Maggio R., Vogel Z., and Wess J. Coexpression studies with mutant muscarinic/adrenergic receptors provide evidence for intermolecular "cross-talk" between G-protein-linked receptors. *P. Natl. Acad. Sci. USA* **90**, 3103–3107 (1993).

[114] Fotiadis D., Liang Y., Filipek S., Saperstein D.A., Engel A., and Palczewski K. Rhodopsin dimers in native disc membranes. *Nature* **421**, 127–128 (2003).

[115] Mercier J.F., Salahpour A., Angers S., Breit A., and Bouvier M. Quantitative assessment of beta 1- and beta 2-adrenergic receptor homo- and heterodimerization by bioluminescence resonance energy transfer. *J. Biol. Chem.* **277**, 44925–44931 (2002).

[116] Percherancier Y., Berchiche Y.a., Slight I., Volkmer-Engert R., Tamamura H., Fujii N., Bouvier M., and Heveker N. Bioluminescence resonance energy transfer reveals ligand-induced conformational changes in CXCR4 homo- and heterodimers. *J. Biol. Chem.* **280**, 9895–9903 (2005).

[117] Guo W., Urizar E., Kralikova M., Mobarec J.C., Shi L., Filizola M., and Javitch J.a. Dopamine D2 receptors form higher order oligomers at physiological expression levels. *EMBO J.* **27**, 2293–2304 (2008).

[118] Dorsch S., Klotz K., Engelhardt S., Lohse M., and Bünemann M. Analysis of receptor oligomerization by FRAP microscopy. *Nat. Methods* **6**, 225–230 (2009).

[119] Lambert N.a. GPCR dimers fall apart. *Science Signaling* **3**, pe12 (2010).

[120] Romano C., Yang W.L., and O'Malley K.L. Metabotropic glutamate receptor 5 is a disulfide-linked dimer. *J. Biol. Chem.* **271**, 28612–28616 (1996).

[121] Huang J., Chen S., Zhang J.J., and Huang X.Y. Crystal structure of oligomeric β(1)-adrenergic G protein-coupled receptors in ligand-free basal state. *Nat. Struct. Mol. Biol.* **20**, 419–425 (2013).

[122] Milligan G. The role of dimerisation in the cellular trafficking of G-protein-coupled receptors. *Curr. Op. Pharmacol.* **10**, 23–29 (2010).

[123] Dunham J.H. and Hall R.a. Enhancement of the surface expression of G protein-coupled receptors. *Trends Biotechnol.* **27**, 541–545 (2009).

[124] Franco R., Casadó V., Cortés A., Mallol J., Ciruela F., Ferré S., Lluis C., Canela E.I., Corte A., Ferre S., and Casado V. G-protein-coupled receptor heteromers: function and ligand pharmacology. *Brit. J. of Pharmacol.* **153 Suppl**, S90–S98 (2008).

[125] Gomes I., Gupta A., Filipovska J., Szeto H.H., Pintar J.E., and Devi L.a. A role for heterodimerization of mu and delta opiate receptors in enhancing morphine analgesia. *P. Natl. Acad. Sci. USA* **101**, 5135–5139 (2004).

[126] Rashid A.J., So C.H., Kong M.M.C., Furtak T., El-Ghundi M., Cheng R., O'Dowd B.F., George S.R., and Dowd B.F.O. D1-D2 dopamine receptor heterooligomers with unique pharmacology are coupled to rapid activation of Gq/11 in the striatum. *P. Natl. Acad. Sci. USA* **104**, 654–659 (2007).

[127] Fiorentini C., Busi C., Gorruso E., Gotti C., Spano P., and Missale C. Reciprocal Regulation of Dopamine D1 and D3 Receptor Function and Trafficking by Heterodimerization. *Mol. Pharmacol.* **74**, 59–69 (2008).

[128] Canals M., Marcellino D., Fanelli F., Ciruela F., De Benedetti P., Goldberg S.R., Neve K., Fuxe K., Agnati L.F., Woods A.S., Ferré S., Lluis C., Bouvier M., and Franco R. Adenosine A2A-dopamine D2 receptor-receptor heteromerization: qualitative and quantitative assessment by fluorescence and bioluminescence energy transfer. *J. Biol. Chem.* **278**, 46741–46749 (2003).

[129] Guixà-González R., Bruno A., Marti-Solano M., and Selent J. Crosstalk within GPCR Heteromers in Schizophrenia and Parkinson's Disease: Physical or Just Functional? *Curr. Med. Chem.* **19**, 1119–1134 (2012).

[130] Armentero M.T., Pinna A., Ferré S., Lanciego J.L., Müller C.E., and Franco R. Past, present and future of A(2A) adenosine receptor antagonists in the therapy of Parkinson's disease. *Pharmacol. Therapeut.* **132**, 280–299 (2011).

[131] Prezeau L., Rives M.L., Comps-Agrar L., Maurel D., Kniazeff J., and Pin J.P. Functional crosstalk between GPCRs: with or without oligomerization. *Curr. Op. Pharmacol.* **10**, 6–13 (2010).

[132] Pin J.p., Neubig R., Bouvier M., Devi L., Filizola M., and Javitch J.A. International Union of Basic and Clinical Pharmacology . LXVII . Recommendations for the Recognition and Nomenclature of G Protein-Coupled Receptor Heteromultimers. *Pharmacol. Rev.* **59**, 5–13 (2007).

[133] Botelho A.V., Huber T., Sakmar T.P., and Brown M.F. Curvature and hydrophobic forces drive oligomerization and modulate activity of rhodopsin in membranes. *Biophys. J.* **91**, 4464–4477 (2006).

[134] Shan J., Khelashvili G., Mondal S., Mehler E.L., and Weinstein H. Ligand-Dependent Conformations and Dynamics of the Serotonin 5-HT2A Receptor Determine Its Activation and Membrane-Driven Oligomerization Properties. *PLoS Comput. Bio.* **8**, e1002473 (2012).

[135] Mondal S., Johnston J.M., Wang H., Khelashvili G., Filizola M., and Weinstein H. Membrane Driven Spatial Organization of GPCRs. *Sci. Rep.* **3**, 2909 (2013).

[136] Goddard A.D., Dijkman P.M., Adamson R.J., and Watts A. *Lipid-Dependent GPCR Dimerization.*, volume 117. Elsevier Inc., 1 edition (2013).

[137] Karplus M. and McCammon J.A. Molecular dynamics simulations of biomolecules. *Nat. Struct. Biol.* **9**, 646–652 (2002).

[138] Caflisch A. and Paci E. Molecular dynamics simulations to study protein folding and unfolding. *Protein Science Encyclopedia* **05**, 1143–1169 (2005).

[139] MacKerel Jr. A.D., Brooks III C.L., Nilsson L., Roux B., Won Y., and Karplus M. CHARMM: The Energy Function and Its Parameterization with an Overview of the Program. In P. V R Schleyer Et Al (Editor), *The Encyclopedia of Computational Chemistry*, number 10, Sp. Iss. SI in The Encyclopedia of Computational Chemistry, 271–277. John Wiley & Sons: Chichester (1998).

[140] Cornell W.D., Cieplak P., Bayly C.I., Gould I.R., Merz K.M., Ferguson D.M., Spellmeyer D.C., Fox T., Caldwell J.W., and Kollman P.A. A Second Generation Force Field for the Simulation of Proteins, Nucleic Acids, and Organic Molecules. *J. Am. Chem. Soc.* **117**, 5179–5197 (1995).

[141] Christen M., Hünenberger P.H., Bakowies D., Baron R., Bürgi R., Geerke D.P., Heinz T.N., Kastenholz M.A., Kräutler V., Oostenbrink C., Peter C., Trzesniak D., and van Gunsteren W.F. The GROMOS software for biomolecular simulation: GROMOS05. *J. Comput. Chem.* **26**, 1719–1751 (2005).

[142] Jorgensen W.L., Maxwell D.S., and Tirado-Rives J. Development and Testing of the OPLS All-Atom Force Field on Conformational Energetics and Properties of Organic Liquids. *J. Am. Chem. Soc.* **118**, 11225–11236 (1996).

[143] Marrink S.J., Risselada H.J., Yefimov S., Tieleman D.P., de Vries A.H., and Vries A.H.D. The MARTINI force field: coarse grained model for biomolecular simulations. *J. Phys. Chem. B* **111**, 7812–7824 (2007).

[144] Hess B. and Kutzner C. GROMACS 4: Algorithms for highly efficient, load-balanced, and scalable molecular simulation. *J. Chem. Theory Comput.* **4**, 435–447 (2008).

[145] Phillips J.C., Braun R., Wang W., Gumbart J., Tajkhorshid E., Villa E., Chipot C., Skeel R.D., Kalé L., and Schulten K. Scalable molecular dynamics with NAMD. *J. Comput. Chem.* **26**, 1781–1802 (2005).

[146] Harvey M.J., Giupponi G., and Fabritiis G.D. ACEMD: accelerating biomolecular dynamics in the microsecond time scale. *J. Chem. Theory Comput.* **5**, 1–9 (2009).

[147] Brooks B. and Bruccoleri R. CHARMM: A program for macromolecular energy, minimization, and dynamics calculations. *J. Comput. Chem.* **4**, 187–217 (1983).

[148] Shaw D.E., Dror R.O., Salmon J.K., Grossman J.P., Mackenzie K.M., Bank J.A., Young C., Deneroff M.M., Batson B., Bowers K.J., Chow E., Eastwood M.P., Ierardi D.J., Klepeis J.L., Kuskin J.S., Larson R.H., Lindorff-Larsen K., Maragakis P., Moraes M.A., Piana S., Shan Y., and Towles B. Millisecond-scale Molecular Dynamics Simulations on Anton. In *Proceedings of the Conference on High Performance Computing Networking, Storage and Analysis*, SC '09, 39:1—-39:11. ACM, New York, NY, USA (2009).

[149] Simons K. and Vaz W.L.C. Model systems, lipid rafts, and cell membranes. *Annu. Rev. Biophys. Biomol.* **33**, 269–295 (2004).

[150] Vattulainen I. and Rog T. Lipid simulations: a perspective on lipids in action. *Cold Spring Harbor Biol.* **3**, 1–13 (2011).

[151] Berkowitz M.L. Detailed molecular dynamics simulations of model biological membranes containing cholesterol. *Biochim. Biophys. Acta* **1788**, 86–96 (2009).

[152] Bennett W.F.D. and Tieleman D.P. Computer simulations of lipid membrane domains. *Biochim. Biophys. Acta* **1828**, 1765–1776 (2013).

[153] Sabra M.C. and Mouritsen O.G. *Numerical Computer Methods, Part C*, volume 321 of *Methods in Enzymology*. Elsevier (2000).

[154] Khelashvili G.a. and Scott H.L. Combined Monte Carlo and molecular dynamics simulation of hydrated 18:0 sphingomyelin-cholesterol lipid bilayers. *J. Chem. Phys.* **120**, 9841–9847 (2004).

[155] Tieleman D.P. Methods and Parameters for Membrane Simulations. In M.S.P. Sansom and P.C. Biggin (Editors), *Molecular Simulations and Biomembranes : From Biophysics to Function*, num-

ber 20 in RSC Biomolecular Sciences, 1–26. The Royal Society of Chemistry (2010).

[156] Andersen H.C. Molecular dynamics simulations at constant pressure and/or temperature. *J. Chem. Phys.* **72**, 2384–2393 (1980).

[157] Nosé S. and Klein M. Constant pressure molecular dynamics for molecular systems (1983).

[158] Martyna G.J., Tobias D.J., and Klein M.L. Constant pressure molecular dynamics algorithms. *J. Chem. Phys.* **101**, 4177–4189 (1994).

[159] Feller S.E., Zhang Y., Pastor R.W., and Brooks B.R. Constant pressure molecular dynamics simulation: The Langevin piston method. *J. Chem. Phys.* **103**, 4613–4621 (1995).

[160] Berendsen H.J.C., Postma J.P.M., van Gunsteren W.F., DiNola a., and Haak J.R. Molecular dynamics with coupling to an external bath. *J. Chem. Phys.* **81**, 3684 (1984).

[161] Hünenberger P. Thermostat algorithms for molecular dynamics simulations. *Adv. Polym. Sci.* **173**, 105–149 (2005).

[162] Koynova R. and Caffrey M. Phases and phase transitions of the phosphatidylcholines. *Biochim. Biophys. Acta* **1376**, 91–145 (1998).

[163] Higgins M.J., Polcik M., Fukuma T., Sader J.E., Nakayama Y., and Jarvis S.P. Structured water layers adjacent to biological membranes. *Biophys. J.* **91**, 2532–2542 (2006).

[164] Fukuma T., Higgins M.J., and Jarvis S.P. Direct imaging of individual intrinsic hydration layers on lipid bilayers at Angstrom resolution. *Biophys. J.* **92**, 3603–3609 (2007).

[165] Cheng J.X., Pautot S., Weitz D.a., and Xie X.S. Ordering of water molecules between phospholipid bilayers visualized by coherent anti-Stokes Raman scattering microscopy. *P. Natl. Acad. Sci. USA* **100**, 9826–9830 (2003).

[166] Klauda J.B., Venable R.M., Freites J.A., O'Connor J.W., Tobias D.J., Mondragon-Ramirez C., Vorobyov I., MacKerell A.D., and Pastor R.W. Update of the CHARMM all-atom additive force field for lipids: validation on six lipid types. *J. Phys. Chem. B* **114**, 7830–7843 (2010).

[167] Tristram-Nagle S., Petrache H.I., and Nagle J.F. Structure and interactions of fully hydrated dioleoylphosphatidylcholine bilayers. *Biophys. J.* **75**, 917–925 (1998).

[168] Nagle J.F. and Tristram-Nagle S. Structure of lipid bilayers. *Biochim. Biophys. Acta Biomembranes* **1469**, 159–195 (2000).

[169] Robinson D., Besley N., O'shea P., and Hirst J. Water order profiles on phospholipid/cholesterol membrane bilayer surfaces. *J. Comput. Chem.* **32**, 2613–2618 (2011).

[170] Steinbauer B., Mehnert T., and Beyer K. Hydration and Lateral Organization in Phospholipid Bilayers Containing Sphingomyelin : A 2 H-NMR Study. *Biophys. J.* **85**, 1013–1024 (2003).

[171] Humphrey W., Dalke A., and Schulten K. VMD: visual molecular dynamics. *J. Mol. Graph.* **14**, 33–38 (1996).

[172] Jo S., Lim J.J.B., Klauda J.J.B., and Im W. CHARMM-GUI membrane builder for mixed bilayers and its application to yeast membranes. *Biophys. J.* **96**, 50–58 (2009).

[173] Jo S., Kim T., and Im W. Automated builder and database of protein/membrane complexes for molecular dynamics simulations. *PloS One* **2**, e880 (2007).

[174] Metcalf R. and Pandit S.a. Mixing properties of sphingomyelin ceramide bilayers: a simulation study. *J. Phys. Chem. B* **116**, 4500–4509 (2012).

[175] Saiz L. and Klein M.L. Structural properties of a highly polyunsaturated lipid bilayer from molecular dynamics simulations. *Biophys. J.* **81**, 204–216 (2001).

[176] Vattulainen I., Falck E., Patra M., Karttunen M., Hyvo M.T., and Hyvönen M.T. Lessons of slicing membranes: interplay of packing, free area, and lateral diffusion in phospholipid/cholesterol bilayers. *Biophys. J.* **87**, 1076–1091 (2004).

[177] Gapsys V., de Groot B.L., and Briones R. Computational analysis of local membrane properties. *J. Comput.-Aided Mol. Design* **27**, 845–858 (2013).

[178] Róg T., Martinez-Seara H., Munck N., Oresic M., Karttunen M., and Vattulainen I. Role of cardiolipins in the inner mitochondrial membrane: insight gained through atom-scale simulations. *J. Phys. Chem. B* **113**, 3413–3422 (2009).

[179] Cheng M.H., Liu L.T., Saladino A.C., Xu Y., and Tang P. Molecular dynamics simulations of ternary membrane mixture: phosphatidylcholine, phosphatidic acid, and cholesterol. *J. Phys. Chem. B* **111**, 14186–14192 (2007).

[180] Hall A., Róg T., Karttunen M., and Vattulainen I. Role of glycolipids in lipid rafts: a view through atomistic molecular dynamics simulations with galactosylceramide. *J. Phys. Chem. B* **114**, 7797–7807 (2010).

[181] Pandit S., Vasudevan S., Chiu S.W., Mashl R.J., Jakobsson E., and Scott H.L. Sphingomyelin-cholesterol domains in phospholipid membranes: atomistic simulation. *Biophys. J.* **87**, 1092–1100 (2004).

[182] Zidar J., Merzel F., Hodoscek M., Rebolj K., Sepcić K., Macek P., and Janezic D. Liquid-ordered phase formation in cholesterol/sphingomyelin bilayers: all-atom molecular dynamics simulations. *J. Phys. Chem. B* **113**, 15795–15802 (2009).

[183] Guixà-González R., Sadiq S.K., Dainese E., Pastor M., De Fabritiis G., and Selent J. Molecular Modeling and Simulation of Membrane Lipid-Mediated Effects on GPCRs. *Curr. Med. Chem.* **20**, 22–38 (2013).

[184] Collins M.D. Interleaflet coupling mechanisms in bilayers of lipids and cholesterol. *Biophys. J.* **94**, L32–L34 (2008).

[185] Longo G.S., Schick M., and Szleifer I. Stability and liquid-liquid phase separation in mixed saturated lipid bilayers. *Biophys. J.* **96**, 3977–3986 (2009).

[186] Mori T., Ogushi F., and Sugita Y. Analysis of lipid surface area in protein-membrane systems combining Voronoi tessellation and Monte Carlo integration methods. *J. Comput. Chem.* **33**, 286–293 (2012).

[187] Vermeer L.S., de Groot B.L., Réat V., Milon A., and Czaplicki J. Acyl chain order parameter profiles in phospholipid bilayers: computation from molecular dynamics simulations and comparison with 2H NMR experiments. *Eur. Biophys. J.* **36**, 919–931 (2007).

[188] Hassan-Zadeh E., Baykal-Caglar E., Alwarawrah M., and Huang J. Complex roles of hybrid lipids in the composition, order, and size of lipid membrane domains. *Langmuir* **30**, 1361–1369 (2014).

[189] Kucerka N., Perlmutter J.D., Pan J., Tristram-Nagle S., Katsaras J., and Sachs J.N. The effect of cholesterol on short- and long-chain monounsaturated lipid bilayers as determined by molecular dynamics simulations and X-ray scattering. *Biophys. J.* **95**, 2792–2805 (2008).

[190] Bartels T., Lankalapalli R.S., Bittman R., Beyer K., and Brown M.F. Raftlike mixtures of sphingomyelin and cholesterol investigated by solid-state 2H NMR spectroscopy. *J. Am. Chem. Soc.* **130**, 14521–14532 (2008).

[191] de Joannis J., Coppock P.S., Yin F., Mori M., Zamorano A., and Kindt J.T. Atomistic simulation of cholesterol effects on miscibility of saturated and unsaturated phospholipids: implications for liquid-ordered/liquid-disordered phase coexistence. *J. Am. Chem. Soc.* **133**, 3625–3634 (2011).

[192] Zhao G., Subbaiah P.V., Mintzer E., Chiu S.W., Jakobsson E., and Scott H.L. Molecular dynamic simulation study of cholesterol and conjugated double bonds in lipid bilayers. *Chem. Phys. Lipids* **164**, 811–818 (2011).

[193] Frenkel D., Smit B., and Ratner M.A. *Understanding Molecular Simulation: From Algorithms to Applications*, volume 50. Academic Press (1997).

[194] Martinez-seara H. and Ro T. Biomolecular Simulations. In L. Monticelli and E. Salonen (Editors), *Molecular Dynamics Simulations of Lipid Bilayers: Simple Recipe of How to Do It*, volume 924 of *Methods in Molecular Biology*, 407–429. Humana Press, Totowa, NJ (2013).

[195] Pandit S.a., Jakobsson E., and Scott H.L. Simulation of the early stages of nano-domain formation in mixed bilayers of sphingomyelin, cholesterol, and dioleylphosphatidylcholine. *Biophys. J.* **87**, 3312–3322 (2004).

[196] Róg T., Pasenkiewicz-Gierula M., Vattulainen I., and Karttunen M. What happens if cholesterol is made smoother: importance of methyl substituents in cholesterol ring structure on phosphatidylcholine-sterol interaction. *Biophys. J.* **92**, 3346–3357 (2007).

[197] Martinez-Seara H., Róg T., Karttunen M., Vattulainen I., and Reigada R. Cholesterol induces specific spatial and orientational order in cholesterol/phospholipid membranes. *PloS One* **5**, e11162 (2010).

[198] Pitman M.C., Suits F., Mackerell A.D., and Feller S.E. Molecular-level organization of saturated and polyunsaturated fatty acids in a phosphatidylcholine bilayer containing cholesterol. *Biochemistry* **43**, 15318–15328 (2004).

[199] Filippov A., Orädd G., and Lindblom G. Lipid lateral diffusion in ordered and disordered phases in raft mixtures. *Biophys. J.* **86**, 891–896 (2004).

[200] Niemelä P., Ollila S., Hyvönen M.T., Karttunen M., Vattulainen I., and Hyvo M.T. Assessing the nature of lipid raft membranes. *PLoS Comput. Biol.* **3**, e34 (2007).

[201] Lindblom G. and Orädd G. Lipid lateral diffusion and membrane heterogeneity. *Biochim. Biophys. Acta* **1788**, 234–244 (2009).

[202] Filippov A., Munavirov B., Gröbner G., and Rudakova M. Lateral diffusion in equimolar mixtures of natural sphingomyelins with dioleoylphosphatidylcholine. *Magnet. Reson. Imag.* **30**, 413–421 (2012).

[203] Apajalahti T., Niemelä P., Govindan P.N., Miettinen M.S., Salonen E., Marrink S.J., and Vattulainen I. Concerted diffusion of lipids in raft-like membranes. *Faraday Discuss.* **144**, 445–481 (2010).

[204] Javanainen M., Hammaren H., Monticelli L., Jeon J.H., Miettinen M.S., Martinez-Seara H., Metzler R., and Vattulainen I. Anomalous and normal diffusion of proteins and lipids in crowded lipid membranes. *Faraday Discuss.* **161**, 397–417 (2013).

[205] Niemelä P., Miettinen M.S., Monticelli L., Hammaren H., Bjelkmar P., Murtola T., Lindahl E., and Vattulainen I. Membrane proteins diffuse as dynamic complexes with lipids. *J. Am. Chem. Soc.* **132**, 7574–7575 (2010).

[206] Mobarec J.C., Sanchez R., and Filizola M. Modern homology modeling of G-protein coupled receptors: which structural template to use? *J. Med. Chem.* **52**, 5207–5216 (2009).

[207] Yarnitzky T., Levit A., and Niv M.Y. Homology modeling of G-protein-coupled receptors with X-ray structures on the rise. *Curr. Op. Drug Discov. Develop.* **13**, 317–325 (2010).

[208] Rodríguez D., Bello X., and Gutiérrez-de Terán H. Molecular modelling of G protein-coupled receptors through the Web. *Mol. Inform.* **31**, 334–341 (2012).

[209] Eswar N., Eramian D., Webb B., Shen M.Y., and Sali A. Protein structure modeling with MODELLER. *Methods Mol. Biol.* **426**, 145–159 (2008).

[210] Eswar N., Webb B., Marti-Renom M.A., Madhusudhan M.S., Eramian D., Shen M.Y., Pieper U., and Sali A. Comparative protein structure modeling using MODELLER. *Current Protocols in Protein Science* **Chapter 2**, Unit 2.9 (2007).

[211] Kandt C., Ash W.L., and Peter Tieleman D. Setting up and running molecular dynamics simulations of membrane proteins. *Methods* **41**, 475–488 (2007).

[212] Wolf M.G., Hoefling M., Aponte-Santamaría C., Grubmüller H., and Groenhof G. g_membed: Efficient insertion of a membrane protein into an equilibrated lipid bilayer with minimal perturbation. *J. Comput. Chem.* **31**, 2169–2174 (2010).

[213] Scott K.a., Bond P.J., Ivetac A., Chetwynd A.P., Khalid S., and Sansom M.S.P. Coarse-grained MD simulations of membrane protein-bilayer self-assembly. *Structure* **16**, 621–630 (2008).

[214] Javanainen M. Universal Method for Embedding Proteins into Complex Lipid Bilayers for Molecular Dynamics Simulations. *J. Chem Theory Comput.* **In Press** (2014).

[215] Mertz B., Struts A.V., Feller S.E., and Brown M.F. Molecular simulations and solid-state NMR investigate dynamical structure in rhodopsin activation. *Biochim. Biophys. Acta* **1818**, 241–251 (2012).

[216] Lee J.Y. and Lyman E. Agonist dynamics and conformational selection during microsecond simulations of the A(2A) adenosine receptor. *Biophys. J.* **102**, 2114–2120 (2012).

[217] Li J., Jonsson A.L., Beuming T., Shelley J.C., and Voth G.a. Ligand-Dependent Activation and Deactivation of the Human Adenosine A2A Receptor. *J. Am. Chem. Soc.* **135**, 8749–8759 (2013).

[218] Selent J., Sanz F., Pastor M., and De Fabritiis G. Induced effects of sodium ions on dopaminergic G-protein coupled receptors. *PLoS Comput. Biol.* **6** (2010).

[219] Dror R.O., Arlow D.H., Borhani D.W., Jensen M.O., Piana S., and Shaw D.E. Identification of two distinct inactive conformations of the beta2-adrenergic receptor reconciles structural and biochemical observations. *P. Natl. Acad. Sci. USA* **106**, 4689–4694 (2009).

[220] Romo T.D., Grossfield A., and Pitman M.C. Concerted interconversion between ionic lock substates of the beta(2) adrenergic receptor revealed by microsecond timescale molecular dynamics. *Biophys. J.* **98**, 76–84 (2010).

[221] Dror R.O., Arlow D.H., Maragakis P., Mildorf T.J., Pan A.C., Xu H., Borhani D.W., and Shaw D.E. Activation mechanism of the β2-adrenergic receptor. *P. Natl. Acad. Sci. USA* **108**, 18684–18689 (2011).

[222] Vardy E. and Roth B.L.L. Conformational ensembles in GPCR activation. *Cell* **152**, 385–386 (2013).

[223] Romo T.D. and Grossfield A. Unknown Unknowns: the Challenge of Systematic and Statistical Error in Molecular Dynamics Simulations. *Biophys. J.* **106**, 1553–1554 (2014).

[224] Grossfield A. Convergence of molecular dynamics simulations of membrane proteins. *Proteins* **67**, 31–40 (2007).

[225] Romo T.D. and Grossfield A. Validating and improving elastic network models with molecular dynamics simulations. *Proteins* **79**, 23–34 (2011).

[226] Provasi D., Bortolato A., and Filizola M. Exploring molecular mechanisms of ligand recognition by opioid receptors with metadynamics. *Biochemistry* **48**, 10020–10029 (2009).

[227] Provasi D. and Filizola M. Putative active states of a prototypic g-protein-coupled receptor from biased molecular dynamics. *Biophys. J.* **98**, 2347–55 (2010).

[228] Provasi D., Artacho M.C., Negri A., Mobarec J.C., and Filizola M. Ligand-induced modulation of the free-energy landscape of G protein-coupled receptors explored by adaptive biasing techniques. *PLoS Comput. Biol.* **7**, e1002193 (2011).

[229] Khelashvili G., Grossfield A., Feller S.E., Pitman M.C., and Weinstein H. Structural and dynamic effects of cholesterol at preferred sites of interaction with rhodopsin identified from microsecond length molecular dynamics simulations. *Proteins* **76**, 403–417 (2009).

[230] Khelashvili G., Mondal S., Andersen O.S., and Weinstein H. Cholesterol modulates the membrane effects and spatial organization of membrane-penetrating ligands for G-protein coupled receptors. *J. Phys. Chem. B* **114**, 12046–12057 (2010).

[231] Mondal S., Khelashvili G., Shan J., Andersen O.S., and Weinstein H. Quantitative Modeling of Membrane Deformations by Multihelical Membrane Proteins: Application to G-Protein Coupled Receptors. *Biophys. J.* **101**, 2092–2101 (2011).

[232] Ingólfsson H.I., Lopez C.a., Uusitalo J.J., de Jong D.H., Gopal S.M., Periole X., and Marrink S.J. The power of coarse graining in biomolecular simulations. *Wiley Interdiscipl. Rev.: Comput. Mol. Sci.* **00**, 225–248 (2013).

[233] Monticelli L., Kandasamy S.K., Periole X., Larson R.G., Tieleman D.P., and Marrink S.J. The MARTINI Coarse-Grained Force Field: Extension to Proteins. *J. Chem. Theory Comput.* **4**, 819–834 (2008).

[234] Schäfer L.V., de Jong D.H., Holt A., Rzepiela A.J., de Vries A.H., Poolman B., Killian J.A., and Marrink S.J. Lipid packing drives the segregation of transmembrane helices into disordered lipid domains in model membranes. *P. Natl. Acad. Sci. USA* **108**, 1343–1348 (2011).

[235] Domański J., Marrink S.J., and Schäfer L.V. Transmembrane helices can induce domain formation in crowded model membranes. *Biochim. Biophys. Acta* **1818**, 984–994 (2012).

[236] Parton D.L., Klingelhoefer J.W., and Sansom M.S.P. Aggregation of model membrane proteins, modulated by hydrophobic mismatch, membrane curvature, and protein class. *Biophys. J.* **101**, 691–699 (2011).

[237] Dunton T.a., Goose J.E., Gavaghan D.J., Sansom M.S.P., and Osborne J.M. The Free Energy Landscape of Dimerization of a Membrane Protein, NanC. *PLoS Comput. Biol.* **10**, e1003417 (2014).

[238] Periole X., Knepp A.A.M., Sakmar T.P., Marrink S.J., and Huber T. Structural determinants of the supramolecular organization of

G protein-coupled receptors in bilayers. *J. Am. Chem. Soc.* **134**, 10959–10965 (2012).

[239] Periole X., Cavalli M., Marrink S.J., and Ceruso M.a. Combining an Elastic Network With a Coarse-Grained Molecular Force Field: Structure, Dynamics, and Intermolecular Recognition. *J. Chem. Theory Comput.* **5**, 2531–2543 (2009).

[240] Provasi D., Johnston J.M., and Filizola M. Lessons from free energy simulations of delta-opioid receptor homodimers involving the fourth transmembrane helix. *Biochemistry* **49**, 6771–6776 (2010).

[241] Johnston J.M., Aburi M., Provasi D., Bortolato A., Urizar E., Lambert N.a., Javitch J.a., and Filizola M. Making Structural Sense of Dimerization Interfaces of Delta Opioid Receptor Homodimers. *Biochemistry* **50**, 1682–1690 (2011).

[242] Periole X., Huber T., Marrink S.J., and Sakmar T.P. G protein-coupled receptors self-assemble in dynamics simulations of model bilayers. *J. Am. Chem. Soc.* **129**, 10126–10132 (2007).

[243] Johnston J.M., Wang H., Provasi D., and Filizola M. Assessing the Relative Stability of Dimer Interfaces in G Protein-Coupled Receptors. *PLoS Comput. Bio.* **8**, e1002649 (2012).

[244] Johnston J.M. and Filizola M. Differential Stability of the Crystallographic Interfaces of Mu- and Kappa-Opioid Receptors. *PLoS ONE* **9**, e90694 (2014).

[245] Giorgino T. Computing 1-D atomic densities in macromolecular simulations: The density profile tool for VMD. *Comput. Phys. Commun.* **185**, 317–322 (2014).

[246] Allen W.J., Lemkul J.A., and Bevan D.R. GridMAT-MD: A grid-based membrane analysis tool for use with molecular dynamics. *J. Comput. Chem.* **30**, 1952–1958 (2009).

[247] Mori T., Ogushi F., and Sugita Y. Analysis of lipid surface area in protein-membrane systems combining voronoi tessellation and monte carlo integration methods. *J. Comput. Chem.* **33**, 286–293 (2012).

[248] Lukat G., Kr??ger J., and Sommer B. APL@Voro: A Voronoi-Based Membrane Analysis Tool for GROMACS Trajectories. *J. Chem. Inf. Model.* **53**, 2908–2925 (2013).

[249] Lukat G., Sommer B., and Krüger J. Membrane simulation analysis using Voronoi tessellation. *J. ChemInf.* **6**, O23 (2014).

[250] Guixà-González R., Rodriguez-Espigares I., Ramírez-Anguita J.M., Carrió-Gaspar P., Martinez-Seara H., Giorgino T., and Selent J. MEMBPLUGIN: studying membrane complexity in VMD. *Bioinformatics* **30**, 1478–1480 (2014).

[251] Soubias O. and Gawrisch K. The role of the lipid matrix for structure and function of the GPCR rhodopsin. *Biochim. Biophys. Acta* **1818**, 234–240 (2012).

[252] Khelashvili G., Albornoz P.B.C., Johner N., Mondal S., Caffrey M., and Weinstein H. Why GPCRs behave differently in cubic and lamellar lipidic mesophases. *J. Am. Chem. Soc.* **134**, 15858–15868 (2012).